RIGA TECHNICAL UNIVERSITY

Shravan Koundinya Vutukuru

INTERACTION ANALYSIS OF SIMPLE FORM OBJECTS WITH FLUID AND CONTROL OPTIMIZATION

Doctoral Thesis

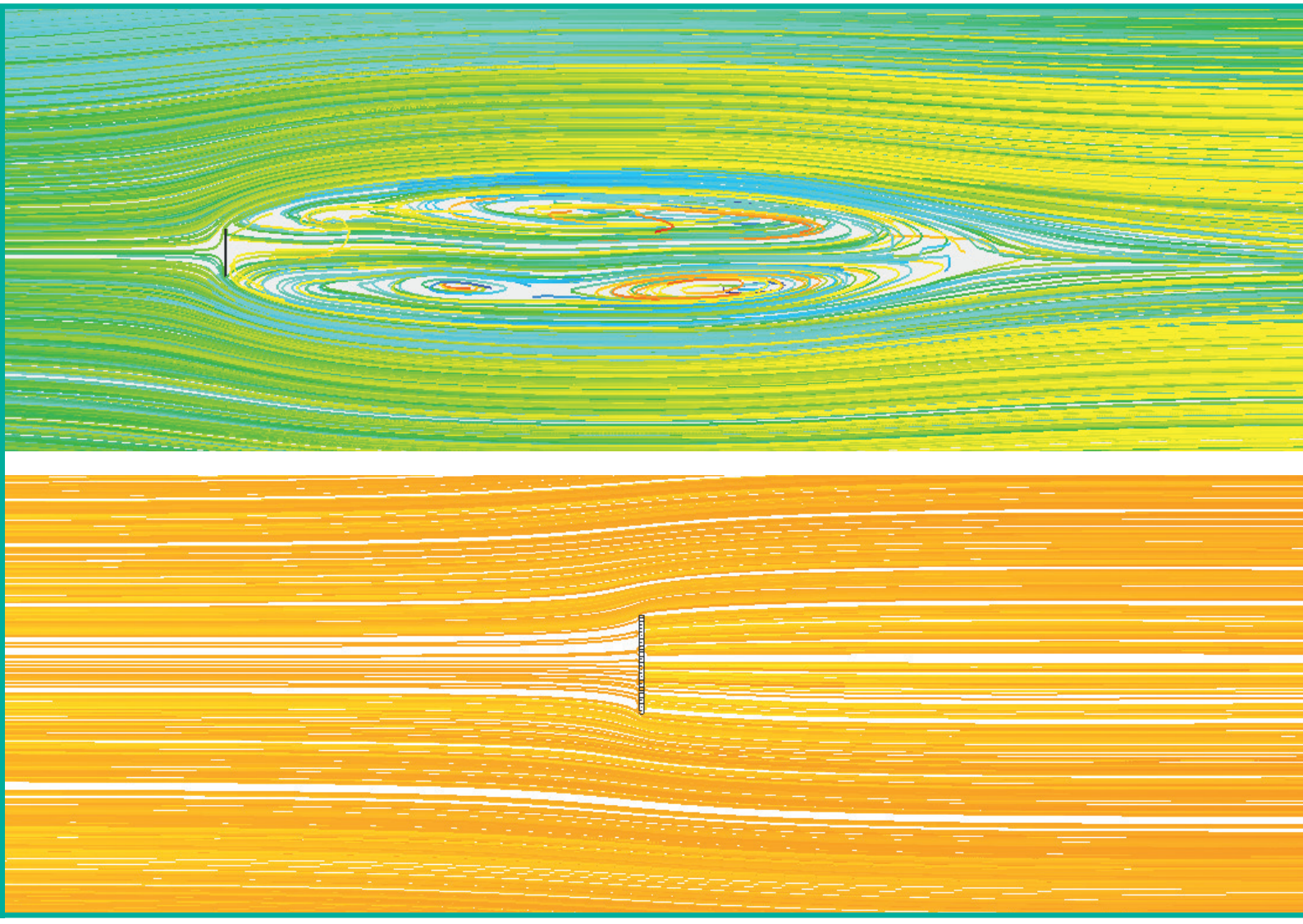

RTU Press
Riga 2021

RIGA TECHNICAL UNIVERSITY
Faculty of Mechanical Engineering, Transport and Aeronautics
Institute of Mechanics and Mechanical Engineering

Shravan Koundinya Vutukuru
Doctoral Student of the Study Programme "Engineering Technology, Mechanics and Mechanical Engineering"

INTERACTION ANALYSIS OF SIMPLE FORM OBJECTS WITH FLUID AND CONTROL OPTIMIZATION

Doctoral Thesis

Scientific Supervisor:

Professor Dr. sc. ing.
IGORS TIPĀNS

Professor Dr. habil. sc. ing.
JĀNIS VĪBA

RTU Press
Riga 2021

Vutukuru, S. K. Interaction Analysis of Simple Form Objects with Fluid and Control Optimization. Doctoral Thesis. Riga: RTU Press, 2021. 112 p.

Published in accordance with the decision of the Promotion Council "P-04" of 13 May 2021, Minutes No. 45.

The Doctoral Thesis was developed with the financial support of the Doctoral Research grant of RTU and Faculty of Mechanical Engineering, Transport and Aeronautics.

DOCTORAL THESIS PROPOSED TO RIGA TECHNICAL UNIVERSITY FOR THE PROMOTION TO THE SCIENTIFIC DEGREE OF DOCTOR OF SCIENCE

To be granted the scientific degree of Doctor of Science (Ph. D.), the present Doctoral Thesis has been submitted for the defence at the open meeting of RTU Promotion Council at on 17 September 2021 14.30 at the Faculty of Mechanical Engineering, Transport and Aeronautics of Riga Technical University, 6B Kipsalas Street, Room 521.

OFFICIAL REVIEWERS

Professor Emeritus Dr. sc. ing. Alģimantas Bubulis
Kaunas University of Technology, Lithuania

Professor emeritus Dr. sc. ing. Ēriks Kronbergs
Latvia University of Life Sciences and Technologies, Latvia

Assistant Dr. sc. ing. Marina Čerpinska
Riga Technical University, Latvia

DECLARATION OF ACADEMIC INTEGRITY

I hereby declare that the Doctoral Thesis submitted for the review to Riga Technical University for the promotion to the scientific degree of Doctor of Science (Ph. D.) is my own. I confirm that this Doctoral Thesis had not been submitted to any other university for the promotion to a scientific degree.

Shravan Koundinya Vutukuru ……. (signature)

Date: ……

The Doctoral Thesis has been written in English. It consists of Introduction; 6 chapters; Conclusions; 136 figures; the total number of pages is 112. The Bibliography contains 70 titles.

ACKNOWLEDGEMENT

I thank my parents for their moral support during all my student days right from high school to the doctoral studies and also for their showers of blessings that helped me bring out this thesis in time.

I wish to express my sincere gratitude to my supervisor Senior Researcher Igors Tipans , Director of International Cooperation and Foreign Students Department who is well known for his tireless efforts and constant support to all foreign students studying at Riga Technical University.

I take this opportunity to express my sense of gratitude to my supervisor Professor Janis Viba for his esteemed guidance and helpful criticism,working with whom was a big turning point in my life.

I also would like to express my gratitude to Professor Aleksandrs Urbahs, then the Director of Transport Department at RTU, who took me into this program.

A special thanks to all my Professors, colleagues and Team Design Factory at the RTU who shared their valuable ideas and also for guiding me inspite of their very busy schedule.

Riga, April, 2021.

ANOTĀCIJA

Šķidruma plūsmas un ķermeņa - šķidruma mijiedarbības pētījumiem ir sena vēsture, taču interesanti ir tas, ka joprojām nav izpētītas nestacionāras ķermeņa kustības un nestacionāras šķidruma mijiedarbības parādības. Risinājums ir ļoti sarežģīts tāpēc, ka pastāv milzīga vienādojumu sistēma, kas sastāv no visiem telpiskā uzdevuma elementiem, kuri ir savienoti kopā starp visiem telpas un laika posmiem. Turklāt, apsverot telpiskos aspektus parciālo diferenciālo vienādojumu sistēmas risināšanai, virkne sarežģījumu rodas no risinājuma metodes veida (galīgas starpības, galīgi tilpumi, galīgi elementi) un arī no mezglu veidošanas metodēm (kustīgas, strukturētas vai nestrukturētas). Lai gan ir pieejami mūsdienīgi komerciāli šķidruma un struktūras mijiedarbības modeļi, tie aprobežojas ar vienkāršiem ķermeņiem un prasa biežas tīkla maiņas metodes, kas ir laikietilpīgas un dārgas skaitļošanas procesos.

Dotajā darbā īpaši tiek pievērsta uzmanība tikai cieta ķermeņa un šķidruma (gaisa) mijiedarbībai. Šeit netiek ievērota plūsmas blīvuma deformācija vai plūsmas atdalīšanās parādība. Tai vietā tiek piedāvāta alternatīva aptuvena pieeja mijiedarbības fenomena aprakstam un tā priekšrocību pētīšanai. Tuvinātās teorijas pamatideja pašreizējā darbā ir tāda, ka lai būtu vienkāršota pieeja analīzei, tiek izmantots prizmas formas vienkāršots ķermeņa matemātiskais modelis, ignorējot šķidruma (gaisa) viskozitāti. Tāpēc šī ir aptuvena teorija nestacionāru ķermeņa un šķidruma kustību mijiedarbības fenomenam. Tam nolūkam tiek izmantotas līdzīgas stacionāras nekustīgas ķermeņa un šķidruma mijiedarbības, kas veiktas ar programmas ANSYS aprēķiniem (2D telpā un 3D telpā), kur stacionārs RANS vienādojums tiek atrisināts ar turbulences modeļa palīdzību. Darbā apspriestā koncepcija piedāvā alternatīvu pieeju “telpa-laiks” programmēšanas metodēm. Tā palīdzēs atrisināt tehnoloģiskos uzdevumus attiecībā uz vienkāršas formas objektu optimizāciju un sintēzi, kam nepieciešami milzīgi skaitļošanas apjomi. Tā, piemēram, tiek pētīta jauna zinātnes iespēja attiecībā uz autonomiem robotiem (zem ūdens esoša robotzivs ar vienu un diviem astes izpildmehānismiem), kur tiek piedāvāta iebūvēta spēka bloka tehnika (enerģijas ieguve no apkārtējās vides), kas tiek analizēta, pamatojoties tikai uz kustīgā šķidruma un kustīgā ķermeņa mijiedarbības parādību.

Eksperimenti vienkāršas formas objektiem tika veikti ARMFIELD vēja tunelī, kas ir pieejams Rīgas Tehniskajā universitātē, piemēram, ar nemainīgu ātrumu 10 m/s, kas tika validēti ar datorprogrammu ANSYS 3D telpā.

Visas jaunākās izstrādātās metodes, to priekšrocības un nozīmīgums saistībā ar šķidruma struktūras mijiedarbību ir apkopoti literatūras pārskata sadaļā, izmantojot dažādas datu bāzes, kas pieejamas internetā.

Izstrādātais darbs, kas uzrakstīts angļu valodā, aptver 112 lpp. Darbā ir 136 attēli, kā arī atsauces uz 70 literatūras avotiem.

SUMMARY

Fluid and rigid body interaction is an age old phenomenon but interestingly, a good approximated solution for the phenomenon pertaining to non-stationary body-fluid interaction is still non-existent. The solution is much more complicated due to huge system of simultaneous partial differential equations that are framed from multi-degrees of freedom, all elements in the spatial domain coupled together between all timesteps. Additionally, when considering the spatial aspects of solving the system of partial differential equations there arise a range of complexities from the type of solution technique (finite-differences, finite-volume, finite-element) and also from meshing techniques (moving, structured or unstructured). Even though advanced commercial fluid-structure interaction solvers are available, they are limited to simple objects and require frequent remeshing techniques that are time consuming and computationally expensive.

The promotion work specifically focuses solely on rigid body-fluid (air) interaction and do not consider flow reattachment or flow separation phenomenon and offers an alternative approach to study the interaction phenomenon and its advantages. The basic idea of the approximated theory in the current work is to have a simplified approach through a straightforward mathematical model without considering the viscous nature of fluid medium (air). Therefore this is an **approximate theory** for non-stationary body and fluid interaction phenomenon considering inputs (post-processing results) from stationary rigid body-fluid interaction performed in ANSYS Fluent (2D and 3D) where the steady state RANS equation is solved with the help of turbulence model. The concept discussed in the work will offer an alternative approach for "space-time" programming techniques and also help to solve the engineering tasks of optimization and synthesis for simple form objects without requiring huge computational efforts. A new world of science for autonomous robots (underwater robotic fish with single and dual tail actuator) is explored where in an on-board power pack technique (energy scavenging from surrounding medium) is proposed that is analyzed purely based on the fluid and rigid body interaction phenomenon.

Experiments on simple form objects were performed in ARMFIELD wind tunnel available at Riga Technical University at a constant speed of 10 m/s and validated with the computer programm ANSYS Fluent (in 3D).

All the latest techniques, advantages and importance related to fluid-structure interaction phenomenon are summarized in the literature review section through various databases available over internet.

Promotion work is written in English, it contains 112 pages, 136 images, and references to 70 sources of literature.

LIST OF FIGURES

1. INTRODUCTION

Undoubtedly, fluid-rigid body interaction phenomenon is one of the most widely occuring activity in nature. Any body immersed in fluid experiences this phenomenon of fluid-structure interaction. The task of fluid, rigid-body association is complicated when influence of interaction and response becomes very much stronger. The rigid body-fluid interaction plays a key role in the design aspect by influencing the decisions for design of new systems that are of contemporary interests.

One of the earliest contributions to the phenomenon of fluid structure interaction was studied by Issac Newton. Newton explained in his book "Principia",1687 that fluid flow can be considered as a uniform, rectilinear stream of particles and upon striking a surface inclined at an angle Θ, the normal momentum of the particles was transfereed to the surface but the tangential momentum would be preserved thereby the particles moved along the surface after collision. The hydrodynamic force was found to be varied as $\sin^2 \Theta$ (known as Newtons sine square law). In contrast, Euler noted that the fluid moving towards the body before reaching bends its direction and its velocity changes so that when the fluid reaches the body the fluid flows past it along the surface, and there exists only pressure at the points of contact. For large angles of inclination, this force is proportional to the $\sin^2 \Theta$ and proportional to $\sin\Theta$ for small incidence angles.

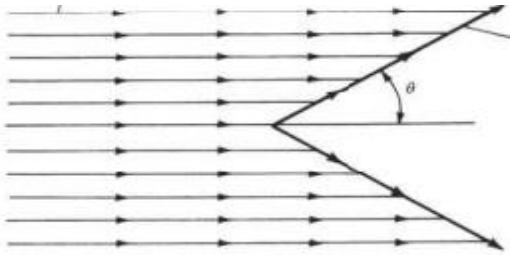

Fig. 1. 1. Uniform stream of particles from left to right on inclined surface, particles moving in tangential direction to the surface of the body after collision.

One of the main challenges in the field of fluid-rigid structure interaction is the fluid-structure coupling. This challenge till date is solved by using two different methods:

1. Non-moving grid
2. Moving grid.

The moving grid techniques are computationally time consuming and mostly require high performing systems for complex geometries there by making it computationally expensive.

The present work focusses on non-moving techniques and by studying in detail the stationary rigid body-fluid interaction phenomenon a simple mathematical model is proposed that helps solve the tasks of moving objects without requiring "space-time" programming practices. Further, vibration through fluid-body interaction/impact is taken up, and a new approach for energy scavenging through non-rotating techniques

(vibration/oscillation) from the surrounding medium is proposed through the parametric and control optimization of the body immersed in fluid flow.

Topicality

The rigid body and fluid flow interaction is a very important phenomenon that needs to be explored because of its wide occurence in nature and for its high demand in understanding various engineering and medical applications. One of the best use of this interaction (fluid–rigid body) phenomenon is to investigate the possiblility of obtaining the energy from the surrounding medium (air, water) when the object is immersed in the fluid. Broadly, there are three main possibilities of interactions with the fluid: (a) stationary rigid body-fluid interaction (still fluid), (b) stationary rigid body in a fluid flow, (c) non-stationary rigid body in a fluid flow.

This completed work of author's and his colleagues covers the following areas that are directly related to the concept or phenomenon of fluid structure interaction: (a) approximate analytical method for fluid-stationary rigid body interaction phenomenon that is of importance to understand non-stationary body motion in fluid flow, (b) interaction analysis of simple form objects, (c) parametric and control optimization of fluid-rigid body interaction problem, (d) synthesis of new devices for energy scavenging through motion modelling of simple form objects and their interaction phenomenon, (e) experiments pertaining to simple form objects subjected to fluid (air)flow. The actual work is carried in two directions - to investigate non-stationary body motion in fluid by analyzing stationary rigid-body interaction phenomenon and to extend the interaction phenomenon of non-stationary body motion by simple form objects for the synthesis of new energy scavenging systems and for the tasks of parametric and control optimization of bodies in fluid flow.The term "energy extraction" or "energy scavenging" refers to the activity that is related to the generation of energy which is the "green" or "clean" energy.

Research Objective

In the current work, the main objective of the research is to study the interaction of fluid with the stationary rigid body in the fluid flow and to extend the concept (through the post-processing results of the steady state case of the stationary body in fluid) for non-stationary motion of the object when immersed in the fluid medium (air or water) alongside the Newtonian mechanics (considering the velocities of vectors in different direction). This concept of mathematical modelling through **approximate** differential equations of motion can be solved numerically through integration that helps overcome the complicated task of "space–time" programming techniques for solution of simple engineering issues.

The theory/concept of non-stationary motion in fluid medium is further extended to obtain or scavenge energy from fluid-body interaction and in the synthesis of new systems or to analyze the diving or flying objects in fluid flow.

Practical application of the thesis

1. The theory and methodology for the interaction of objects with fluid for different cases of stationary object, still fluid, and non-stationary object in a flowing fluid can be used in the systhesis of new “clean energy” devices and also for the design of flying and diving robots /machines.
2. The results of computer modelling for 2D and 3D are helpful to solve the task of form optimization.
3. Control of robotic fish tail actuator (single or dual) can be used for energy restoration to recharge on-board power pack.
4. A patent application has been developed/submitted that is based on the fluid-rigid body interaction principle with a linear generator under the title “ Wind energy conversion device”.

Research Novelty

1.Comercially available software for computational fluid dynamics study with “space-time” programming techniques involves constant re-meshing for geometries in non-stationary motion when subjected to fluid flow and additionally, are computationally very expensive and at the same time they offer approximate solution at the end. It is therefore important to look for an alternative approach that helps to perform simple engineering tasks related to non-stationary rigid body motion in a fluid medium (air or water) with out requiring labour intensive space time programming techniques.

2.The proposed method (theory) and methodologies in the work suggest the use of classsical mechanical methods for understanding the physics of non-stationary rigid body-fluid interaction in a continuous medium (air or water) ignoring the viscosity of the fluid medium and thereby it is possible to obtain dissipative forces through reduction of their principal vectors and principal moments at the centre of mass of the rigid-object (system). The obtained corresponding equivalent relations allow to form differential equations of body motion, which are numerically integrated accordingly. Upon integration, it is possible to perform parametric optimization with a computer and synthesize new efficient systems for use of energy during fluid movement or to create new “green energy” systems for fluid flow around a rigid body object, or to realise a flying or diving object in a fluid medium.

Structure of the Thesis and Main Results

The structure of the thesis is summarized in 6 chapters.

In Chapter 1, Introduction on the topic and latest advancements and state of the art research are reviewed.

In Chapter 2, a new approximate analytical method through a mathematical model for fluid-rigid body interaction is analysed and summarized in scientific publication

No. 8, with the three main topics covered:

1. Fluid-rigid body interaction phenomenon with motionless fluid.
2. Stationary rigid body object interaction with air (fluid) at low speeds.
3. Moving object in a fluid flow (at low speeds).

The Chapter 3 summarizes the scientific publications No. 2,3,5,6 on fluid (air) flow, with the following main topics covered:

1. Analysis of simple rigid body-fluid flow interaction phenomenon for steady and unsteady case;
2. Interaction phenomenon for flow object interaction (concave and convex side prism)
3. The Chapter 4 summarizes other studies of fluid dynamics in scientific publications No. 2, 3 and 7 with four main topics covered:

1. Variable area rigid body structure vibrations in fluid flow for energy extraction; optimization task.
2. Variable area rigid body structure model for vibrations in a fluid flow for energy extraction and a mathematical model of the horizontal motion of one tail or dual tail of a fish robot in a fluid;
3. Vibration damping of fluid-rigid body interactions at low speeds;
4. Control optimization methods (force and area control) for horizontal and vertical motion of the body.

The Chapter 5 summarizes other studies of fluid dynamics in scientific publications No. 3 and 7 with the following main topics covered:

1. Synthesis of new devices for the purpose of energy scavenging;

The Chapter 6 summarizes other studies of fluid dynamics in scientific publications No.3, 5 and 6 with the following main topics covered:

1. Experiments related to flat plate .
2. Experiments related to perforated plate.
3. Validation of the interaction phenomenon theory (mathematical model).

Research Hypothesis

The main hypothesis of the work is based on the hypothesis of Newtonian mechanics:

1. Superposition principle equation of motion for the particle system in the fluid medium (diferential form);
2. Rigid-body and fluid particles impact in the windward side (pressure zone), Pressure at the leeward side (suction zone) is created by the fluid particles;
3. Viscosity of the fluid medium is ignored.
4. The fluid is assumed to be incompressible (density constant).
5. In the pressure zone, the vector of the absolute velocity of the fluid flow V_0 is the same at all contact points of the object.

All the above hypothesis have been analyzed through numerical simulations and experiments performed by using wind tunnel as well as the movement of the pendulum in open air. As a result, a new and a better approximated scientific theory was developed.

The new theory differs from all the existing theories in that it is not always necessary to perform "space–time" analysis of non-stationary rigid body-fluid interactions. The interaction phenomenon of non-stationary rigid body and fluid flow interaction could be well understood through a stationary rigid body and fluid flow interaction phenomenon which means there is no need to perform extensive "space-time" programming techniques for simple engineering tasks.

Research methodology

The research is completely devoted to extensive study of fluid and rigid body interaction phenomenon by using simple form objects in air (continuum). The interaction phenomenon is carried out in two directions: first, computer numerical simulations for the fluid- stationary rigid body interaction phenomenon are performed in ANSYS Fluent where the steady state RANS (Reynolds Average Navier Stokes Equation) is solved by using turbulence model and interaction force along the flow direction, otherwise called drag is estimated. Secondly, a mathematical model (differential equations) by using laws of classical mechanics is then developed that considers the post processing result from the computer program (coefficient of interaction - concept of zones, presence of pressure side and suction side) and is extended for non-stationary interaction behaviour by taking into consideration the flow velocity (relative velocities if they are vectors in different direction), fluid density, spring constant, linear damper (that is simulated for linear generator) and geometry parameters of the body that is immersed in fluid flow (air), and all the graphical results are illustrated by using MATHCAD. All simulations are carried out for a Reynolds number of 108287,92 (only at subsonic speeds).

The following conclusions are drawn

1. The concept of zones (pressure side and suction side) is a reality and exists for all types of geometry when immersed in air flow.
2. At high speeds (hypersonic speeds), the concept of zones is not applicable due to shock interactions and related static pressure rise and compressibility effects (density change).
3. Complex mesh motion techniques are not always required when solving simple engineering tasks with simple form objects.
4. The task of form optimization could be taken up effectively for specific engineering assignments.
5. The nature of flow (laminar or turbulent), geometry parameters, density effects are more significant as compared to viscous nature of the fluid medium under consideration (only for air).
6. Since the approach is purely mathematical, complex geometries can also be analysed.

The results obtained are in good agreement only for rigid body.

Thesis approbation and publications

Scientific articles indexed in SCOPUS or WOS database

1. Tipans I., Viba J., Irbe M., Vutukuru S. K. 2020. Investigation of dual varying area flapping actuator of a robotic fish with energy recovery. *Agron. Res.* 18, 1046–1055.
2. Tipans I., Viba J., Irbe M., Vutukuru S. K. 2019. Analysis of non-stationary flow interaction with simple form objects. *Agron. Res.* 17, 1227–1234.

Full-text conference papers published in conference proceedings indexed in SCOPUS or WOS database

3. Vutukuru S. K., Tipans I., Viba J., Irbe M. 2020. Form optimization and interaction analysis of plane symmetry prism in air. *Engineering for Rural Development.* vol. 19, pp. 739–746.
4. Spade K., Vaicis I., Vutukuru S. K., Irbe M. 2020. Analysis of granule layer impact interaction on vibrating 2D prism. *Engineering for Rural Development.* vol. 19, pp. 1463–1469.
5. Vutukuru S., Viba J., Tipans I., Viksne I., Irbe M. 2019. Analysis of flat plate vibrations by varying frontal area to the flow. *Engineering for Rural Development.* vol. 18, pp. 1408–1414.
6. Tipans I., Viba J., Vutukuru S. K., Irbe M. 2019. Vibration analysis of perforated plate in non-stationary motion. *Vibroengineering Procedia.* vol. 25, pp. 48–53.
7. Tipans I., Viba J., Vutukuru S. K., Irbe M. 2021.Varying area vibrating structure in a fluid for energy gain. *Advances in Systems Engineering. Lecture Notes in Mechanical Engineering. Springer, Singapore.* pp.757-770.
8. Tipans I., Viba J., Vutukuru S. K., Irbe M. 2021. Optimization of energy extraction using definite geometry prisms in air. *Latvian Journal of Physics and Technical Sciences*. Vol.58(2), pp. 19-31.
9. Tipans I., Viba J., Vutukuru S. K., Irbe M. 2021. Action of pendulum in transient fluid flow. *Engineering for Rural Development.* vol. 20, pp. 275–280.
10. Beresnevich V., Vutukuru S.K., Irbe M., Kovals E., Eiduks M., Burbeckis K., Viba J. Wind energy conversion generator. *Engineering for Rural Development.* Vol- 20. pp.955-960.

New Invention (Patent application).

11. Vēja enerģijas pārveidošanas iekārta (Wind energy conversion device) submitted on 18-12-2020, R.T.U., LVP2020000092.

Author's Contribution to Publications

All scientific publications have been written in collaboration with supervisors Professor Jānis Vība and Senior Researcher Igors Tipāns as co-authors and consultant

Martins Irbe in the development of publications. The work on scientific publications was collectively planned and accomplished by the authors. The percentage of research work contributed by the author to scientific publications is summarized in Table 1.

Table 1.

Contribution to the Development of Scientific Publications

Publication No.	Activity	Contribution
1.	Experimental equipment design, literature, experiments, data processing, numerical modelling	75 %
2.	Research of literature, simple form object analysis, numerical modelling and graphical representation, 2D & 3D flow simulations	75 %
3.	Research of literature, design, prototyping, 2D&3D flow simulation, wind tunnel experiments, data processing and graphical representation,mathematical modelling	75 %
4.	Modelling of granular fraction motion by using approximate force determination method for pressure and suction zones	5%
5.	Rigid body shape geometry optimization analysis of fluid and body interactions, experimental model setup, experiments in wind tunnel, 2D & 3D simulations.	75%
6.	Analysis, optimization and synthesis of non-stationary fluid and body interaction, wind tunnel experiments, numerical modelling, 3D simulations, experimental setup of model.	100%
7.	Parametric optimization, research literature review, numerical modelling, body motion analysis,	40%
8.	Geometry design and research literature review.	100%
9.	Experiments , simulation and result analysis	50%
10.	Literature review, results analysis and Mathematical simulation.	50%

Thesis for Assertion

1. Standard explanations found in the literature on interaction of fluid and rigid body are not accurate: it has been proved that the lowest pressure does not always occur at the visually longest fluid flow line, i.e. as the highest local velocity. In fact, there is a suction phenomenon, which then also reduces

pressure.

2. Viscosity may be ignored in engineering calculations for fluid-rigid body interaction analysis only for air medium. This is justified because all computer modelling programs which include viscosity are also approximate. Also, considering the interaction phenomenon, the shape of the object, nature of flow (laminar or turbulent) are of primary importance.
3. In the analysis of air-rigid body interactions, the principle of superposition for non-stationary body motion or relative motion in the fluid flow can be applied, i.e. the interaction phenomenon can be divided into two zones: the pressure zone and the suction zone. The laws of classical mechanics including Brownian random motion of particles are to be considered for better analysis.
4. The approximate theory obtained in the description of the interaction between air and a rigid body can be applied to the engineering estimates for the description of interaction between water and rigid body considering the density and viscous effects.
5. The differential equations of fluid-rigid body interaction obtained in the work can be applied to solve analytical, optimization, and synthesis problems without using complex and time-consuming approximate "space-time" programming methods.

1.1. Focus and main tasks

The main focus of the present work is to investigate in detail the stationary rigid body in fluid (air) interaction phenomenon and to extend the interaction concept for non-stationary body fluid interaction without requiring "space-time" programming techniques and also the application of the interaction phenomenon in performing engineering tasks of energy scavenging, synthesis of new devices through control and parametric optimization. A simple and straightforward mathematical model is proposed (according to the classical laws of mechanics) that is based on fluid-rigid body interaction phenomenon for simple form objects. The interaction is in detail analysed by using ANSYS software in a uniform flow at low speeds and then the space around this interaction is split into zones (Fig. 1.2). The task of optimization is considered (in terms of perturbation in parameters and for area control). All calculations and experiments are performed for prevailing wind conditions in Latvia (at 10m/s).

The research carried out in the work is summarized in the following main directions as a thematically merged set of scientific publications:

1. **New approach for fluid-rigid body interaction phenomenon**
   - A simplified theory for studying the rigid body interaction phenomenon is proposed by the theory of superposition when the body is subjected to a fluid flow.
   - Interaction analysis is carried out for objects in different fluid flow conditions (windless, stationary and non-stationary motion).

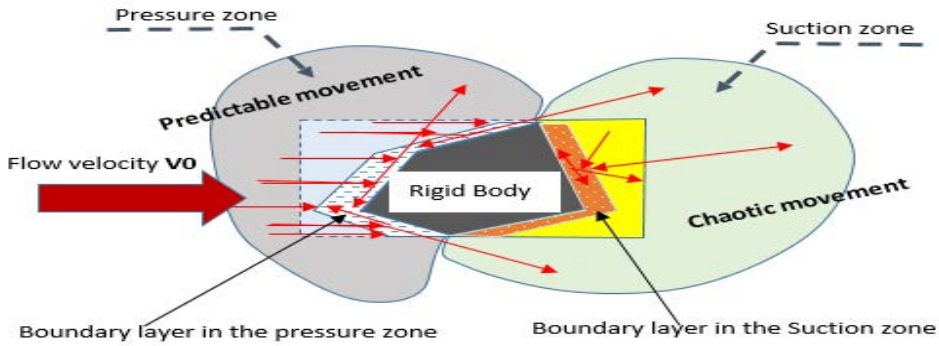

Fig. 1. 2 Concept of zones(pressure and suction zones) for a body immersed in fluid(air).

- A mathematical interaction model was proposed to understand the interaction phenomenon.

2. **Interaction of simple form objects**
   - Simple form objects like diamond, square, perforated plate and star prism interaction analysis in fluid flow (air) was carried out and verified through computer programms by using ANSYS.
   - A simple and straightforward mathematical model is proposed by studying the interaction phenomenon for convex and concave broken side prisms.
   - ANSYS results are discussed and the new theory is validated.
3. **Approximation for interaction phenomenon**
   - Interaction analysis of simple form objects like flat plate, diamond, perforated plate and star prisms (all stationary objects) at steady flow of 10m/s, pressure plots of star prism and error estimation for calculating *C* coefficient of interaction for simple form objects (diamond, flat plate and perforated plate).
   - Interaction phenomenon extended for the investigation of concave and convex broken side prisms immersed in a fluid flow.
   - Concept of diving and flying objects is analysed.
   - ANSYS simulation results are discussed.
4. **Parametric and control optimization for interaction phenomenon**
   - On board energy scavenging task by using simple form object like flat plate, perforated plate as a model for flapping/oscillating robotic fish tail is analysed through the parametric optimization.
   - Damping due to excitation and due to impact, and also due to harmonic excitation from fluid and structure interaction are analysed and explained.
   - Control optimization for robotic fish movement (horizontal, vertical) with force and control action is analysed.
5. **Synthesis of new energy scavenging systems**
   - Efficient and innovative energy scavenging systems of 1D.O. F, 2D.O.F and

3D. O. F are analysed, and the process and results of theoretical interaction models are discussed and explained.

6**. Experiments**

- Experiments to validate the theory by using simple pendulum in still air is performed.
- New flapping/oscillating device is investigated.
- Innovative patented application for the purpose of energy scavenging from fluid flow by a flat plate is mentioned.

1.2.Fluid-structure interaction analysis literature review

Usually the FSI (Fluid-Structure Interaction) are solved in one of the following approaches.

1. Monolithic approach – fluid and structure equations are treated simultaneously
2. Partitioned approach – fluid and structure displacement are solved individually.
3. Loosely coupled and strongly coupled partitioned approach – single solution (one time for fluid and another time for structure) per time step is used.
4. Direct coupled FSI uses partitioned approach for solving. Both sequential staggered solution scheme (explicit) and iterative staggerd scheme are supported by using third –party solver.

5. Practically coupled FSI was solved without real time coupling. An iterative staggered algorithm called multi –iterative coupling was used(MIC) [1].

Further, an overview of advanced techniques/methods to solve the task of fluid-structure interaction is mentioned, most of which either require high computational work or remeshing or space-time discretization-programming techniques.

A better method compared to moving and deforming techniques with no restriction on closeness between objects and their complex motion is studied were continuity and momentum equations include motion effects [2]. Different types of mesh moving techniques for fluid-structure interaction were studied and compared. A new use of space-time discretization that could be extended for a full-time space Galerkin discretization was examined [3]. Fixed mesh technique by using arbitrary Lagrangian-Eulerian approach for flow problems in moving domain were studied and for every time step results were displayed on a background mesh [4]. An algorithm for space-time finite element meshes was used to obtain numerical results for transient Navier-Strokes equations for an adaptive moving mesh in time was presented [5]. New XFEM approach was proposed based on fixed grid method, which does not take into account most of fluid unknown characteristics, this method is advantageous as simulations of deforming structures could be performed effectively [6]. Easily understandable and less complex method for space-time mesh that allows a refinement of selected locations within the domain was proposed[7]. Advantage of saving the computational time and to account for flexibility of unstructured meshes and improving the scope of compressible fluid flow was mentioned [8]. Solution for non-stationary fluid body problems by using high-order finite element

method based on space-time discontinuous Galerkin (DG) procedure was proposed and extended to explain the dynamics of parachute motion [9].

Applications of fluid-rigid body interaction physics and the importance of this interaction phenomenon in day to day life is mentioned in the following paragraph.

Wind impacts analysis are performed where effects of wind impact for a HAWT is analysed by using high fidelity fluid–structure interactions simulations (CFD) and computational structure mechanics (CSM). Flow patterns, loads and performance of impacted blades were studied in detail [10]. Considering the flexibility of the structure, efficient computational model for interaction phenomenon of fluid–structure in steady state flow for a wind turbine with flexible blades was proposed [11]. A detailed analysis is performed for optimal control problem involving linearized fluid-structure interaction model with a delay term in structural damping. A distributed control acting on the fluid domain-structure domain or both is taken into consideration. Numerical results are validated with theoretical results[12]. To account for other types of fluid structure interaction, non-linear fluid structure-interaction problem is taken up, and the existence of a weak solution by designing a hybrid approximation scheme that deals with non-linearities in the system is obtained[13]. A computational framework is developed to analyse body fluid structure interaction (BFSI) phenomenon of oscillating flexible stabilizer connected to the end of the body[14]. A high fidelity FSI model is developed by coupling (CFD) and (FE) finite element to investigate the response of a wind turbine structure[15]. Coupled fluid structure interaction for a vibrating–assisted rotary percussion drilling tool is presented[16]. Fluid–structure interaction phenomenon investigation for horizontal axis in tidal current turbine (HATCT) is performed. Number of cycles and safety factor at different equivalent alternating stresses was predicted[17]. Keeping in view the effect of wind and rotating speed including vibration through fluid-structure interactions for a wind turbine blade a good study was conducted[18]. Wind flow and motion/deformation behaviour for rotating wind turbine are experimented in wind tunnel[19]. Effects of velocity profile on large scale wind turbine for variation in load and fatigue life through coupled fluid structure interaction modelling is performed[20]. One and two way fluid structure interactions to account for unsteady flow field and structural vibration of a wind turbine blade was studied [21]. Further, fluid structure interaction under shear and waves was carried out [22]. Under dynamic excitation, ultimate strength for turbine runner blade is established [23]. Cerebral aneurysm wall for its deformation was studied[24]. Importance of fluid structure interaction in 3D modelling of Marfan syundrome with elastic and hyperelastic materials is investigated[25]. Stability of 2D FSI system using mixed boundary conditions around an unstable stationary solution was performed [26]. Vibration response and analysis for hydrocyclone under periodic exitation by implementing FSI techniques is taken up [27]. Aero-hydraulic pipe under friction coupling is studied[28]. Simulation study for travelling wave valve less micro pump and its role in fluid delivery is performed[29]. Modelling for a flexible structure–fluid interaction is studied in detail. The work emphasizes more on physical understanding and dramatic reductions in computational costs using by reduced order models, time-

linearization and methods from dynamical system theory were analyzed[30]. Efficient method to tackle the problem of monolithic approach is discussed and tested on a NACA0009 symmetric hydrofoil. Transient analysis is performed by time marching solution, by updating the shape of the mesh at each time step (integrating the obtained modal forces with the CFD grid) [31].

On a broader view, the more complex problems due to fluid-structure interaction analysis is that of moving or changing domain, structural deformation due to interaction forces by fluid, conflict of description of fluid was investigated (Eulerian vs Lagrangian) [32]. A space-time parallel algorithm with space-time adaptive mesh refinement (AMR) is developed and experimented that shows the algorithm is promising for CFD applications that can take advantage of the time parallelism. Given the same solution accuracy, speedups are recognised for the use of space-time parallelization over the time-sequential integration on Couette flow and Stokes' second problem [33]. Advantage of paralel–in-time method for time periodic problems was successfully implemented on Stokes second problem and a speedups of 13 times over the time-sequential algorithm without loss of accuracy was achieved[34]. Multigrid-reduction-in-time algorithm (MGRIT) for solving 2D and 3D spaced diffusion equations was demonstrated. A significant speedup in comparison to sequential time marching approach was achieved[35]. A key difficulty in using time-stepping routines for the MGRIT algorithm is that the cost of the time integrator on coarse time grids must be less expensive than on the fine grid to allow for speedup over sequential time stepping on the fine grid in order to overcome this problem, reducing the costs of the coarse-level problems by adding spatial coarsening is considered, and effects of spatial coarsening on MGRIT convergence applied to two numerical models of an induction machine, one with linear material laws and a full nonlinear model was investigated, a significant speedup in the simulation time was achieved[36]. New error estimates are used to analyze the choice of space-time discretizations when testing parallel-in-time methods, error estimates for the one-dimensional advection equation based on Runge–Kutta and finite difference discretization by using general space-time discretization schemes[37]. Solution to optimal control problem governed by a parabolic PDE through space-time spectral allocation method that helps to reduce the problem to a system consisting of easily solvable algebraic equations was investigated[38]. Solution to linear system of equations arising from parabolic equation discretization through the space-time additive Schwarz method is presented. It was also concluded that space–time method outperforms the traditional time stepping method as the number of processes becomes very large[39]. Highly parallel space-time domain decomposition methods for parabolic problem using the class of space–time Schwarz methods are presented and discussed [40]. The variation of pressure with rotation of plate at different air velocity and the forces acting on a pendulum type flat plate against air flow are studied. The angles of the flat plate were varied and it was found that as the velocity of the incomming air is increased there is a more flapping/oscillations of the plate that can be used for the purpose of energy scavenging [41].

Application of fluid-structure interaction through simulation for drawing ocean wave energy was studied for various different wave conditions [42]. The complex physics behind fluid and structure interaction and their applications in the field of ocean engineering was discussed in detail [43]. In depth fluid-structure interaction for wind turbines at offshore was presented by a comprehensive simulation methodology, flow around the 3D oscillating foil was compared with experimental results [44].Challenges that are encountered when dealing with fluid-structure interaction problems particularly related to slender structures was addressed [45]. An improved tool that helps to predict the flutter speed for flow induced vibrations of bridges was developed [46]. Fluid-structure interactions for studying the performance of energy extraction process of a new innovative flapping foil was experimentally studied [47]. Implementation and validation at high Reynolds number for a fully passive flapping foil turbine by means of a strongly coupled model was presented [48]. A theoretical performance of oscillating airfoils subjected to unsteady, laminar flow for the pupose of drawing energy was investigated [49]. In order to stabilize the dynamics of fluid-structure interaction problem, an optimization problem was taken up to control the inflow [50]. Principal mechanisms for propulsive forces in flexible oscillating bodies in fluid medium and their control over formation of large scale vortices was reviewed pertaing to marine forms[51]. Higher order schemes which properly conserve kinetic and mechanical energy in the system through partially non-conservative formulation was investigated [52]. Problems encountered during viscous flows inside of a deformable structure were addressed [53]. Insights into the complex flow nature near the rotor and in the wake and also the deformation of the blades along with the interaction of solid and fluid field of an horizontal axis marine current turbine by using large eddy simulations were performed. The results showed good agreement with the experiments and showed the influence of support on blade trembling and on the power co-efficient[54]. Good results were achieved for the comparison of CFD simulations and experiments for speculating far wake in case of a horizontal axis tidal turbines[55]. Numerical study was conducted for a floating point absorber, a wave energy conversion device using RANS (Reynolds Averaged Navier Stokes) based on Computational Fluid Dynamics (CFD)[56]. In order to predict the performance of a two body wave energy convertor a time domain model which was supposed to be very efficient in terms of speed has been developed[57].

1.3.Applications of interaction analysis

The fluid– rigid body interaction analysis is basically performed to predict and mitigate the following interaction phenomenon

1. Flutter
2. Galloping
3. Sloshing
4. Vortex Induced Vibrations (V.I.V)

The above mentioned interaction application for fluid-structure finds wide demand in the field of aerospace technologies (wing flutter, flow over turbine blades), biomedicine

(elastic artery modelling for stent design), automotive technologies (design of heat exchangers) and marine engineering (safe and functional marine structures).

1.4. Further research on the topic

The main part of the present work specifically focuses solely on rigid body-fluid (air) interaction, it does not consider flow reattachment or flow-separation phenomenon and offers an alternative approach to study the interaction phenomenon and its advantages. The main basic idea of the approach/methodology in the current work is to have a simplified approach for interaction phenomenon through a straightforward mathematical model and is not considering the viscous nature of fluid medium or air. Therefore it is an approximate theory for non-stationary body-fluid interactions that considers inputs (post processing results) from stationary rigid body-fluid interaction model performed in ANSYS Fluent software where the steady state RANS equation is solved with the help of k-ε realizable turbulence model.

The concept discussed in the work will offer an alternative approach for "space-time" programming techniques and also will help to solve engineering tasks of optimization and synthesis for simple form objects without requiring huge computational efforts.

The novelty of interaction analysis approach is that the main part of the current research work for fluid–rigid body interaction phenomenon is discussed in detail in the subsequent sections. It is believed that the approach discussed helps to solve simple engineering tasks without requiring time consuming programming techniques.

2. NEW APPROACH FOR FLUID (AIR)-RIGID BODY INTERACTION

In this chapter, three different cases for the fluid-rigid body interaction are presented. The fluid is considered continous and flow is assumed to be ideal and laminar.The three cases include:

(a) moving body (prism) in still fluid (air);

(b) stationary body (prism) in airflow;

(c) moving body (prism) in airflow.

The complicated task of rigid body (prism) and air interaction is simplified by using a new theoretical approach (superposition principles) by taking into account the upstream and downstream rigid body (prism) and air interaction phenomenon which was found to be different under varying speeds. The mathematical model in the present work is applicable only for bodies that undergo rectilinear translation motion Fig.2.1-2.2. The body-fluid interaction for a moving body in still fluid and moving body in air flow are explained by considering a body of arbitrary shape.

2.1.Object interaction with still fluid

The space around rigid body-fluid interaction is investigated in detail and mathematical model is proposed by taking into consideration the very small fluid element (in air) in the pressure zone and according to the theorem on change in linear momentum [58] and [59] in differential form by a superposition principle is proposed in the present work, by taking into account the projection of the area normal N_1 before and after collisions (fluid - body interaction), we obtain (1) from Brownian interaction for the prism in air (Fig.2.1-2.2):

$$\begin{aligned} m_{10} \cdot VB_1 - (-m_{10} \cdot VB_1) &= -N_1 \cdot dt, \\ m_{10} &= VB_1 \cdot dt \cdot dL_1 \cdot B \cdot \rho, \\ p_{10} &= \frac{|N_1|}{dL_1 \cdot B}, \end{aligned} \tag{1}$$

where

m_{10} – Brownian interaction mass;

VB_1 – an average air normal velocity in pressure zone;

N_1 – normal force on air in a small element;

dt – infinitely small time interval;

dL_1 – width of a small element;

B – prism height in the direction perpendicular to the plane of motion;

ρ – density;

p_{10} – atmospheric pressure at pressure zone.

Due to prism-air interaction at the windward side (pressure side) (2):

$$\begin{gathered} m_1 \cdot v \cdot \cos(\beta_1) - 0 = \Delta N_1 \cdot dt, \\ m_1 = v \cdot \cos(\beta_1) \cdot dt \cdot dL_1 \cdot B \cdot \rho, \\ \Delta p_1 = \frac{|\Delta N_1|}{dL_1 \cdot B}, \end{gathered} \tag{2}$$

where m_1 – mass due to air interactions in boundary layer;
v – prism velocity;
β_1 – angle between velocity v and normal N_1;
ΔN_1 – change in normal force acting on prism;
Δp_1 – pressure increase at windward side.

From (1), (2) it is possible to find the unknowns. The two unknowns could be solved by using the following (3) and (4):

$$p_{10} = 2 \cdot {VB_1}^2 \cdot \rho \cdot dt, \tag{3}$$

$$\Delta p_1 =\cdot v^2 \cdot \rho \cdot dt \cdot (\cos(\beta_1))^2, \tag{4}$$

For (1) – (4) for the leeward side (suction zone) of the interaction space, the task is complicated with the amount of momentum differentials in the suction zone. For that reason, two different hypotheses are proposed. Two hypotheses could be validated either experimentally or by using numerical computer programs.

First hypothesis

In suction zone reduction in pressure Δp_{21} over the surface is assumed constant and proportional to the square of the velocity v as presented in (5) and (6):

$$\Delta p_{21} = -\rho \cdot C_1 \cdot v^2, \tag{5}$$

$$p_{20} = 2 \cdot {VB_2}^2 \cdot \rho \cdot dt; \tag{6}$$

where, C_1 – constant, found by experiments or numerical modeling;
VB_2 – average air normal velocity (suction zone).

Second hypothesis

In suction zone reduction in pressure Δp_{22}, over the surface is assumed to be varying and is proportional to the square of the velocity v, and also depends on the normal N_2 to the surface area, and also the angle β_2, thereby (7), (8):

$$\Delta p_{22} = -v^2 \cdot \rho \cdot C_2 \cdot \cos(\beta_2), \tag{7}$$

$$p_{20} = 2 \cdot {VB_2}^2 \cdot \rho \cdot dt; \tag{8}$$

where C_2 is a constant, found in the same way as C_1.

The obtained differential relations (3)-(8) can be used in engineering analysis tasks only at low speeds and for body or objects that undergo rectilineear translation motion. For all practical engineering calculations, it is recommended to adopt $VB_1 = VB_2$ at low speeds,

and limited by $v << VB_1$ and $v << VB_2$, then $p_{01} = p_{02} = p_0$, where p_0 is the mean atmospheric pressure around the prism.

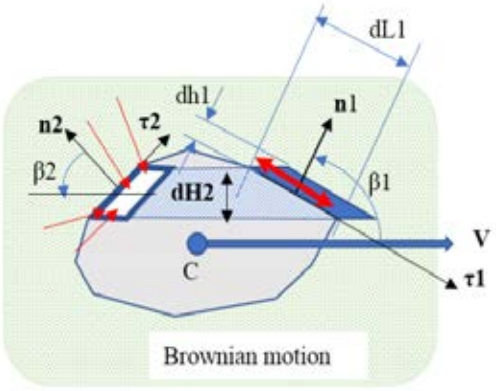

Fig. 2. 1. Rectilinear translation motion body interaction in still air.

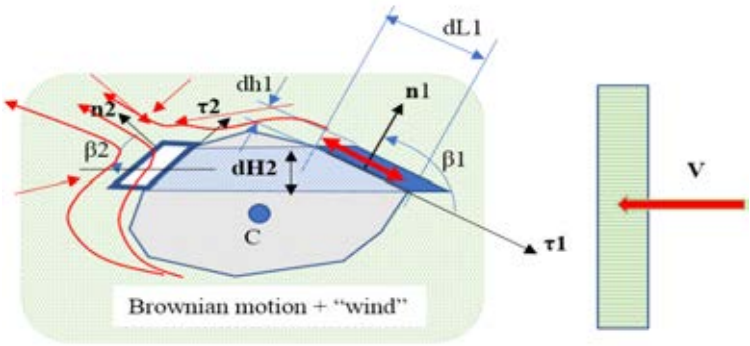

Fig. 2. 2 Model of stationary prism with fluid (air) interactions.

2.2. Stationary rigid-body (flat plate) in air at low speeds

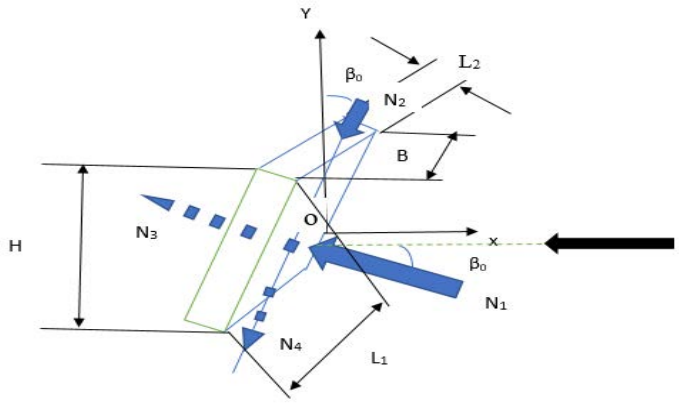

Fig. 2. 3 Stationary rectangle flat plate in a fluid flow.

where, L_1, B – length and width of flat plate sides;

L_2 – thickness of the plate;

A_1, A_2 – area;

N_1, N_2 –forces at the centre of additional pressure in the pressure sides;

N_3, N_4 –forces at the centre of plate vacuum (thin) side;

V – flow velocity from right to left.

Interaction phenomenon for fluid–rigid body (simple flat plate geometry) to obtain the mathematical correlation according to the theorem of change in linear momentum is explained in Fig.2.3. for the pressure side of the flow the differential form given by (9), (10)

$$dm \cdot v \cdot \cos(\beta_{fp}) = dN \cdot dt, \tag{9}$$

$$dm = v \cdot \cos(\beta_{fp}) \cdot dL \cdot dt \cdot B \cdot \rho, \tag{10}$$

where dm – mass of the element volume in flow stream velocity v;

β_{fp} – the angle between the flow and the surface (flat plate);

dN – the impact force in the direction of the normal surface of the elemental area;

t – time;

dL – the elemental length of the surface;

B – width of the object, constant for a two-dimensional body;

ρ – density of air.

Integrating (9), (10) forces N_1, N_2 perpendicular to sides are obtained, given by (11), (12).

$$N_1 = A_1 \cdot v^2 \cdot \rho \cdot \left(\cos(\beta_{fp})\right)^2, \tag{1 1}$$

$$N_2 = A_2 \cdot v^2 \cdot \rho \cdot (\sin(\beta_{fp}))^2, \tag{12}$$

where

A_1, A_2 – area of sides on the pressure and suction sides respectively.

At the suction - vacuum side in the downstream along the edge of the body it is realized that there exists constant pressure as shown in Fig.3.8 which is proportional to the density ρ multiplied by the flow velocity squared as represented in the (13), (14):

$$N_3 = A_1 \cdot v^2 \cdot \rho \cdot C, \tag{13}$$

$$N_4 = A_2 \cdot v^2 \cdot \rho \cdot C, \tag{14}$$

where C– constant (interaction coefficient) is dependent on form (shape) and speed of the incoming flow. The value of C or interaction coefficient can be determined experimentally or by numerical simulations. For subsonic cases the value of C ranges between 0 and 1 [$(0<C<1)$].

For the centre of the plate *O*, there are two components arising from interaction forces given by (15), (16) respectively:

$$f_x = -H \cdot B \cdot \rho \cdot v^2 \cdot \left(C + \frac{(cos(\beta_{fp})^3 + d \cdot sin(\beta_{fp})^3)}{\cos(\beta_{fp}) + d \cdot \sin(\beta_{fp})}\right) \quad (15)$$

$$f_y = L_1 \cdot B \cdot \rho \cdot v^2 \cdot \left(C \cdot (\sin\left(\beta_{fp}\right) - d \cdot \cos(\beta_{fp})\right) + \sin(\beta_{fp}) \cdot \left((\cos\left(\beta_{fp}\right)\right)^2 + d \cdot (\cos(\beta_{fp}))^3) \quad (16)$$

As shown in Fig. 2.3, $H = L_1 \cdot \left(\cos\left(\beta_{fp}\right) + d \cdot \sin\left(\beta_{fp}\right)\right)$, $d = \frac{L_2}{L_1}$ (17)

where d – the ratio of edges L_2/L_1,

f_x –horizontal force component, otherwise called as a drag force;

f_y –vertical force component, otherwise called as a lifting force;

H – section height perpendicular to flow.

Equation (15), (16) can be used to obtain the coefficient of interaction C as discussed in the subsequent section below. Fig. 2.4 shows the mathematical model for the concept of zones.

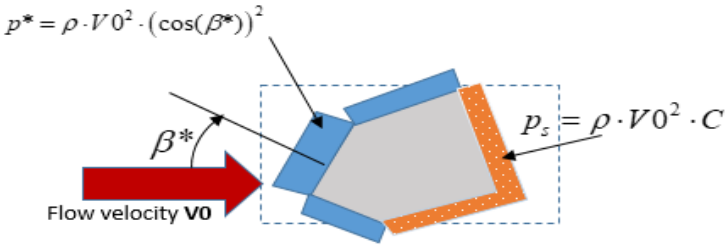

Fig. 2. 4. Concept of zones (pressure and suction zones) for a body immersed in fluid (air), a mathematical model.

2.3. Moving object in a running fluid

Interaction of a non-stationary prism in a running stream (air) is shown in Fig. 2.5

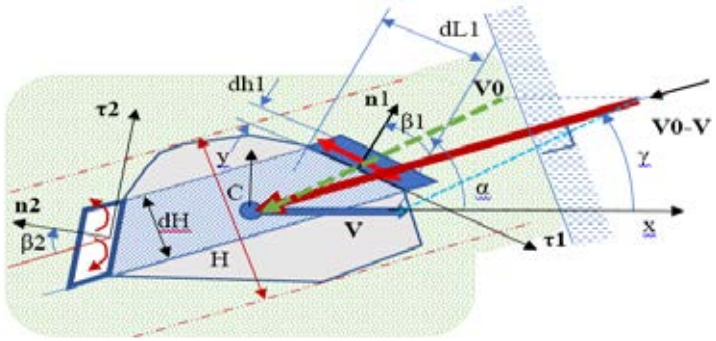

Fig. 2. 5 Model of non-stationary prism in airflow.

The relative velocity Vr vector in the windward or pressure zone must be recalculated by determining the angle γ from the elementary parallelograms with normal N_1 and N_2 as shown in Fig.2.5. By plotting the vectors V and V_0 on the horizontal (x) and vertical (y) axes, we obtain (18), (19):

$$V_r = \sqrt{(-V_0 \cdot \cos(\alpha) - V)^2 + (-V_0 \cdot \sin(\alpha))^2} \tag{18}$$

$$\cos(\gamma) = \frac{-V_0 \cdot \cos(\alpha) - V}{\sqrt{(-V_0 \cdot \cos(\alpha) - V)^2 + (-V_0 \cdot \sin(\alpha))^2}} \tag{19}$$

where Vr – relative velocity,
V_0 – vector of wind velocity,
V – rectilinear translation motion velocity of a prism,
α - velocity flow angle.

In the further sections of the work we illustrate the possibility to optimize the form of the prism or 3D object in order to obtain the desired effect or criterion along with the task of motion control and also real system synthesis based solely on the fluid-structure interaction.

2.4 Conclusions

1. In this work a new method is developed for estimating approximate flow and rigid body interaction for three different tasks.
2. An alternate approach for solid body-fluid (air) interaction phenomenon by splitting the interaction space in the fluid into zones (pressure and suctions zones) was found to be successful technique in analysing the rigid body-fluid interaction phenomenon.
3. The results of the work are only valid when the body undergoes rectilinear translation motion.The theory explained in this section is purely mathematical in approach and could be easily extended for fluid–structure interaction analysis of complex form bodies.

3. APPROXIMATION FOR INTERACTION PHENOMENON

In the Chapter 2 the fluid-rigid body interaction is studied and analysed for three different cases. In the present section the interaction phenomenon is examined for typical simple forms through computer programms and application of the interaction case is in detail discussed to explain the diving and flying movements of objects in fluid.

ANSYS Fluent was used to perform numerical simulations. The RANS (Reynolds Averaged Navier Stokes) equation is solved by using k-ε realizable turbulence model. A similar domain, the same depth with similar mesh was used for interaction analysis of all the objects. The residuals converged to 10^{-4} in all cases. All the simulations were performed for a constant air speed of 10 m/s keeping in view the prevailing wind and weather conditions in Riga, Latvia. The length and depth of all the forms are taken to be 0.16 m.

From the results of numerical simulations it is now realized that the region around the fluid–stationary body interaction space can be split into two zones, it means that the theory proposed in the earlier section is valid. In the upstream side there exists a pressure zone and in the downstream side just behind the body there is a suction or a vacuum zone (leeward side), as explained in Figs. 3.3-3.5. In the Fig. 3.1 , the prism forms are named as per the angle formed along the centre line drawn perpendicularly to the flow direction as shown in the Fig. 3.2. It can be seen that from Figs. 3.3-3.5, irrespectively of the geometry of the object the interaction space can be conveniently divided into zones, and the concept of zones is valid for low speeds within subsonic regime and for all orientations of the body to the fluid flow.

The value of interaction constant C from (15) and (16) is to be calculated by using numerical techniques or experiments. The value of *C* (coefficient of interaction) varies for different forms.

3. 1. Approximated theory

The approximated theory discussed in the present work is as follows:

1. The space around the fluid-stationary body interaction is split into zones (pressure zone and suction zone) which is realised through computer numerical simulation ANSYS Fluent for all types of objects (2D and 3D).
2. At the suction side or leeward side there exists a constant static pressure which can be conveniently written by mathematical expression for interaction coefficient in determining interaction force along the fluid flow. This interaction force ortherwise called drag is obtained by considering the change of momentum in differential form (superposition principle).
3. Through Newtonian laws of mechanics (involving vectors of velocity in different directions) for the body motion in fluid the differential equation could be easily integrated and results obtained, in this case labour intensive space-time programming techniques are not required.

4. The importace and significance of interaction coefficient can be well understood for synthesis of new systems and in energy scavenging from fluid–structure interaction phenomenon which will be disccussed in detail in Chapters 4 and 5 of the present work.

3.2. 3D Diamond prism

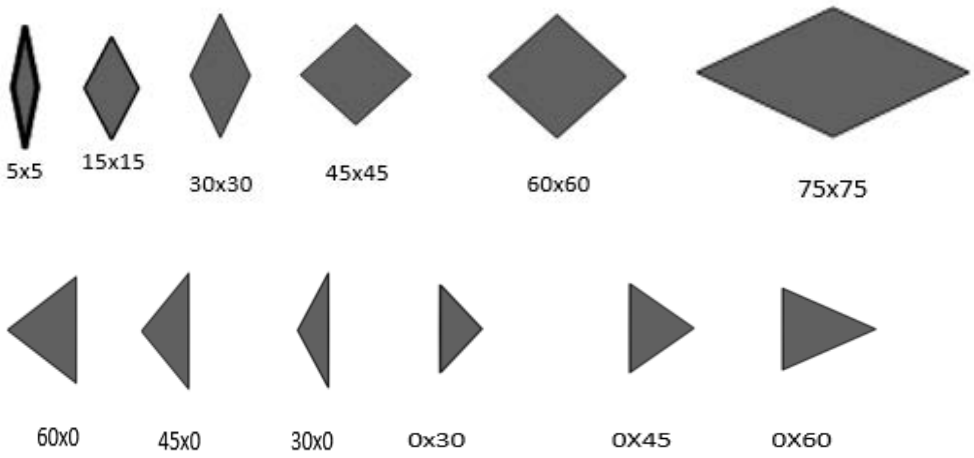

Fig.3.1. All prism shapes.

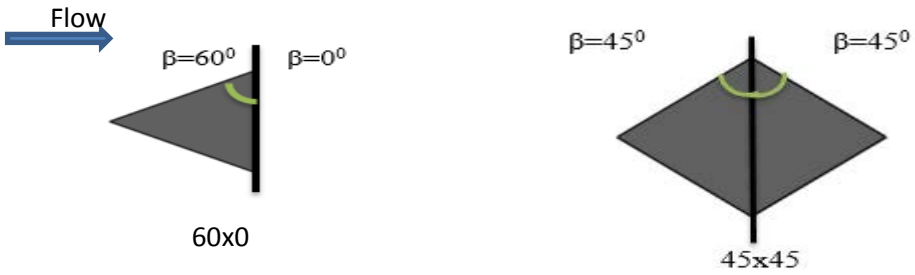

Fig.3.2 Nomenclature of the prism forms.

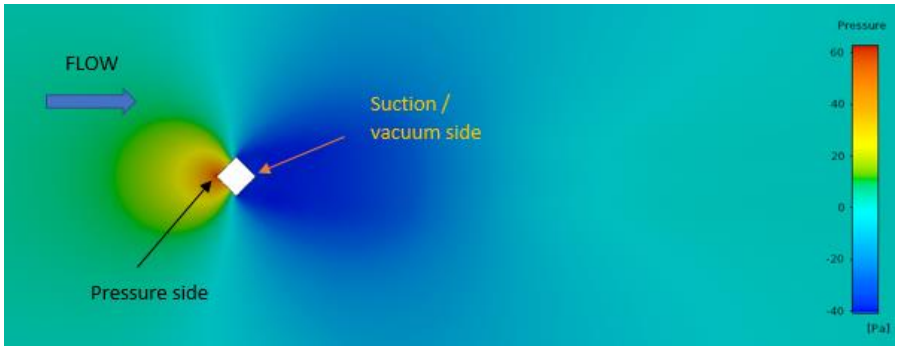

Fig.3.3 Concept of zones for a diamond (45x45) prism at constant speed of 10 m/s.

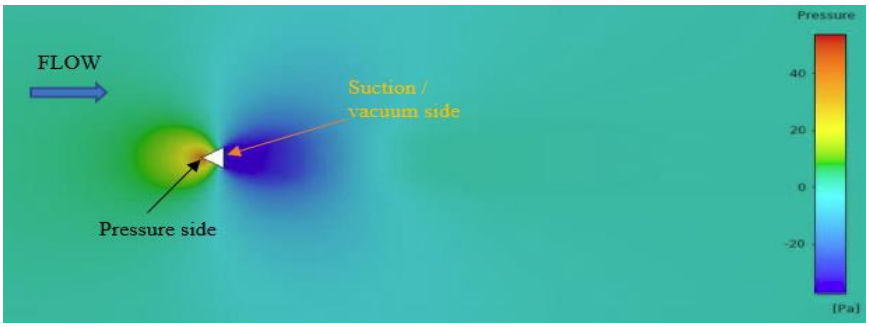

Fig.3.4 Concept of zones for equilateral triangle (60x0) prism at constant speed of 10 m/s.

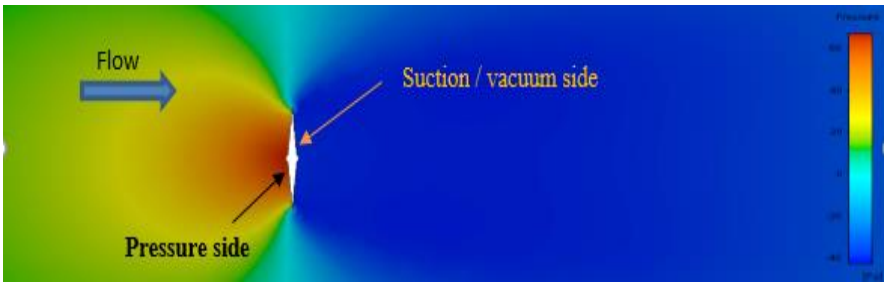

Fig.3.5 Concept of zones for a diamond (5x5) prism at constant speed of 10 m/s.

A mathematical model similar to the flat plate with the same technique is extended for a diamond form. An approximation for the diamond shaped rigid body f_{xd} along the direction of flow is given by (20).

$$f_{xd} = -H \cdot B \cdot v^2 \cdot \rho \cdot [C + \cos(\beta_d)^2] \tag{20}$$

Where

B – body width,

H – height perpendicular to the flow,

β_d – the angle between the flow and the surface at the normal point of impact,

ρ – fluid density.

Accordingly , the interaction coefficient C is to be estimated by using (21), (22) and (23): D - theoretical interaction force along the flow (21), D_{ex} – calculated interaction force along the flow (22), and approximated D_p– interaction force as the fifth degree polynomial function (23):

$$D = C + \cos(\beta_d)^2; \tag{21}$$

$$D_{ex} = \frac{f_{xde}}{A \cdot v^2 \cdot \rho} \tag{22}$$

$$D_p(\beta_d) = 1.5 + 3.7266 \cdot {\beta_d}^3 - 1.5249 \cdot {\beta_d}^4 - 0.10135 \cdot {\beta_d}^5 - 2.8129 \cdot {\beta_d}^2 + 0.2823 \cdot \beta_d \tag{23}$$

Where

f_{xde} – interaction force for diamond plate along the flow direction.

From equations (21) and (23) it follows that C = 0.5 when $\beta_d = 0$. Interaction coefficient in case of diamond shaped body is approximated by (24):

$$D = 0.5 + (\cos(\beta_d))^2 \tag{24}$$

The estimation of the accuracy of the approximate formula (24) for a diamond-shaped object at C = 0.5 is explained in Fig.3.6. The percentage of average difference is estimated to be less than 5%.

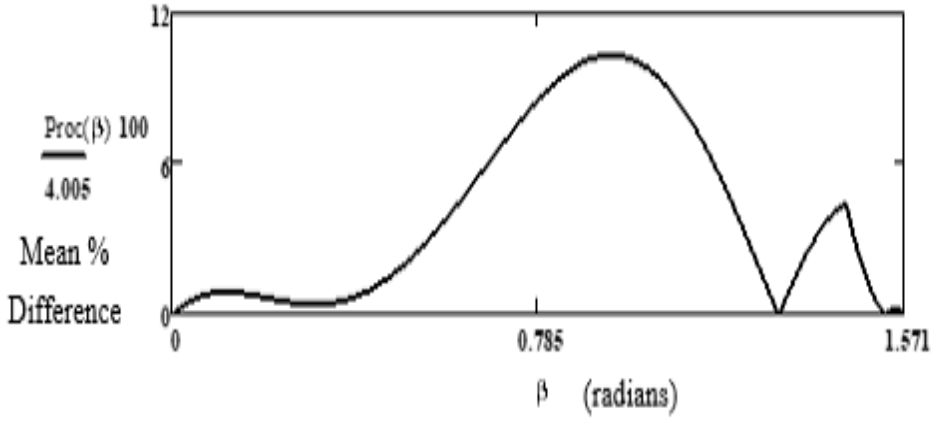

Fig.3.6 β (radians) against percentage difference for approximate formulation (24) when C = 0.5 is expressed in percentage for a diamond form. The mean value is 4%.

3.3. 3D Star prism and flat plate

3.3.1 Steady and unsteady flow for a 3D star prism

A typical form object is considered (star prism) to prove that there exists contant pressure at the downstream leeward side (suction zone). Interaction analysis is provided for a star prism where the steady and unsteady RANS (Reynolds Averaged Navier Stokes Equation) is solved at a air speed of 10m/s. The presence of zones is shown in the Fig.3.7. The static pressure plot confirms the occurence of pressure and suction side for the interaction phenomenon in steady and unsteady environment Fig.3.8. The suction or vacuum zone is realized from the static pressure plot for the star prism and in the suction zone the pressure is almost constant along the length and only varies with the speed, nature of the flow (steady or unsteady) and is form dependent at the edges as shown in Fig.3.8.

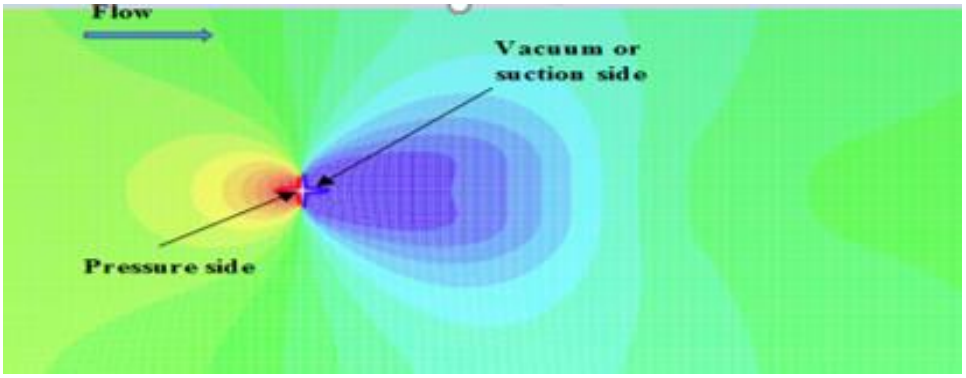

Fig.3.7.Static pressure over stationary star prism at constant speed of 10m/s.

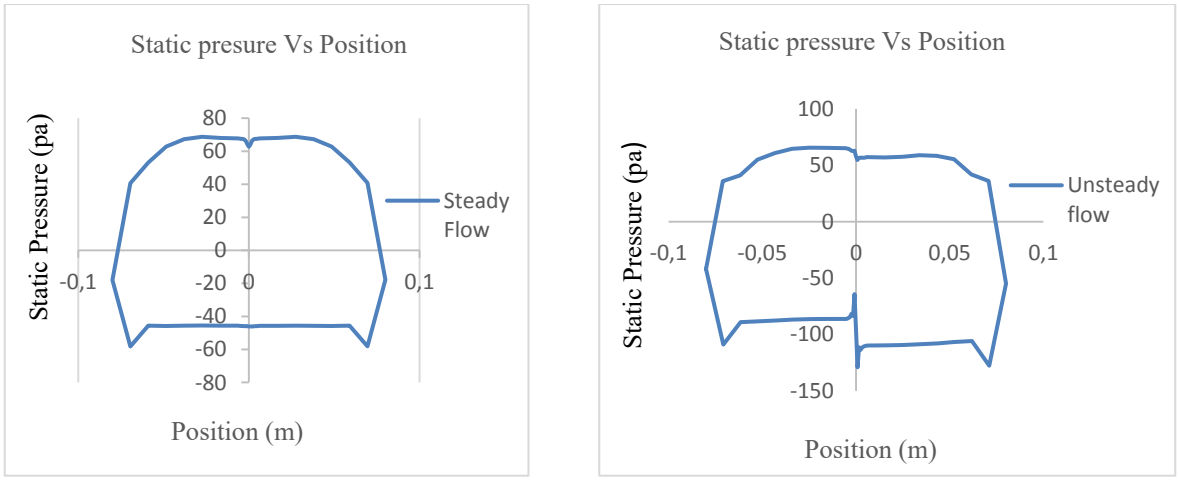

(a) (b)

Fig.3. 8.Static pressure plot for stationary star prism for: (a) steady flow, (b) nsteady flow at constant speed of 10m/s.

3.3.2. Interaction coefficient for high speeds (3D star prism)

In this section the interaction coefficient is analyzed at high speeds for the 3D star prism. It is noted that at supersonic speeds, Mach 1.8, the suction zone at the boundary layer imediately adjacent to the body exists, but due to the change in density effects (compressibility) the value of *C* (interaction coefficient) is difficult to determine. Fig.3.9, Fig. 3.10 shows the pressure contour with shock stand-off at Mach 1.8 for star prism.

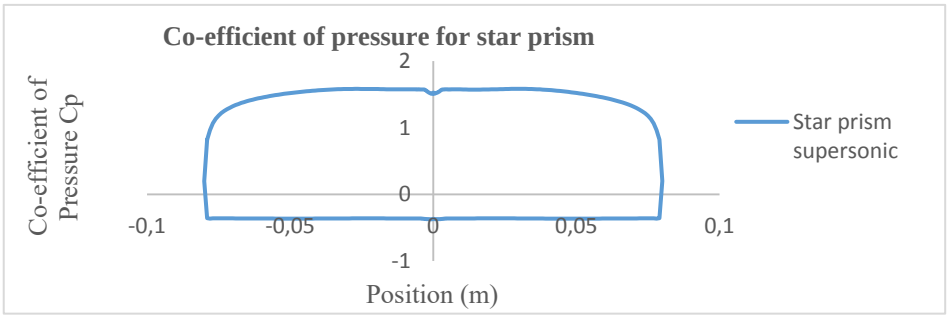

Fig.3. 9.Coefficient of pressure for stationary star prism at Mach 1.8.

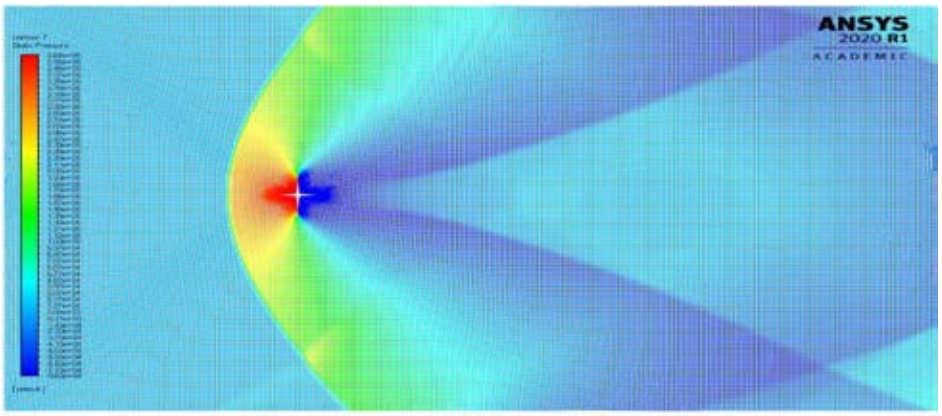

Fig.3.10. Static pressure for stationary star prism at Mach 1.8.

At much higher speeds at Mach 4.8 at the suction zone (or vacuum side) immediately adjacent to the body at the leeward side due to high static the pressure increases across the shock wave and interaction of the shock with the body as shown in Fig. 3.11, the value of *C* (interaction coefficient) is taken to be zero. In Fig.3.12 the contour of the static pressure at Mach 4.8 shows that the shock interacts with prism geometry, due to that complicated phenomenon arises that brings significant change in the pressure distribution (Fig. 3.11).

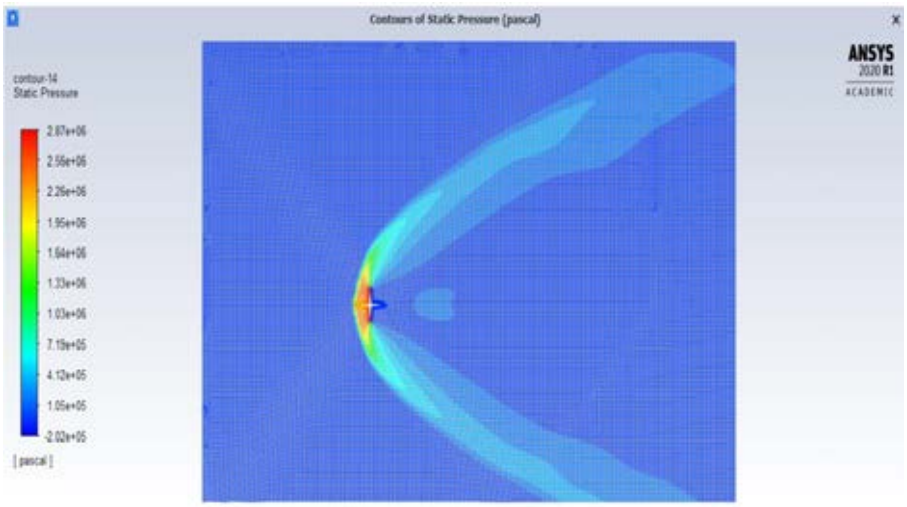

Fig.3. 11. Static pressure contour for stationary star prism at Mach 4.8.

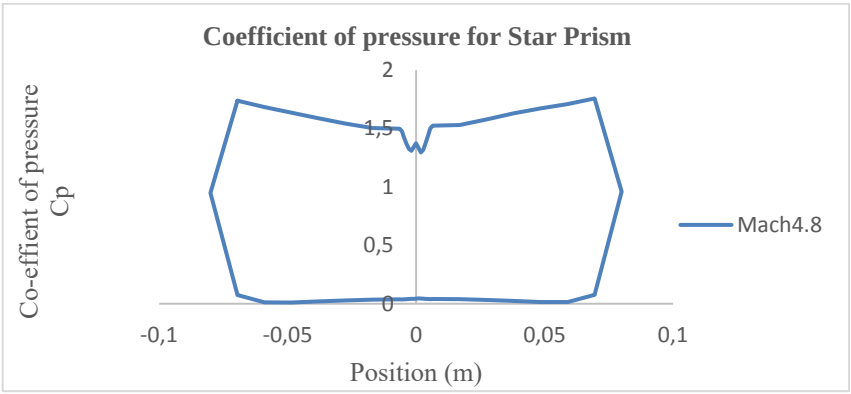

Fig.3.12.Coefficient of pressure for stationary star prism at Mach 4.8.

3.3.3 Interaction coefficient for 2D and 3D flat plate

Flat square plate of 0.16 m x 0.16 m is considered and computer numerical computations were performed supported by experiments. The main idea in selecting the flat plate was that it is the simplest of all forms. Interaction analysis for flat plate (square flat plate) in 3D is shown in Fig 3.13. The streamlines show the formations of recirculating streamliness at the downstream of the plate.

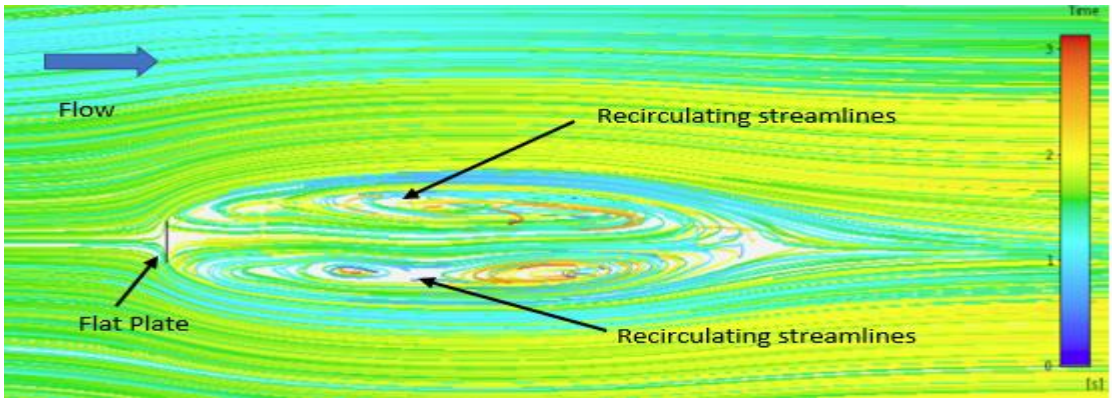

Fig.3.13. Streamline for the flat plate, formation of recirculating streamliness downstream of the plate.

Initially, for the coefficient C, 2D numerical simulations for flat plate are investigated. By varying β_{2d}, there exists different interaction phenomenon and mostly encountered fluctuating forces due to the variations in pressure across the body subjected to fluid flow, the mean values of interactions are analyzed and interaction $D_1(\beta_{2d})$ is found out by (25):

$$D_1(\beta_{2d}) = -0.1013532598492 \cdot (\beta_{2d})^5 - 1.5249241156366900458 \cdot (\beta_{2d})^4 + 3.7266204256 \cdot (\beta_{2d})^3 - 2.81293523749905363 \cdot (\beta_{2d})^2 + 0.2823061 \cdot (\beta_{2d}) + 1.5. \quad (25)$$

For ($\beta = 0$), coefficient in (15) is $C = 0.5$, is obtained from (25) and formula (15) can be rewritten in form (26), (27):

$$f_x = -H \cdot B \cdot v^2 \cdot \rho \cdot [D_2(\beta_{2d})] \quad (26)$$

$$D_2(\beta_{2d}) = \left[0.5 + \frac{\cos(\beta_{2d})^3 + d \cdot sin(\beta_{2d})^3}{\cos(\beta_{2d}) + d \cdot sin(\beta_{2d})}\right] \quad (27)$$

From (25), (26) drag force coefficients Df_1 (β_{2d}) and $Df_2(\beta_{2d})$ will be (28) (29):

$$Df_1(\beta_{2d}) = D_1(\beta_{2d}).(\cos(\beta_{2d}) + d \cdot \sin(\beta_{2d})), \quad (28)$$

$$Df_2(\beta_{2d}) = 0.5 \cdot (\cos(\beta_{2d}) + d \cdot \sin(\beta_{2d})) + (\cos(\beta_{2d}))^3 + d \cdot (\sin(\beta_{2d}))^3 \quad (29)$$

Precision of approximation (15) with $C = 0.5$ is shown in Fig.3.14,
where,

$$percent_{12}(\beta_{2d}) = \frac{|Df_2(\beta_{2d})| - |Df_1(\beta_{2d})|}{Df_1(\beta_{2d})}.100$$

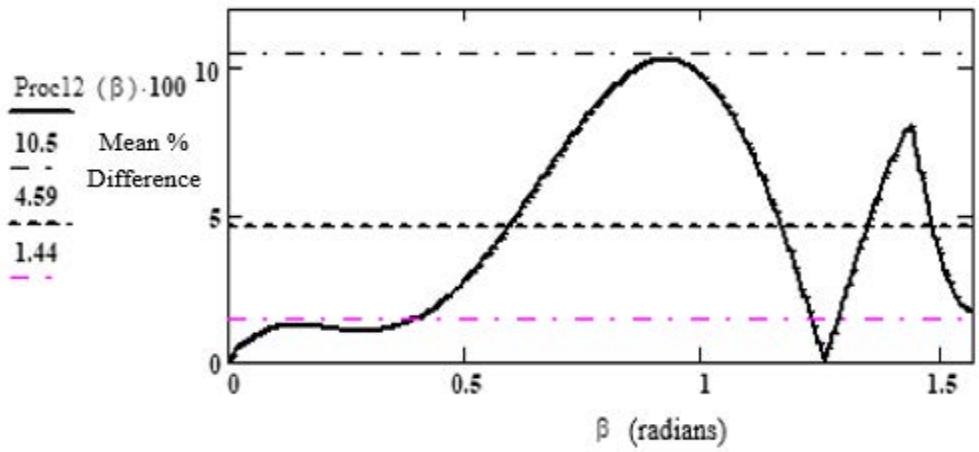

Fig.3.14. Accuracy of square flat plate model (in percentage error) against β (in radians): 10.5 % of maximal error; 4.59% middle value error; 1.44 % middle value error in region $\beta = 0 - \pi/4$.

For a 3D square flat plate (15) is rewritten as follows.

$$f_x = \frac{A \cdot v^2 \cdot \rho}{2}.\left(C + \frac{\cos(\beta_{3d})^3 + d \cdot sin(\beta_{3d})^3}{\cos(\beta_{3d}) + d \cdot sin(\beta_{3d})}\right) \tag{30}$$

where A – wetted area of the body. From the computation results for a drag force (interaction force) at different angles of β_{3d} (shown in Fig.3.15), when approximated to a 5th degree polynomial curve, the equation obtained is

$$D_3(\beta_{3d}) = -8.10^{-12} \cdot {\beta_{3d}}^5 + 2.10^{-8}{\beta_{3d}}^4 + 2.10^{-7}{\beta_{3d}}^3 - 0.0004 \cdot {\beta_{3d}}^2 - 0.0013 \cdot \beta_{3d} + 2.0463 \tag{31}$$

Similarly, for drag force experiments at 10m/s, the results are approximated in the form of a 5th degree polynomial described in equation (32) and shown in Fig.3.15;

$$D_{e3}(\beta_{e3d}) = 10^{-11} \cdot {\beta_{e3d}}^5 + 2.10^{-8} \cdot \beta_{e3d} + 10^{-7} \cdot \beta_{e3d} - 0.004 \cdot {\beta_{e3d}}^2 - 0.0016 \cdot \beta_{e3d} + 2.1796 \tag{32}$$

From (30) estimation of the drag force for the given geometry, the value of constant (interaction co-efficient) $C = 0.31$ is obtained for $\beta_{e3d} = 0^0$. Thereby the interaction force along the flow direction is taken as 1.31. It was observed that the maximum error measured at $\beta = 0^o$ ($\beta_{e3d} = 0^0$ & $\beta_{3d} = 0^0$) from computations and experiments was about

~6 % as analysed from Fig.3.15. From the Fig. 3.15, it could be seen that maximum drag is always achieved when the body is placed normally to the flow.

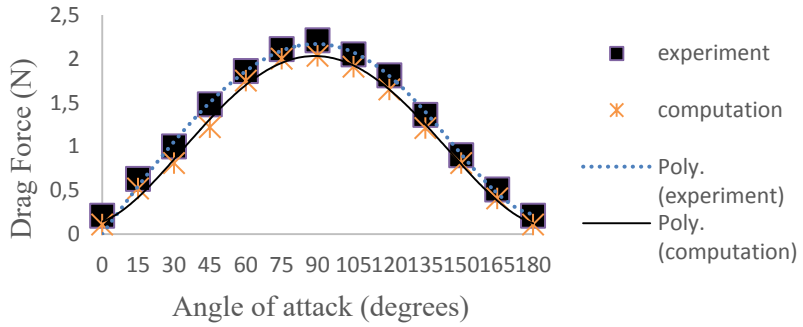

Fig.3. 15.Experimental and numerical results for stationary flat plate at constant speed of 10m/s approximated as a 5th degree polynomial curve.

3.4. 3D Perforated plate

Another simple form object is a perforated flat plate shown in Fig. 3.16. The total area of the perforations was maintained at half the area of the square flat plate. A comparison was done with simple flat plate (square plate) of the same size, and it was found that the simple square flat plate had recirculating streamliness formation downstream, and those recirculating streamliness are swept away for the perforated plate at a speed of 10m/s, Fig.3.19. The drag was also reduced for the perforated plate as compared to the simple flat plate.

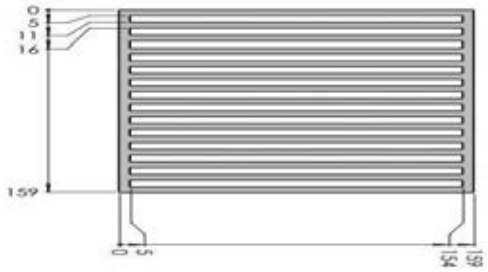

Fig.3.16. Geometry of perforated plate, all dimensions are in mm.

Interaction force (If_x) for perforated plate is given by (33) that includes all elemental (perforated) area , β_p for different angles of perforated plate,

$$If_x = -k \cdot B \cdot H_1 \cdot v^2 \cdot \rho \cdot \left[C + \frac{cos(\beta_p)^3 + d \cdot sin(\beta_p)^3}{cos(\beta_p) + d \cdot sin(\beta_p)} \right], \tag{33}$$

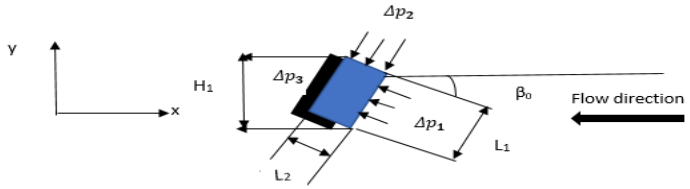

Fig.3. 17 Pressure distribution for a perforated prism element cross section.

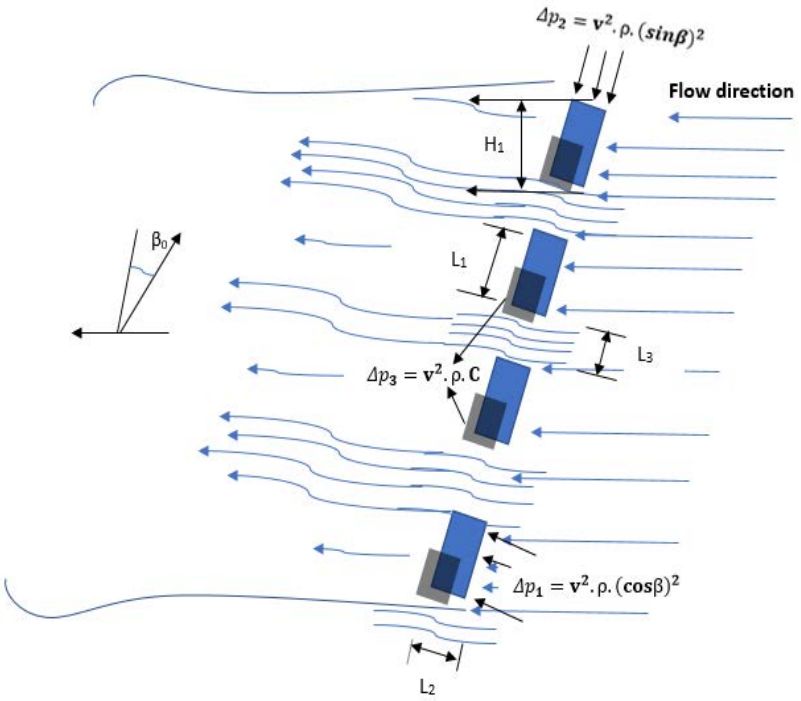

Fig.3. 18.Presure distribution across the cross section of a perforated plate.

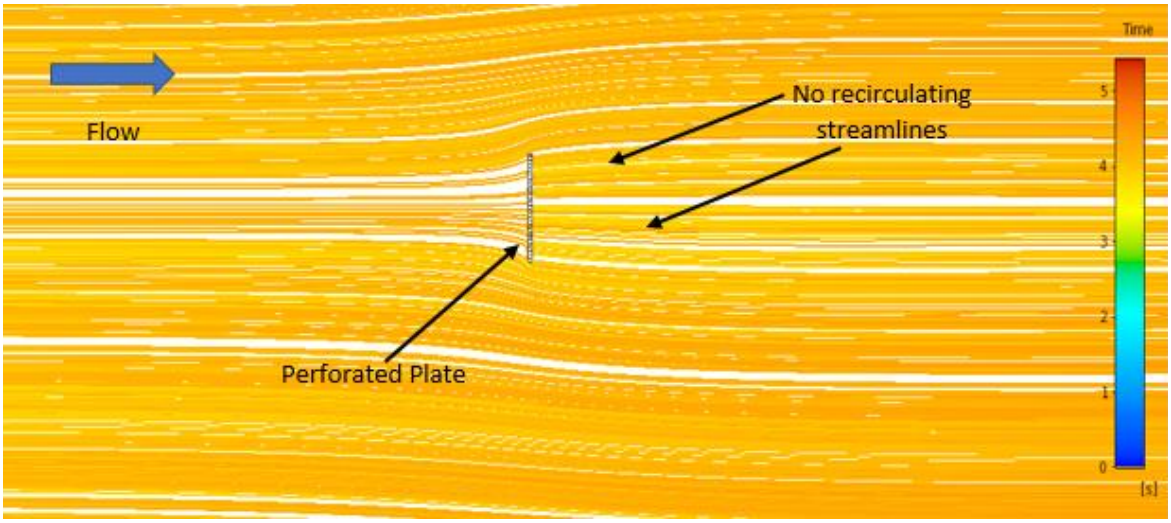

Fig.3.19.Streamline for the perforated flat plate, no recirculating streamliness downstream of the plate.

The pressure due to normal forces for the elementary area of the perforated plate is given by:

$$\Delta p_1 = \frac{dN_1}{dL_1 \cdot B}; \tag{34}$$

$$\Delta p_2 = \frac{dN_2}{dL_2 \cdot B}, \tag{35}$$

where $\Delta p_1, \Delta p_2$ –change in presure on sides for the length L_1 and L_2, Fig.3.17 and pressure distribution for rectangular cross section perforated plate is shown in Fig.3.18.

L_3 – gap of rectangle perforation of prism.

3.5 Flow and object interaction (convex and concave form)

The surfaces formed by fractured planes in the form of convex or concave geometric configurations are investigated and discussed in this section. The main task is to get a solution for flow and object interaction through approximate analytical relationships.

3.5.1 Convex broken side prism model

The four cornered convex broken side prism is shown in Fig.3.20. At the windward sides (p_1, p_2, p_3) the theorem of change in linear momentum in the differential form is applied (36).

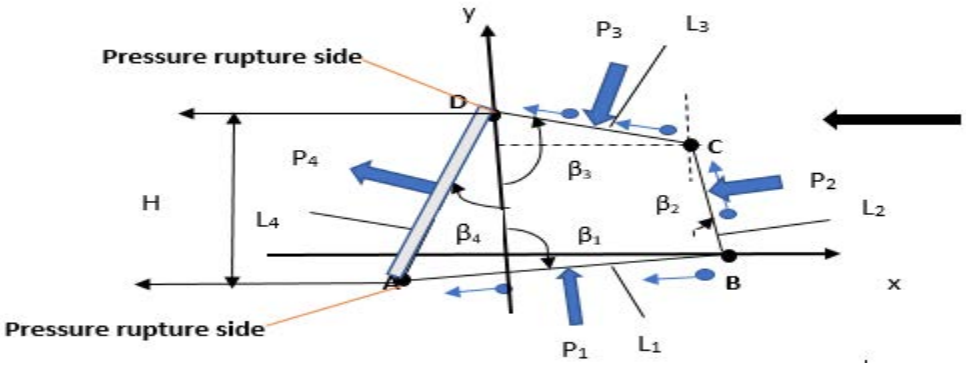

Fig. 3. 20. Interaction model for a convex prism in air.

L_1, L_2 – length of sides, β_1, β_2– frontal angles, H – height of a prism, - symbol of flow direction on the body surface as result of air–body interaction.

$$\boldsymbol{p_1} = [\boldsymbol{V}.(\boldsymbol{\cos(\beta_1)})^{\boldsymbol{2}}.\boldsymbol{\rho}]; \boldsymbol{p_2} = [\boldsymbol{V}.(\boldsymbol{\cos(\beta_2)})^{\boldsymbol{2}}.\boldsymbol{\rho}];$$
$$\boldsymbol{p_3} = V^2 \cdot \rho \cdot \left[(\cos(\beta_3))^2 - C_{12} \cdot C_{23} \cdot (\cos(\beta_2)) \cdot \sin(\beta_3 - \beta_2)\right], \quad (36)$$

where β_1, β_2, β_3- angles relative to the flow (side orientation); C_{12}, C_{23} are constants that observe changes in the flow velocity and also at the break points.

When $C_{12} = C_{23} = 1$, it implies that velocity at the break point does not change and is the same in the fluid flow (~ V).

The pressure p_4 in the suction zone between the edges of the rapture can be determined as follows (37):

$$p_4 = C_4 \cdot V^2.\rho \quad (37)$$

where C_4 is a constant, for example $C_4 = 0.5$.

It should be noted that calculations formulas are applicable to a prism that has convex surfaces in the pressure zone and is limited by (38):

$$0 < \beta 4 < \pi \cdot 2^{-1}; \pi > \beta 4 + \beta 3 > 0; \beta 3 - \beta 2 > 0. \quad (38)$$

From (36) and (37) the following projections of the interaction forces on the horizontal (x) axis and vertical (y)-axes (parallel or perpendicular to the flow respectively) are given by (39), (40):

$$-f_X = V^2 \cdot B \cdot \rho \cdot \{L_1 \cdot [\cos(\beta_1)^3] + L_2 \cdot [\cos(\beta_2)^3] + L_3 \cdot [\cos(\beta_3)^3 - C_{12} \cdot C_{23} \cdot \cos(\beta_2) \cdot \cos(\beta_3) \cdot \sin(\beta_3 - \beta_2)] + L_4 \cdot C_4 \cdot \cos(\beta_4)\}; \quad (39)$$

$$-f_y = V^2 \cdot B \cdot \rho.\{L_1.[\cos(\beta_1)^2].\sin(\beta_1) + L_2.[\cos(\beta_2)]^2.\sin(\beta_2) + L_3.[\cos(\beta_3)^2.\sin(\beta_3) - C_{12} \cdot C_{23} \cdot \cos(\beta_2).\sin(\beta_3).\sin(\beta_3 - \beta_2)] + L_4.C_4.\sin(\beta_4)]\}; \quad (40)$$

Additional geometric links (41), (42) are to be considered or observed for analyzing or optimizing the forces (*Fx* - drag force along flow direction, *Fy*–lifting force perpendicular to flow direction)

$$L_4.\sin(\beta_4) + L_3.\sin(\beta_3) + L_2.\sin(\beta_2) - L_1.\sin(\beta_1) = 0; \quad (41)$$

$$L_4 \cdot \cos(\beta_4) - L_3.\cos(\beta_3) - L_2.\cos(\beta_2) - L_1.\cos(\beta_1) = 0 \quad (42)$$

3.5.2 Concave broken side prism model

When considereing the concave broken side prism, impact force N_3 on the edge of the inner breakage should be taken into account. The force N_3 is perpendicular to the edge of length L_3 as shown in the Fig.3.21. Changing the direction from edge L_2 to edge L_3 there arises an impact force N_3 given by (43):

$$N_3 = L_2 \cdot B \cdot \rho \cdot V^2 \cdot \cos(\beta_2) \cdot \sin(\beta_2 - \beta_3) \cdot [0.5 + 0.5 \cdot sin(\beta_2 - \beta_3)] \quad (43)$$

Here the criterion for taking concave case is when $\sin(\beta_2 - \beta_3) \geq 0$.

In case of absence of theoretical force N_3, flow is to be smooth over the entire surface with the length L_3, it is recommended that (39) and (40) are used to get good approximation. All the above shown relations help us to solve the task of optimization and synthesis for the interaction of various forms of star shaped prism models. The viscous nature of the fluid medium is ignored.

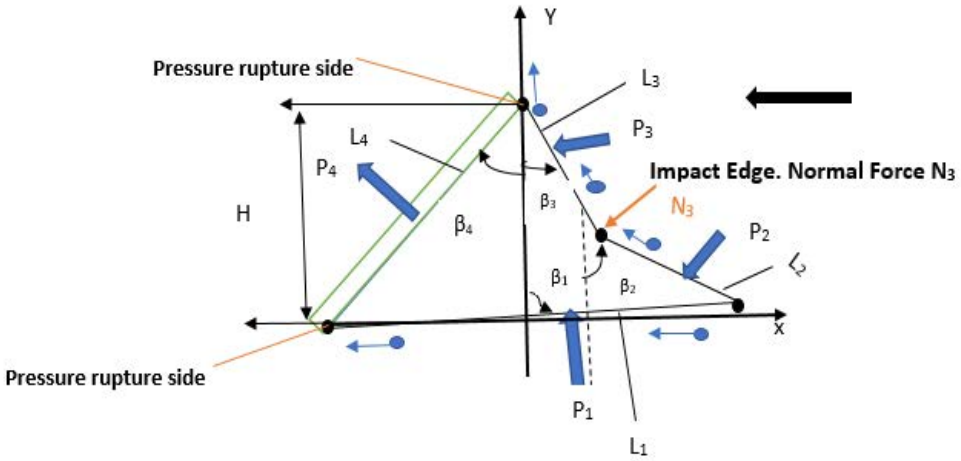

Fig.3. 21.Concave starlike prism in air (flow from right to left).

L_1, L_2, L_3, L_4 – length of sides, β_1, β_2, β_3, β_4 – frontal angles H – height.

3.5.3 3D simple forms interaction force

After analyzing the interaction case for simple forms, it is clear from the computer programming results that unless the object is perforated, there is a presence of recirculating streamlines as it can be seen for a star prism in Fig.3.22. A comparison of computation and theoretical interaction force (drag force) for diffferent prisms is shown in Fig.3.23.

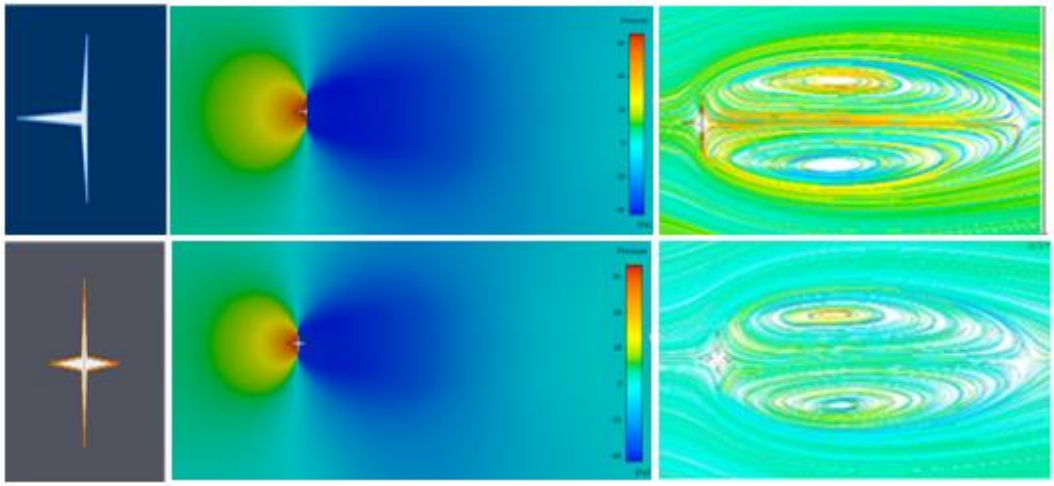

Fig.3.22. Shape, pressure contour, streamlines for different shapes.

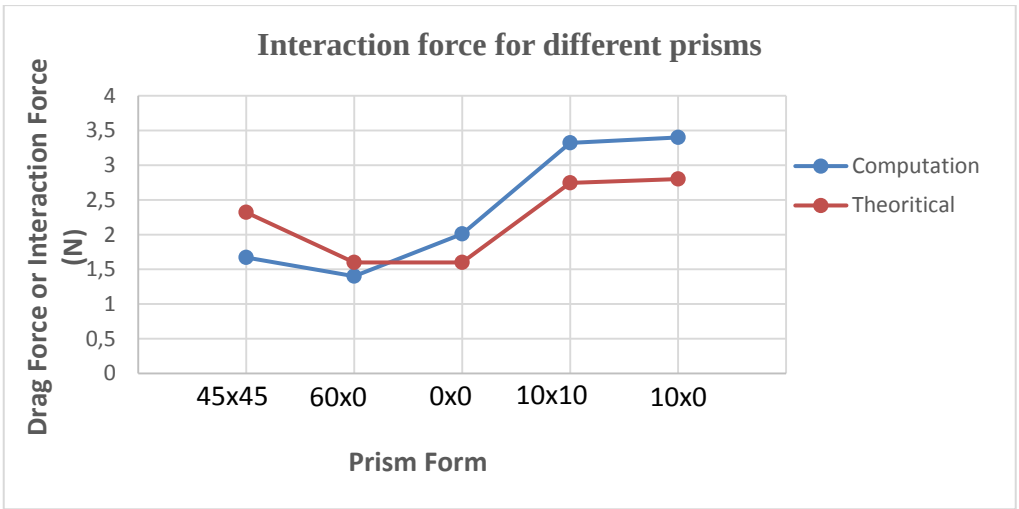

Fig.3.23. Comparison of interaction force for different prisms - numerical computation and theoretical approach.

3.6. Robotic fish tail with fluid interaction for a diving motion

Robotic fish diving motion through the fluid-rigid body interaction phenomenon is demonstracted in this section. The results show the importance of the application of co-efficient of interaction *C* in analyzing the movement of objects in fluid.

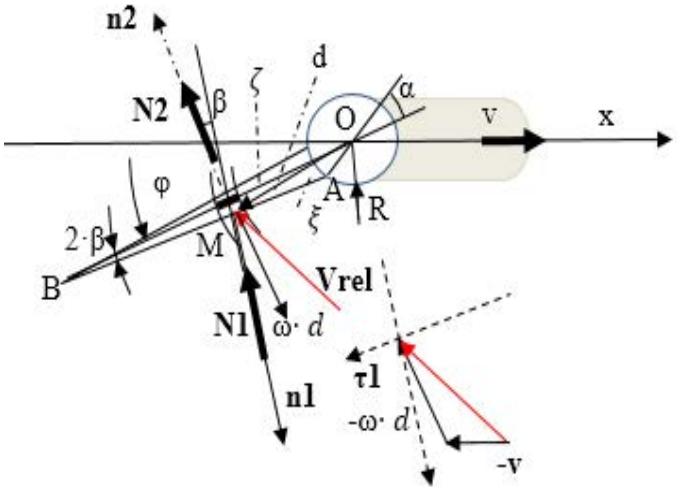

Fig.3.24. Fluid interaction in diving motion for autonomous robotic fish tail.

Assuming a simple linear motion for the robotic fish in water with an efficient mechatronic system and with a triangular tail that could flap or oscillate about the axis O, as shown in Fig. 3.24. for a given time function. The hull and the tail is described as a mechanical system of one degree of freedom (1 DOF) defined by the co-ordinate x.

The differential equation for robotic motion is given by

$$(m_0 + m)\ddot{x} = -N_1 x - N_2 x - b\dot{x}^2 sign(\dot{x}), \tag{44}$$

where m_0 mass of the hull, m is mass of the tail, $\ddot{x}$, $\dot{x}$ are correspondingly the acceleration and velocity of the hull, $N_1 x$ is a fluid interaction component in a pressing zone, $N_2 x$ is a fluid interaction component with the tail in suction zone, $b\dot{x}^2$ is non-linear interaction of the hull with fluid in rectilinear motion, motion velocity v = $\dot{x}$; b is constant. From Fig 3.24. normal forces N_1 and N_2 on two different surface planes are given by (45), (46)

$$|N_1| = B.\rho \left| \int_0^{\beta} (v.sin(\varphi - \beta) + \omega.\xi)^2 d\xi \right|; \tag{45}$$

$$|N_2| = B.\rho.C \left| \int_R^{R2} (v.sin(\varphi) + \omega.\zeta)^2 d\zeta \right|, \tag{46}$$

where ξ is a distance from side AMB and $d\xi$ is a differential of ξ, calculated from (48), ζ is a radial distance along OB in Fig.3.24, C is a constant (co-efficient of interaction), approximately equal to 0.5.

$$\xi = \frac{R \cdot \sin(\gamma)}{\sin(\alpha + \beta - \gamma)}$$
$$d = \frac{R \cdot \sin(\alpha + \beta)}{\sin(\alpha + \beta - \gamma)} \quad (47)$$

The forces N_1x and N_2x can be expressed as ,

$$F_1x = |N_1|.sign\left(v.sin(\varphi - \beta) + \omega.\frac{R + R2}{2}\right).sin(\varphi - \beta); \quad (48)$$

$$F_2x = |N_2|.sign\left(v.sin(\varphi) + \omega.\frac{R + R2}{2}\right).sin(\varphi) \quad (49)$$

For the tail fin, rotation angle and angular velocity are given by (50),(51).

$$\varphi = a[\sin(pt) + 2(\lambda_3)\sin(3pt + \varepsilon_3)]; \quad (50)$$

$$\omega = a[p\cos(pt) + 6p(\lambda_3)\cos(3pt + \varepsilon_3)], \quad (51)$$

All numerical results obtained from MATHCAD are shown in Figs.3.25-3.30 for the following parameters, where the mechatronic constants ε_3 = -1.571, λ_3= ±0.1, p = 5 and a = 0.5.

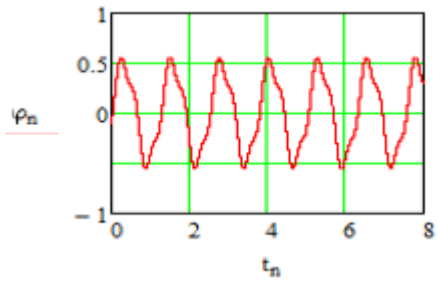

Fig.3.25.Tail rotation angle (radians) in time (seconds).

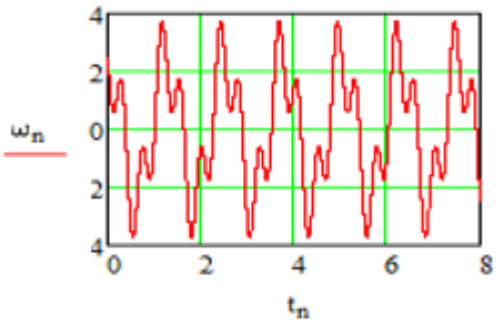

Fig.3.26.Angular velocity (radians/sec) in time (seconds) for the robotic tail fin, $\lambda_3 = -0{,}1$.

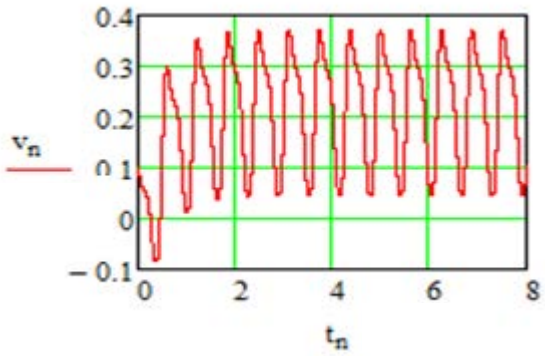

Fig.3. 27. Robotic fish hull velocity (meters/sec) with varying time (seconds); $\lambda_3 = -0{,}1$.

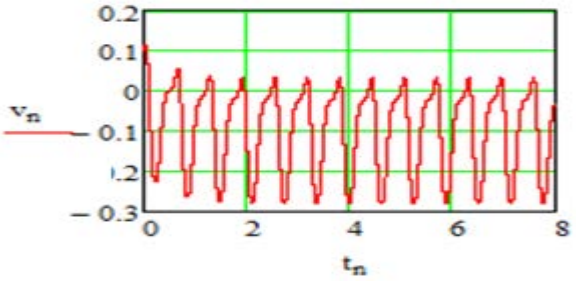

Fig.3.28. Robotic fish hull velocity (meters/sec) in reverse direction varying with time (seconds) for $\lambda_3 = +0{,}1$.

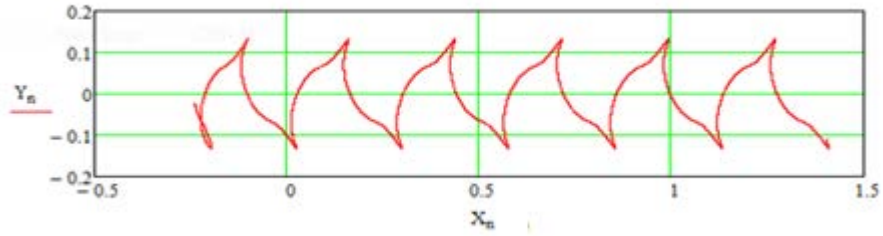

Fig.3. 29. Robotic fish tail edge trajectory (point B), moving forward in plane (X, Y) (meters);$\lambda_3 = -0{,}1$.

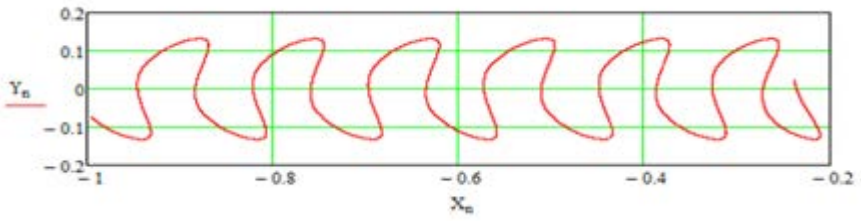

Fig.3. 30. Robotic fish tail edge trajectory (point B), moving backward in plane (X, Y) (meters); $\lambda_3 = +0{,}1$.

3.7. Motion of a sharp prism in vertical plane (flying object)

In this section the importance of the concept of interaction co-efficient C in estimating the physics of the flying objects is demonstrated.

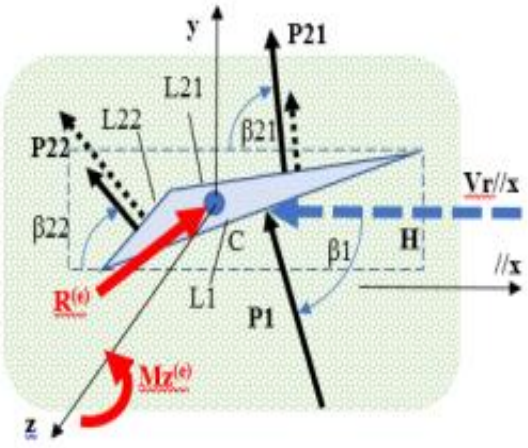

Fig.3. 31. Movement of triangle prism along the wind direction.

For equal angles $\beta_{22} = \beta_{21} = \beta_1$ shown in the Fig.3.31 a case of vertical movement is investigated for object in fluid flow. The motion of a sharpened prism in a vertical plane is described by differential equations (52),

$$m \cdot \ddot{y} = [L \cdot B \cdot \rho \cdot (\dot{x} \cdot \sin(\alpha) - \dot{y} \cdot \cos(\alpha)^2 \cdot (1 + C_1) \cdot \sin(\alpha) \cdot sign(\dot{x} \cdot \sin(\alpha) - \dot{y} \cdot \cos(\alpha)^2] - m \cdot g \quad (52)$$

where $\ddot{y}$ is a projection of acceleration to the vertical plane; α – angle between normal and vertical direction; g – acceleration due to gravity.

The obtained (52) helps in solving analytical and parametric optimization tasks for a given non-stationary motion problem. It is analysed that this object movement is similar to the gliding or diving movement of birds in air and the results of diving motion are shown in Figs.3.32-3.34. All parameters in system SI: $\rho = 1.25; L \cdot B = 0.04; m \cdot g = 2; C_1 = 0.5; \alpha = \frac{\pi}{4}$.

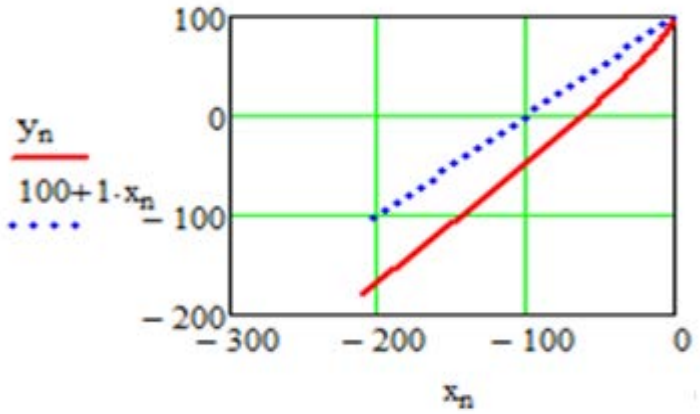

Fig.3. 32.Center of mass trajectory in the vertical plane taken from the coordinates (x, y) = (0, +100) (in meters).

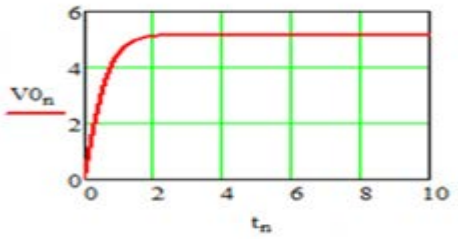

Fig.3. 33. Velocity projection (meters/sec) with varying time (seconds) on prism normal.

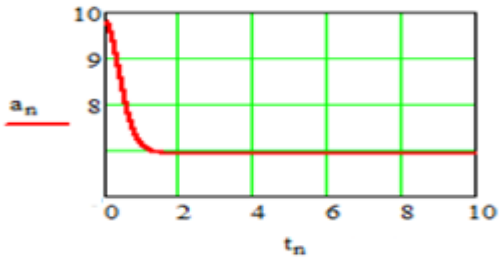

Fig.3. 34. Acceleration (meters/seconds^2) of prism with varying time (seconds).

It can be inferred from the modeling results that the velocity projection perpendicular to the prism reaches the terminal value, and no fluctuation or shift is observed further with the time. The acceleration in the tangential direction becomes constant and there is a linearly increase in velocity component with the time. In real-world applications a prism with a blunt front surface must be considered.

3.8 Conclusions

1. From the results obtained, it is confirmed that the calculations for the fluid-body interaction the task assumes a constant pressure in the boundary layer of the flow suction zone.
2. Theoretically obtained new analytical formulas for the calculation of the interaction forces of a flow in the pressure zone can be used to solve analysis, optimization and synthesis tasks in real objects.
3. Theoretically and by modeling with ANSYS, it is shown that there is a fundamental difference in the interaction forces between convex and concave object forms.
4. For similar shape in compression zone (upstream flow/pressure zone), but different shape in suction zone, the interaction force can be assumed to have almost similar value for all engineering calculations. The interaction force however would change based on the orientation of the body in the fluid flow (at different angles to the fluid flow).
5. In analysing the convex and concave forms, the viscous nature of the fluid-medium (air) has been ignored and is of secondary importance in estimating interaction force

4. PARAMETRIC AND CONTROL OPTIMIZATION FOR INTERACTION PHENOMENON

4.1. Parametric optimization of a star prism

Parametric optimization task is taken up in this section for a star prism model. The star prism model is considered for its form (geometry) that is neither too simple nor too complex. In the parametric optimization problem, the horizontal force F_x (as a criterion) is analyzed with the limitations as mentioned in (41) - (43). The star prism with equal sides $L_2 = L_3$ and with height H = constant and $\beta_1 = 0$, other parameters - V, ρ, B, remain constant. Results of optimization $K(\beta_2) = F_x / (V^2 \cdot \rho \cdot L_2)$ are shown in Figs 4.1.-4.2 for different C_{12}, C_{23} values. This demonstrates that analytical relationships could be obtained which allow parametric optimization of fluid flow interactions.

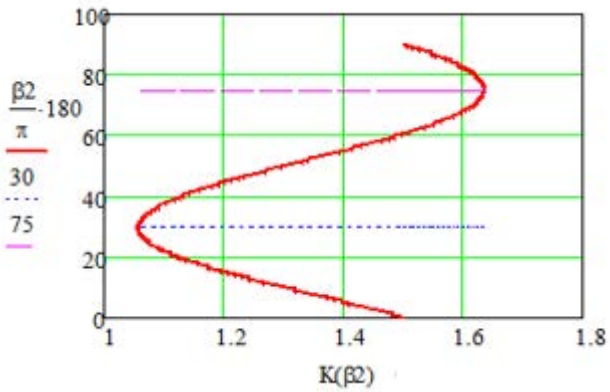

Fig.4. 1.Optimization for a star prism using first criterion: $K(\beta_2)$ – drag coefficient; $C_{12} = C_{23} = 1$ (β_2 in degress).

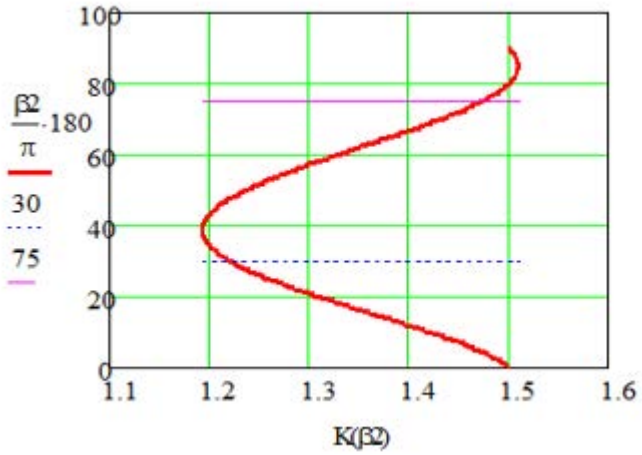

Fig.4. 2.Optimization for a star prism with four sides for the second criterion: $K(\beta_2)$ – drag coefficient; $C_{12} = C_{23} = 0.5$ (β_2 in degress).

4.2. Optimization of energy recovery from the fluid flow

The concept of fluid-rigid body interaction in this section is extended to estimate the energy recovery through a mathematical model. The viscous nature of the medium is not considered by the mathematical model. For all the cases the error is analysed and it was found to be less than 5%.

4.2.1 Perforated plate in fluid flow for energy scavenging (area control action)

Technique of energy extraction by using a perforated plate that could switch between a simple and perforated plate with the help of an efficient mechatronic system is demonstrated by using mathematical model supported by experimental results in Fig 4.4. Moving perforated plate in fluid for energy scavenging is shown in the Fig. 4.3. The basic idea in selecting the perforated plate was to estimate the varying area surface work action for the purpose of energy extraction from fluid. The fluid in this case is assumed to be laminar and incompressible. Details of perforated plate are shown in Fig. 3.16.

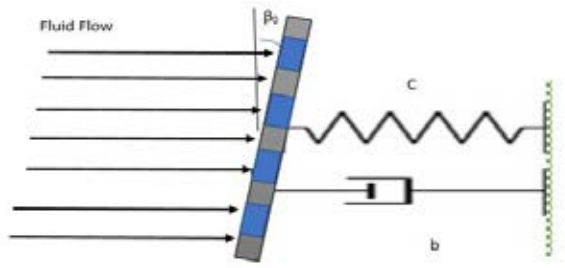

Fig.4.3 Perforated plate model for energy recovery.

The comparison of computational and experimental results shows that an inequality (53) exists as the funcion of inclination angle β. The formula (53) can only be used within the range: $-\frac{\pi}{4} \leq \beta \leq \frac{\pi}{4}$. It was found that the mean value of the constant C for the perforated plate investigated here within mentioned limits is $C = 0.065$.

$$L_3 \geq L_2 \cdot tg(\beta), \tag{53}$$

The mathematical model for the energy extraction concept is given by (54), by taking into consideration the plate relative velocity,

$$m\ddot{x} = -cx - b\dot{x} - A_0 \cdot [1 - a \cdot sign(\dot{x})] \cdot \rho \cdot \{C + [cos(\beta_0)]^2]\}(V + \dot{x})^2 \frac{V + \dot{x}}{|V + \dot{x}|}, \tag{54}$$

the plate in (54) is assumed to have negligible thickness ($d \cong 0$).

Here m – mass, x - displacement of perforated plate, A_0 –area parameter due to interaction; a – constant of area exchange, ρ –density, C –interaction coefficient, β_0 –angle against flow, V – air flow velocity, $a \cdot sign(\dot{x})$ – adaptive control area action.

Modelling results are shown in Figs.4.5 – 4.7 with parameters:
m = 1.56 kg, c = 3061 kg·s^{-2}, b = 5 kg·s^{-1}, A_0 = 0.04 m^2, a = 0.5, C = 0.065, V = 10 m·s^{-1}, ρ = 1.2047 kg·m^{-3}, $\beta_0 = \pi/6$.

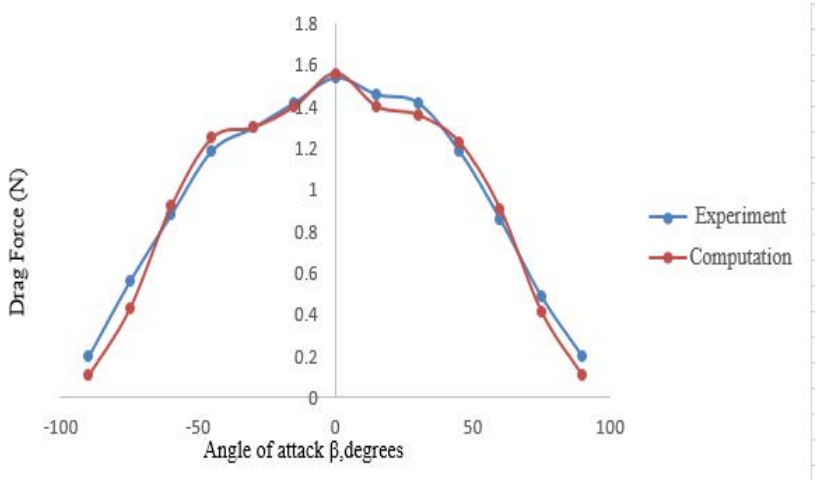

Fig.4.4 Comparison of numerical computation and experiments for perforated plate (stationary case) at 10m/s.

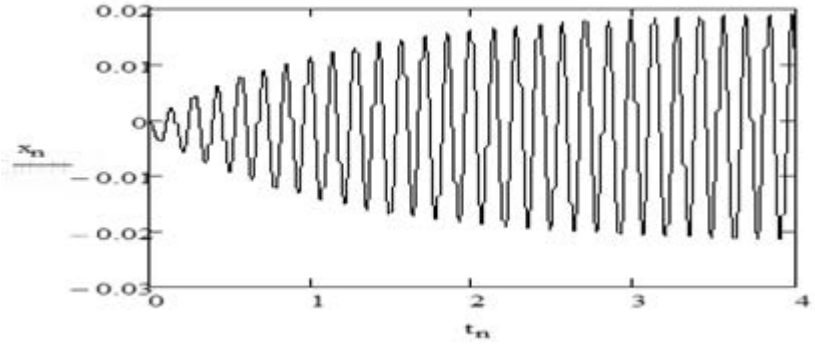

Fig.4.5 Plate displacement (meters) with varying time(seconds).

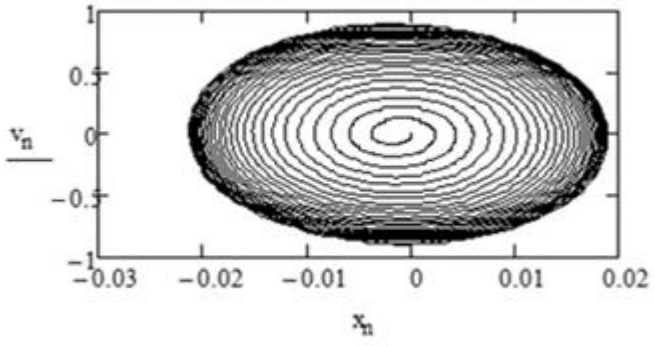

Fig.4.6 Motion in phase plane velocity (meters/sec) vs displacement (meters).

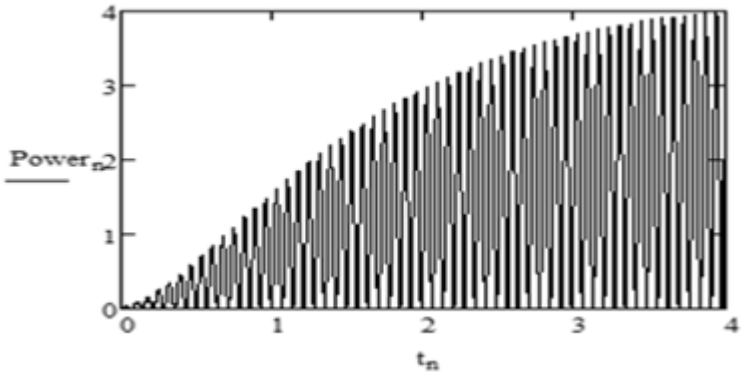

Fig.4.7 Generator power (watts) for varying time (seconds).

4.2.2 Flat plate or diamond in fluid flow for energy scavenging

Considering the thin plate with the depth is ~ 0 , Fig.4.8, the model for energy scavenging includes linear spring with stiffness *c* and linear damping with proportionality coefficient *b*. The relative interaction velocity *Vr*:

$$V_r = (v_f + v_p) \tag{55}$$

where v_f - fluid velocity;

v_p – plate velocity along x- axis.

Differential equation for motion of a plate along horizontal x-axis is expressed in (56):

$$m\ddot{x} = -c \cdot x - b \cdot \dot{x} - A \cdot \rho \cdot [0.5 + \cos(\beta)^2] \cdot ((v_f + v_p)^2 \cdot \frac{(v_f + v_p)}{|(v_f + v_p)|} \tag{56}$$

where

A – surface area of the object under consideration (flat perforated plate),

ρ – density of the fluid,

β– angle of plate against flow.

The energy obtained is represented as a damping force ($-b\dot{x}$), i.e. the damper is simulated for the generator, The power *P* is taken as (57):

$$P = b \cdot (\dot{x})^2 \tag{57}$$

The average power *Pa* is given by (58):

$$P_a = \frac{\int_0^t b \cdot (\dot{x})^2 \cdot dt}{t} \tag{58}$$

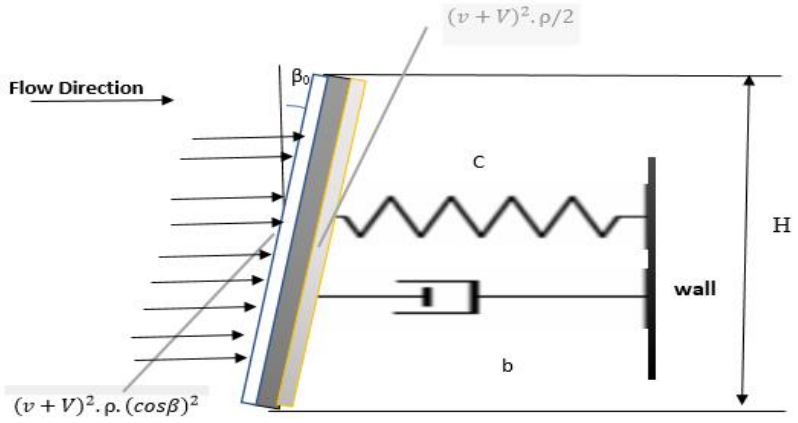

Fig.4. 8. A new model for energy scavenging from a fluid with the help of flat plate (mathematical model).

β Analysis of equation (56) allows to realize that there are five parameters to be studied or calculated for estimating the efficiency of a given system: two parameters (c, b) of the system and three time or phase coordinates control actions (, V and A). Modelling results are shown in Figs.4.9-4.12. For all results , system parameters are :

A = 0.004 m^2; V = 10 m·s^{-1}; ρ = 1.25 kg·m^{-3}. Average power Pa is estimated as a percentage of maximal power P_{max} expressed as a function of flow velocity (59):

$$P_{max} = b \cdot V^2 \cdot \frac{V}{3} \qquad (59)$$

Angle β time control modelling results are shown in Figs 4.9-4.12 for $\beta = \frac{\pi}{2,5}\sin(7t)$:

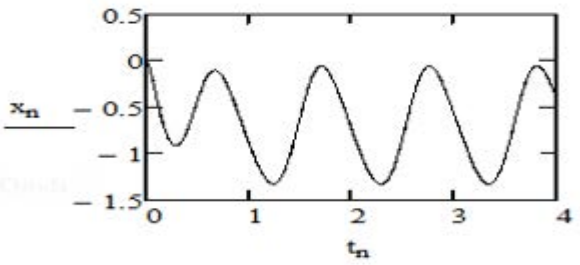

Fig.4.9 Displacement x (meters) as a function of time t(seconds).

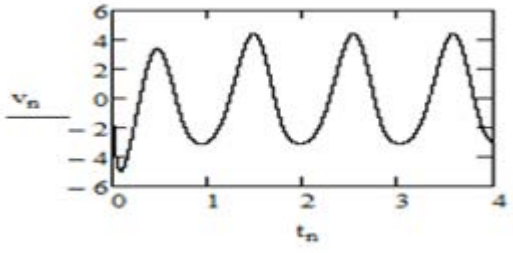

Fig.4.10 Plate centre velocity v (meters/second) as a time function t (seconds).

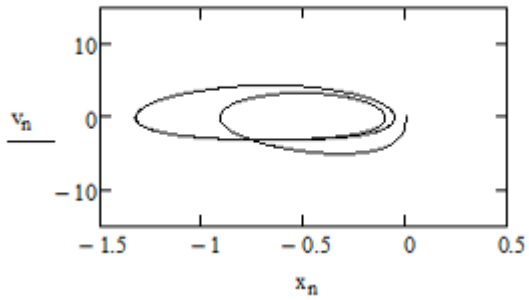

Fig.4.11 Motion in phase plane velocity (meters/second) vs dispalcement (meters).

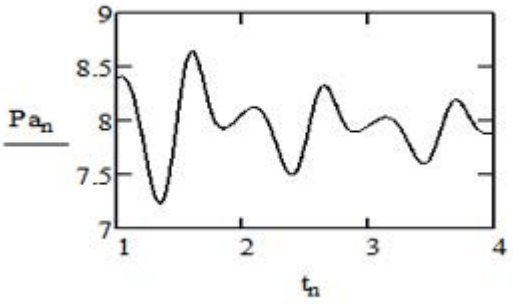

Fig.4.12 Average power *Pa* (watts) in time (seconds) for a generator.

Figs.4.9-4.12, obtained from mathematical modelling show the following results:
1. It is possible to analyse or estimate the optimal parameters of the system (i.e. stiffness, area, frequency, amplitude) for maximum power within given limits.

Additional optimal angle control laws can be obtained such as bi–harmonic $\beta = \frac{\pi}{2,5}[\sin(7t) + 2\sin(14t)]$ or poly-harmonics. Fluid flow velocity V control modelling results are shown in Figs 4.13–4.16. Function $V = V_0 \cdot (2 - 0,5\sin(10t))$ where $V_0 = 10\ m.s^{-1}$.

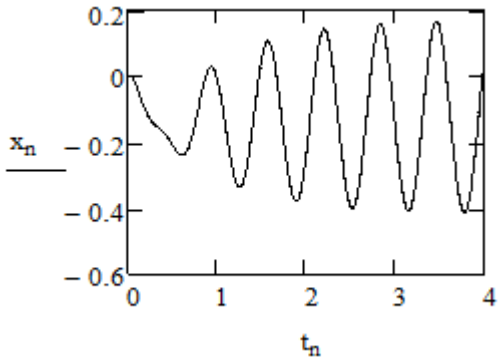

Fig.4. 13. Displacement *x* (meters) as a function of time *t* (seconds).

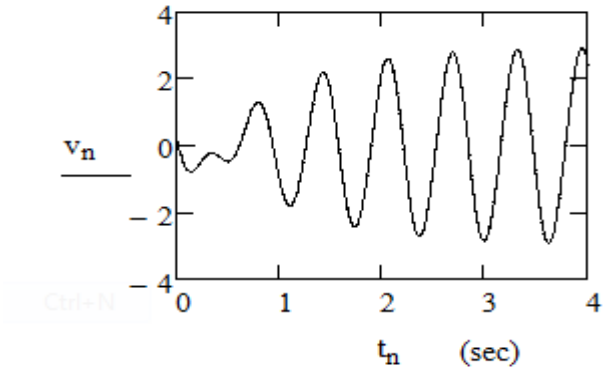

Fig.4. 14. Plate centre velocity *v* (meters/second) for a given time *t* (seconds) .

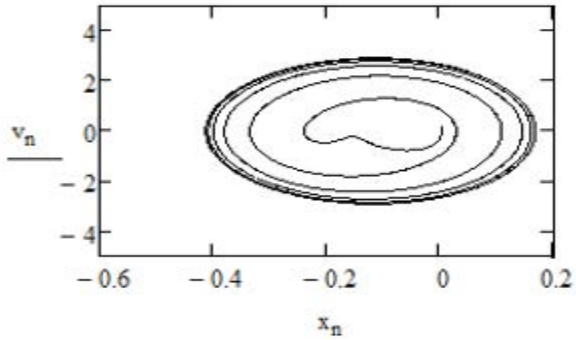

Fig.4. 15. Motion in phase plane for *v = v(x).* Velocity in (meters/seconds) and displacement in (meters)

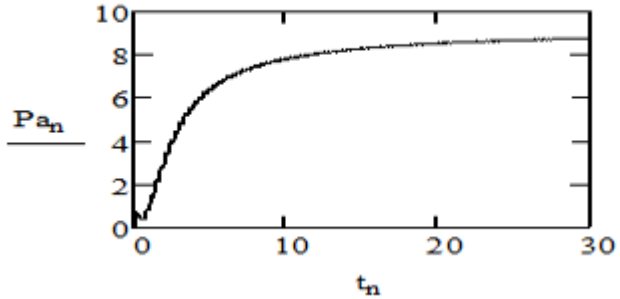

Fig.4. 16.Average power *Pa* (watts) as a function of time *t* (seconds).

Results of the mathematical modelling in the case of the flow velocity as the harmonic time function in Figs.4.13–4.16 shows the following:

1. A new opportunity to generate energy by harmonically changing the flow rate is analysed.
2. Opportunity to use new forms such as harmonic, bi-harmonic, pulse for control of flow is explored.

4.2.3 Energy recovery from a dual varying area actuator of a robotic fish tail (control action)

An innovative and very important application pertaining to Autonomous Underwater Vehicles (A.U.V) is dealt in this section. The concept of on board recharge of power pack utilising the phenomenon of interaction of fluid and rigid body is highligted. The importance of the interaction force coefficient and its significance for the task of on board power pack for a vehicle could be realised in this section. The Autonomous Underwater Vehicle (here the robotic fish) which was designed and experimented as a part of the FILOSE project has a perforated tail fin and is designed in such a way that only during the diving motion the tail form is changed from single to dual tail that could rotate about the axis O as shown in Fig. 4.17. This new technique of diving is assumed to be more efficient as this innovative technique helps to overcome viscous forces of the fluid medium and also to maintain the diving force unceasing. Two perforated plates whose actions are synchronous form the tail fin. The tail fins under locked position is called "Locked-in", as no relative movement between the tails exists. The perforations of the two plates fit in exactly thereby to form a complete flat plate. This single tail fin under extreme angles of propulsive strokes change into perforated plate due to the plates relative motion in that position.

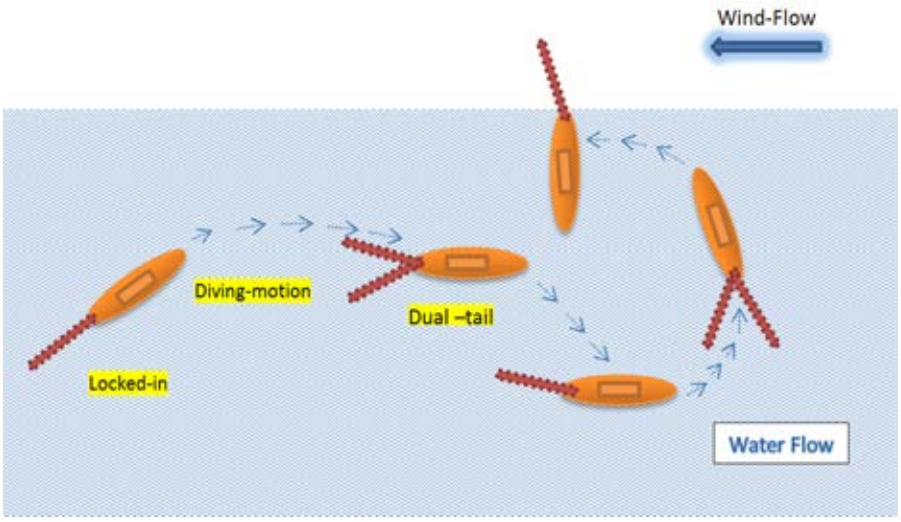

Fig.4.17 Diving motion of the robotic fish inside water with single and dual tail along with the technique of charging from air.

Common technique for both the dual and single tail fin is that at the time of charging, the single tail fin is extended out of water(for dual tail 'Locked in' postion) and the surrounding air medium is used for charging Fig. 4.18. through flapping/curvelinear oscillations.

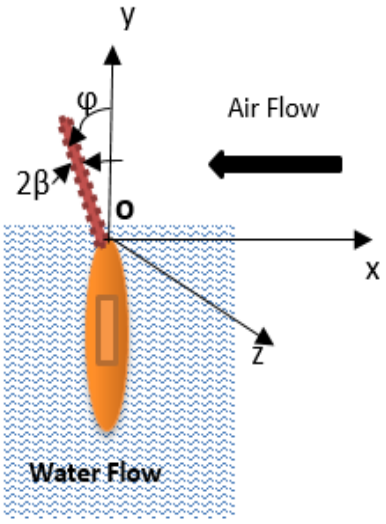

Fig.4.18.Charging action (projecting tail out of water surface).

From Fig. 4.18. taking into account the air interaction,

$$J_z\ddot{\varphi} = Mwin_z - Mel_z(\varphi) - Mgen_z(\dot{\varphi}), \qquad (60)$$

where J_z is a tail mass moment of inertia about rotation axis z; $\ddot{\varphi}$ – angular acceleration;, $\varphi, \dot{\varphi}$ are correspondingly the angle and angular velocity; $Mwin_z$ is an air flow interaction moment; $Mel_z(\varphi)$ is a moment from linear or non-linear elastic spring; $Mgen_z(\dot{\varphi})$ is a linear or non-linear moment from energy generator.

The results of the mathematical modelling are given for a relatively small plate for robot on board power charging as shown in Figs. 4.19-4.22, a case with a linear spring and a linear generator characteristics in the following form is considered:

$$Mel_z = c \cdot \varphi;\ Mgen_z(\dot{x}) = b \cdot \dot{\varphi}, \qquad (61)$$

where c, b are constants.

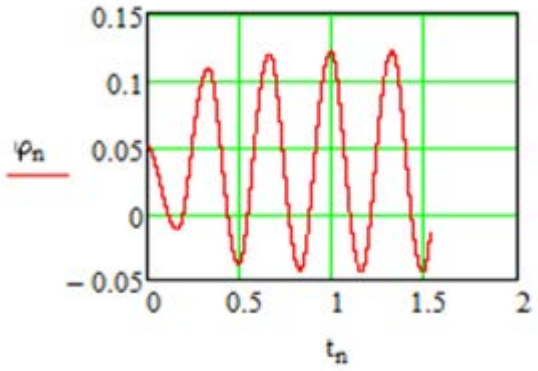

Fig.4.19 Perforated plate angle (radians) varying with the time (seconds) for robotic fish tail.

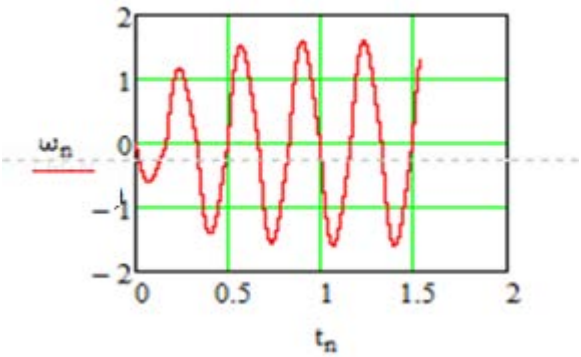

Fig.4.20 Perforated plate angular velocity (radians/sec) varying with time (seconds).

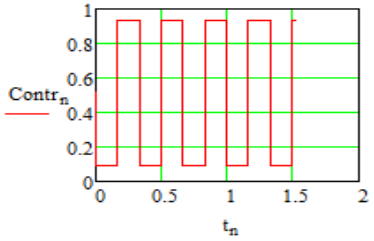

Fig.4.21 Perforated plate area control action with varying time (seconds).

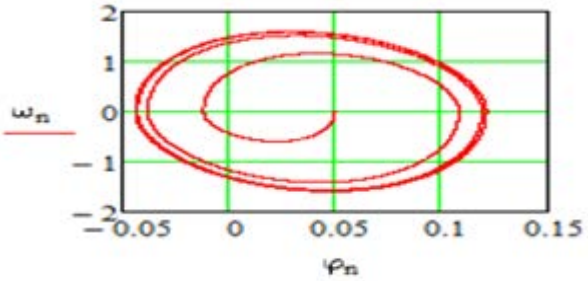

Fig.4.22 Motion in phase plane angular velocity (radians/seconds)vs angular displacement (radians) .

4.2.4. Energy recovery from a single actuator for robotic fish tail

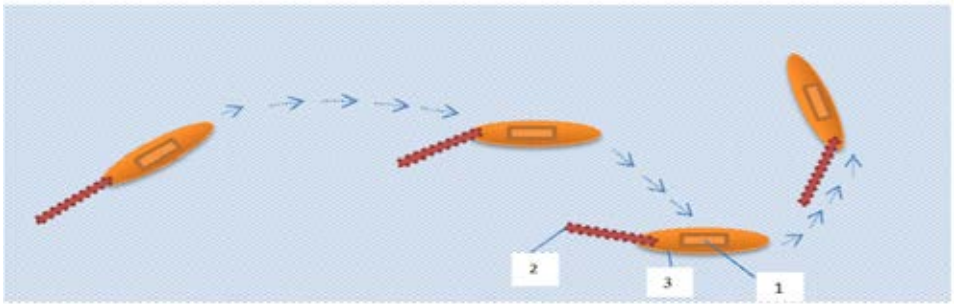

Fig.4.23 Trajectory for robotic fish in water stream for single tail actuator.
1 – On board battery station, 2 – perforated tail fin, 3 - fish hull.

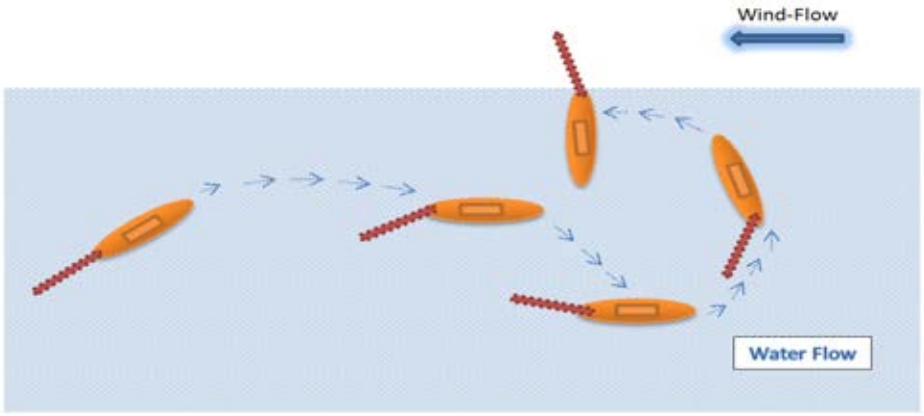

Fig.4.24 Concept of charging for AUVs from a wind flow.

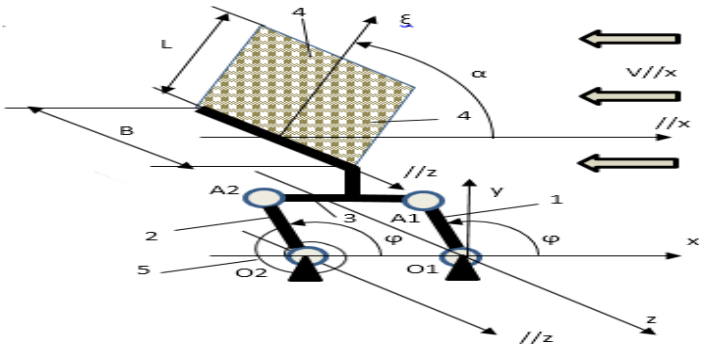

Fig.4.25. Model of perforated tail fin of robotic fish with linear spring.
1, 2 – two rods of the same length, 3 - three-dimensional traverse in plane,
4 - perforated plate with width *B* and length *L*, 5 - torsion spring with rotational,stiffness c, 6 –generator

Wind flow interaction from Fig. 4.25 is given by

$$Q = B \cdot L \cdot MCP \cdot \rho \cdot (1 + C) \cdot [V \cdot sin(\alpha) - \omega \cdot r \cdot \cos(\alpha - \varphi)]^2 \cdot \text{Sign}\,[V \cdot sin(\alpha) - \omega \cdot r \cdot \cos(\alpha - \varphi)], \quad (62)$$

Where, B – width,
L – length,
MCP - function of area mechatronical control of a perforated plate,
ρ - density of fluid (air),
V- wind velocity,
α - plate angle with respect to the wind (fluid flow),
r-length of rods 1and 2,
φ - rods 1 and 2 angle,
ω - angular velocity of rods 1 and 2,
C - constant, taking into account suction (downstream of plate interactions).

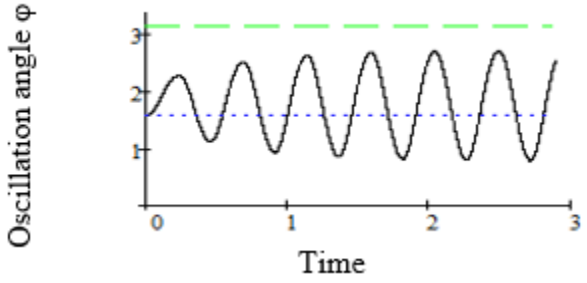

Fig.4.26 Oscillation angle φ (radians) as a function of time t (seconds).

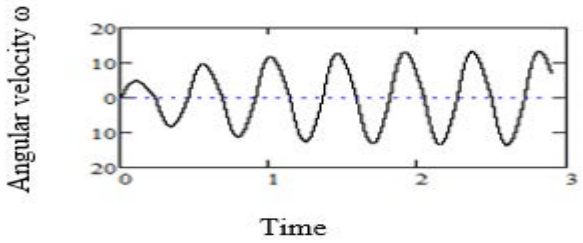

Fig.4.27 Electric generator angular velocity ω (radians/sec) with varying time t (seconds).

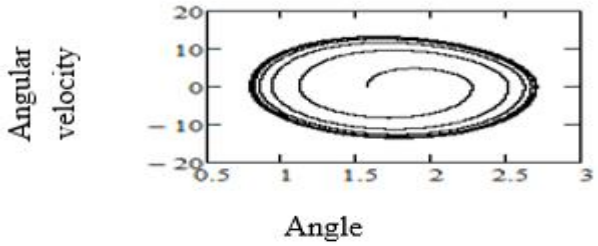

Fig.4.28 Motion in phase plane,angular velocity (radians/second) vs angle displacement (radians).

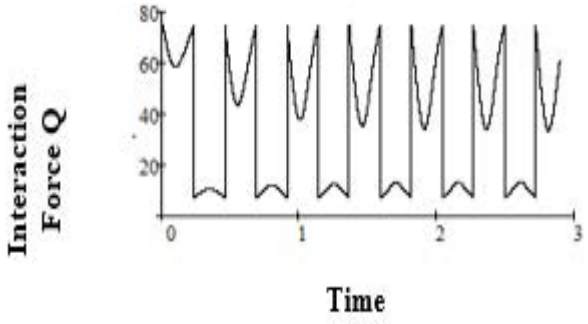

Fig.4.29 Interaction force Q (newtons) in wind flow as a function of time t (seconds).

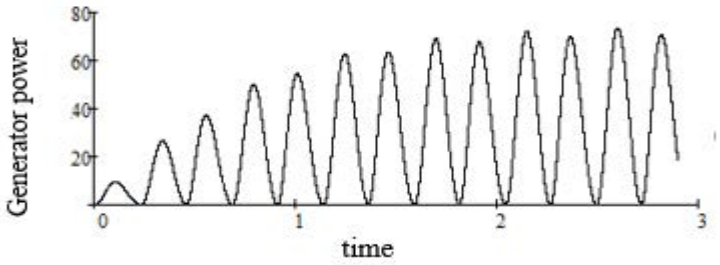

Fig.4.30 Generator power (watts) with varying time (seconds).

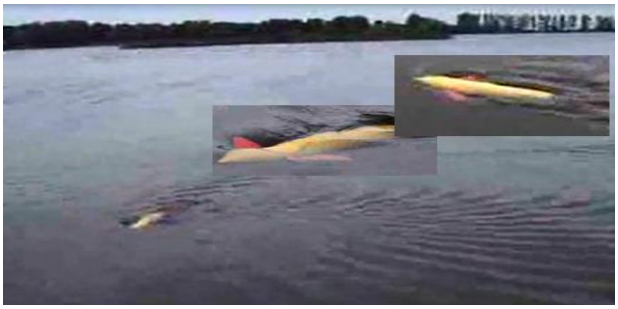

Fig.4.31 Robot fish test in lake.

4.3 Vibration damping from fluid interaction phenomenon through parametric optimization

Parametric optimization is considered with the optimum of a model changes (response of the system) to the full change of parametric variability. The parameters are generally those variables that are relevant to optimization and could be of environmental variables or variables controlled by other discipline engineers (multi-disciplinary expertise).The aim of the current work is to illustrate the technique of parametric optimization in a manner that helps in analyzing, estimating and studying about the systems and related challenges (fluid density effects, maximization of efficiency, etc). In the present section a case of sensitivity analysis based on a technique for parametric optimization is demonstrated which considers the response of the model changes with the perturbation of a parameter. The peculiarities of fluid structure in free damping oscillations are that their operation can be controlled by changing parameters such as: fluid density ρ, interaction cross section area A_0 and shape configuration (drag coefficient), the density being an environment variable (dependent on fluid medium). Therefore, in the optimization of the free oscillation damping process, the effect of the interaction area, size and the type of the spring is analyzed. Only the most typical cases of oscillation excitation and their free damping with pulse and harmonic excitations were analyzed in the subsequent section

4.3.1 1 D.O.F system free vibration damping by impacts and interactions

A case of impact and interactions is analyzed in this section. We consider the wheel of the car suspension system as shown in the Fig. 4.32. When the wheel of the vehicle hits the elevated surface and as the wheel bounces in the fluid (air or water), the free oscillation damping of the typical car suspension system is analyzed by elastic forces for a non–linear spring which is a case of vibration damping through interactions .
The results of the parametric analysis by using MATHCAD are shown in the Figs.4.33-4.37.

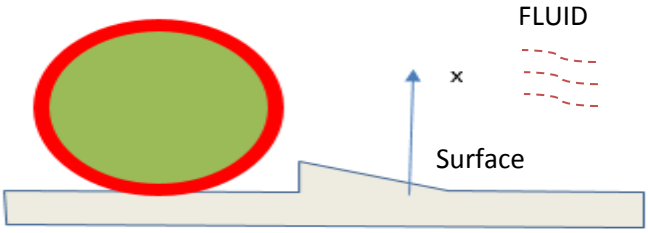

Fig.4.32.Wheel hitting the elevated surface in fluid medium.

Ignoring the viscous nature of the medium, the equations as per the laws of classical mechanics are given by:

$$x_{n+1} = x_n + s \cdot vx_n \tag{63}$$

$$vx_{n+1} = vx_n + \frac{s}{m} \cdot \left[\frac{-\rho \cdot A_0 \cdot D}{2} \cdot (vx_n)^2 \cdot \text{sign}(vx_n) - c \cdot x_n \cdot (0.5 - 0.5 \cdot \text{sign}(x_n)) - m \cdot g\right] \tag{64}$$

$$Contr_n = \frac{-\rho \cdot A_0 \cdot D}{2} \cdot (vx_n)^2 \cdot sign\,(vx_n) \tag{65}$$

The value of mass =30 kg, acceleration due to gravity g= 9.81 m/s^2, spring constant c kg/s^2, density of the fluid ρ, displacement in the nth second x_n, velocity at the nth second vx_n., area A_0 in m^2.

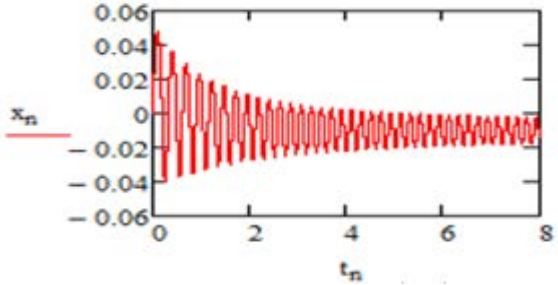

Fig.4.33 Displacement (meters) vs time (seconds)graphics.

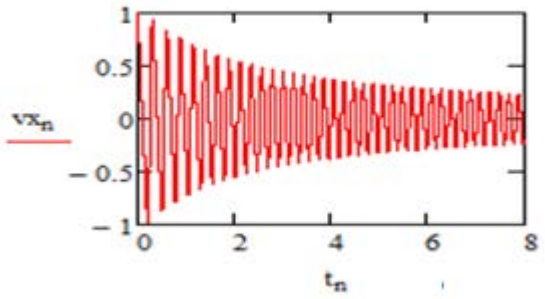

Fig.4.34.Velocity (meters/seconds) vs time (seconds) graphics.

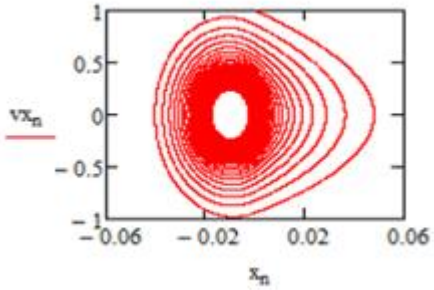

Fig.4.35. Motion in phase plane velocity (meters/seconds) vs displacement (meters).

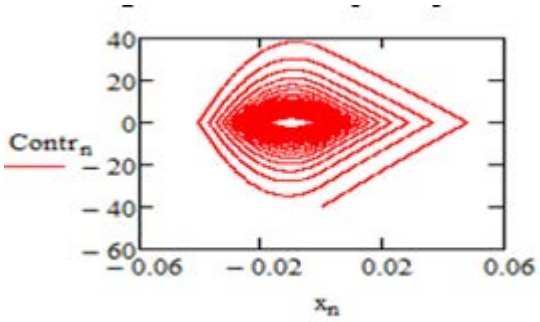

Fig.4.36.Control action vs displacement (meters).

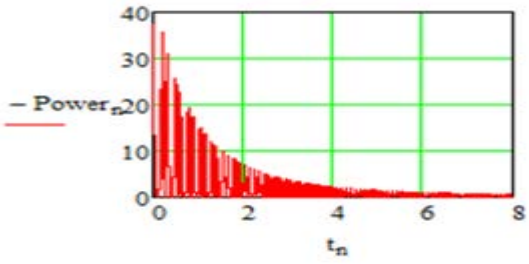

Fig.4.37.Power generated (watts) with varying time (seconds).

It is observed that in order to obtain the same power output in air, the area of the body under consideration is to be large enough.

Conclusions.

1. In air as the medium instead of water, the linear relationship in the elastic force equations shows that the area must increase by 800 times.
2. The free air vibration damping will only be used in low mass energy systems.
3. The analysis shows that quadratic velocity of resistance to force and such dampings are effective for high speeds.
4. At low speeds free vibration damping in case of computer modeling is turned off.

4.3.2. 1D.O.F system with linear and non-linear spring, free vibration damping through harmonic excitation

A resonance case for linear and non-linear spring is taken up in different fluid medium on subjected to a harmonic excitation with a linear spring, resonance $\omega = \sqrt{\frac{c}{m}}$ for water as fluid medium.

The equations according to classical laws of mechanics for the linear spring system are given by (63), (65) and (66), the results are illustrated in Figs.4.38-4.42.

$$vx_{n+1} = vx_n + \frac{s}{m} \cdot [\frac{-\rho \cdot A_0 \cdot D}{2} \cdot (vx_n)^2 \cdot \text{sign}(vx_n) - c \cdot x_n \cdot (1) - m \cdot g + P_0 \cdot \sin(\omega \cdot t_n)] \quad (66)$$

where $P_{0,}$ is the force. $P_0 = \frac{m \cdot g}{5}$.

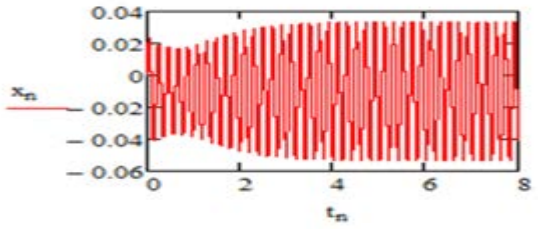

Fig.4.38.Displacement (meters) with varying time (seconds).

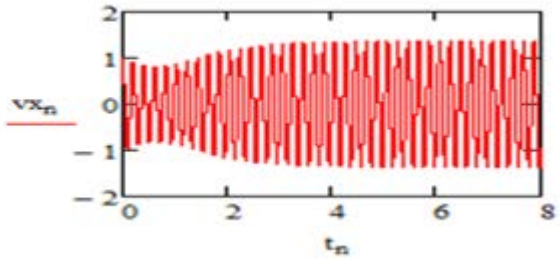

Fig.4.39.Velocity vx_n (meters) with varying time t_n(seconds).

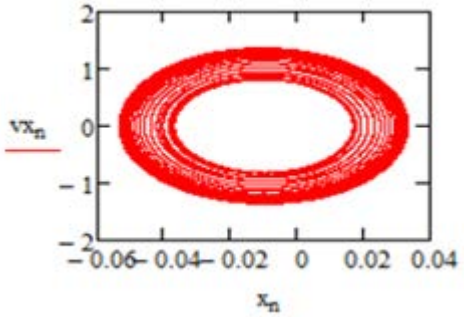

Fig.4.40. Motion in phase plane, Velocity vx_n (meters/second) vs x_n (displacement).

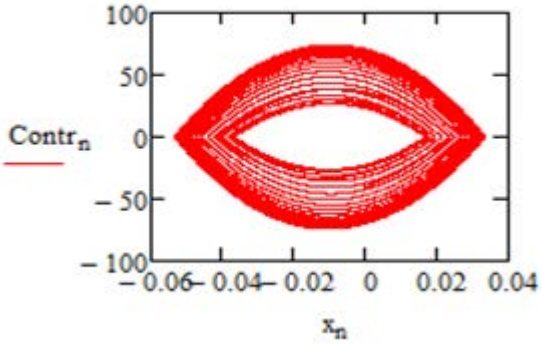

Fig.4.41.Control action with varying time (seconds).

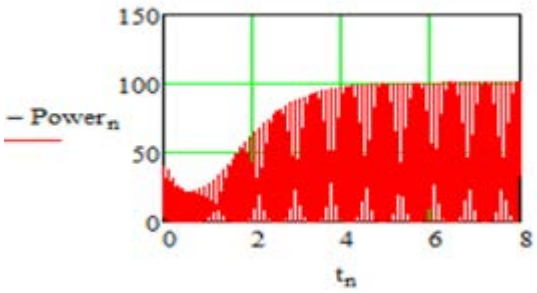

Fig.4.42.Power generated (watts) as a function of time (seconds).

Conclusion.

1. In a linear double-sided spring-force system, the dependence of the damping resistance force on the square of the velocity effectively dampens the resonant motion.
2. The steady state occurs relatively quickly, in around 2 s.

We look at non-linear spring with cubic elasticity $c \cdot x^3$, resonance $\omega = (\frac{\sqrt{\frac{c}{m}}}{3})$, gas as medium. A non–linear spring is used and as the laws of classical mechanics, along with (63), (65) & (67), the results are illustrated in Figs. 4.43-4.48.

$$vx_{n+1} = vx_n + \frac{s}{m} \cdot [\frac{-\rho \cdot A_0 \cdot D}{2} \cdot (vx_n)^2 \cdot \text{sign}(vx_n) - c \cdot (x_n)^3 \cdot (1) - m \cdot g + P_0 \cdot \sin(\omega \cdot t_n)] \quad (67)$$

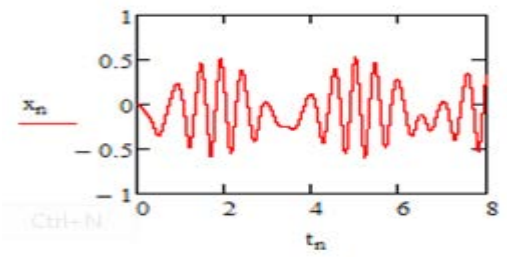

Fig.4.43.Displacement x_n (meters) with varying time t_n (seconds).

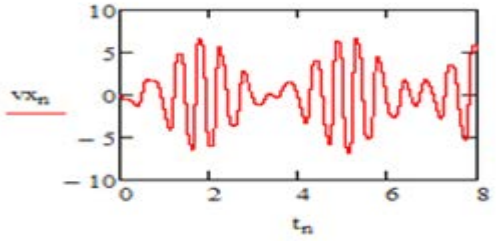

Fig.4.44.Velocity vx_n (meters/second) with varying time t_n (seconds).

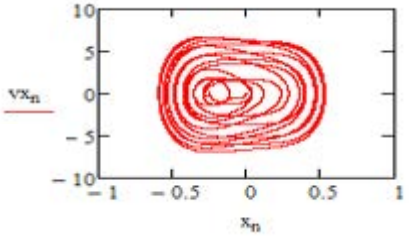

Fig.4.45 Motion in phase plane velocity vx_n (meters/second) vs displacement x_n (meters) .

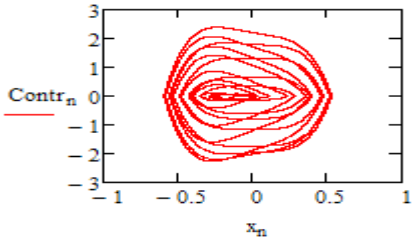

Fig.4.46.Control action with varying displacement x_n (meters) .

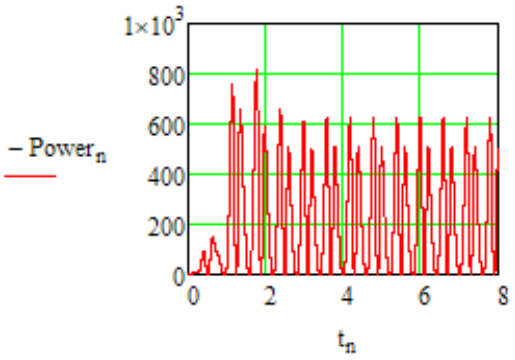

Fig.4.47.Power generated (watts) for water as fluid medium for varying time t_n (seconds).

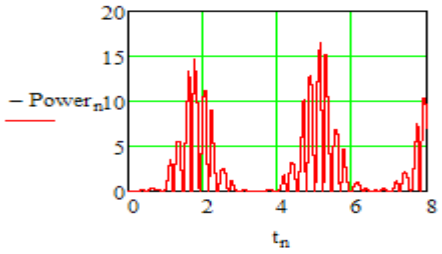

Fig.4.48.Power generated (watts) for gas (air) as working medium for varying time t_n (seconds).

Conclusion.

1. In non-linear double-sided spring-force system, there is no steady trend but repeating fluctuating trend could be seen.
2. The absolute power generated is larger for water than for a working fluid medium.

4.3.3. 1D.O.F system damping for harmonic excitations in water, non - periodic case

The transition process from zero to excitation force frequency was analyzed. The mathematical model is given by (68). The results are illustrated in Figs 4.49-4.54.

$$vx_{n+1} = vx_n + \frac{s}{m} \cdot \left[\frac{-\rho \cdot A_0 \cdot D}{2} \cdot (vx_n)^2 \cdot \text{sign}(vx_n) - c \cdot (x_n)^3 \cdot (1) - m \cdot g + P_0 \cdot \sin(0 \cdot 5t_n)\right] \quad (68)$$

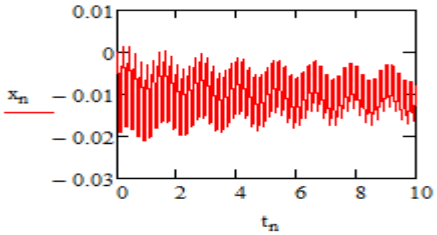

Fig.4.49. Displacement x_n (meters) with varying time t_n (seconds).

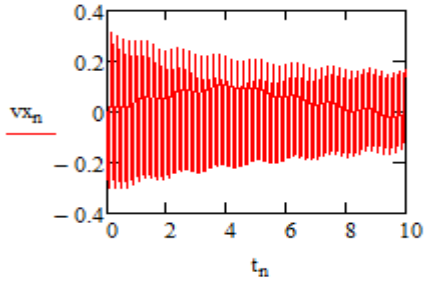

Fig.4.50. Velocity vx_n (meters/second) with varying time t_n (seconds) .

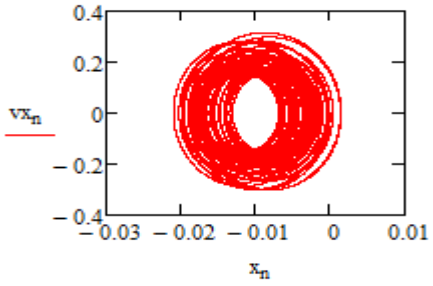

Fig.4.51. Motion in phase plane Velocity vx_n (meters/second) with varying displacement x_n (meters).

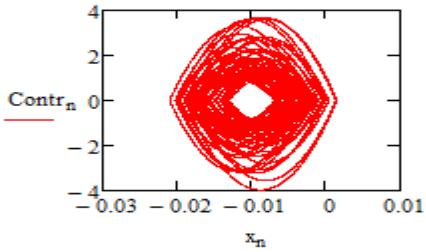

Fig.4.52.Control action with varying displacement x_n (meters).

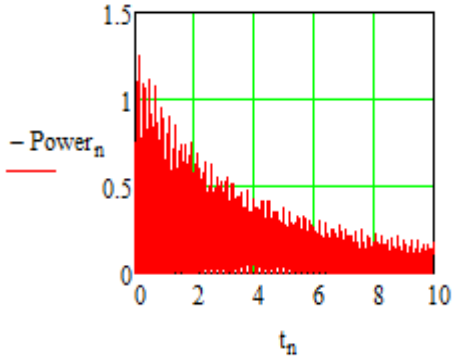

Fig.4.53.Power generated (watts) for water as working medium with varying time t_n (seconds).

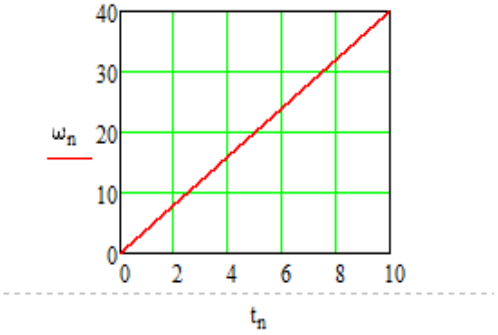

Fig.4.54.Linear trend of frequency (Hertz) with varying time t_n (seconds).

Conclusions.

1. In the considered case, when the frequency of the excitation force changes linearly starting from zero value of the amplitude - the frequency curve does not show rapid increase.
2. From the results it can be seen that the dependence of the force on the square of the velocity effectively dampens the amplitudes over the whole frequency range.
3. It has been shown that the liquid has a much higher efficiency in vibration damping than the gas.

4.4 Control optimization for robotic fish motion in fluid

It is important to control the motion of objects in fluids for the purpose of achieving some desired objective through improved efficiency. In order to achieve a good overall performance of the moving objects in a fluid medium, there is a need of new techniques and methods. The search for new techniques can be divided into two main directions:

- To improve the indicators of technical and economic parameters of the existing moving objects in fluids;
- To develop fundamentally new models.

Each subsequent improvement of the moving objects in fluid after reaching a certain technical level is becoming expensive with a relatively small increase in their efficiency. Therefore, with emerging opportunities for improvement the search for new operating principles of motion of objects in fluid flow is inevitable. Thus great importance is attached to the dynamic synthesis of moving objects in fluid flow. There are two basic approaches to this problem:

- researching and improving similar existing inventions;
- the use of the idea of optimal synthesis, in which the mathematical problem of optimal control is first solved, and after that the structural scheme is synthesized with sufficient objectivity.

Analyzing the problems of modern non–stationary motion objects in fluids, synthesis problems, from the analysis of the current situation, several completely new problems are encountered.

Among them, the following can be highlighted:

1. Optimal control methods and selection of a given subsystem before an unknown structure.

To solve this problem, it is necessary to know the practical purpose of the synthesized system.

Therefore, the optimal synthesis differs significantly from the usual analysis problems in which the functionality of the system is not critical.

2. Determination of constituent elements, form and need.This task is complex and its solution is still unknown.

However, if we start from the consideration that the synthesized system is better if the number of elements is smaller, then in special cases the problem will be solved at the level of engineering assumptions followed by refinement of theoretical calculations.

3. Development of subsystem optimal control methods.

If gaps appear in the coordinates of the system phases, then the optimal control can not always be determined by usual methods of the optimal control theory, and new methods must be found.

4. Synthesis of optimal control in phase plane or time.

The solution to this problem is very topical.

The focus here should be on developing the principles of a new self-regulatory system.

5. Determination of optimal parameters for the selected mechanical system.

Although great progress has been made in this direction with the help of computer technology, precise analytical methods are not available.

The complexity of the problem lies in the fact that it is necessary to set an optimal parameter criterion with the value of the optimum value (higher / lower) and at the same time to comply with stable operating modes.

4.4.1. Control optimization methods

Optimal control theory is a branch of mathematical optimization that deals with finding a control for a dynamical system over a period of time such that an objective function is optimized. It has numerous applications in science, engineering and operations research. A dynamical system may also be introduced to embed operations research problems within the framework of optimal control theory.

Optimal control is an extension of the calculus of variations, and is a mathematical optimization method for deriving control policies. The method is largely due to the work of Lev Pontryagin and Richard Bellman in the 1950s, after contributions to calculus of variations by Edward J. McShane. Optimal control can be seen as a control strategy in control theory.

For solution of task of optimization, various methods of optimal control theory can be used, for example:

- the maximum principle of Pontryaging;
- the classical method of variation calculus;

- method of moments;
- dynamic programming;
- mixed method (usually initially the optimization phase, followed by variation of parameters).

In the subsequent work, the Pontryagin maximum principle is used.

4.4.2. Horizontal motion model optimization with force control.

The model of the horizontal movement of the robot is shown in Fig.4.55

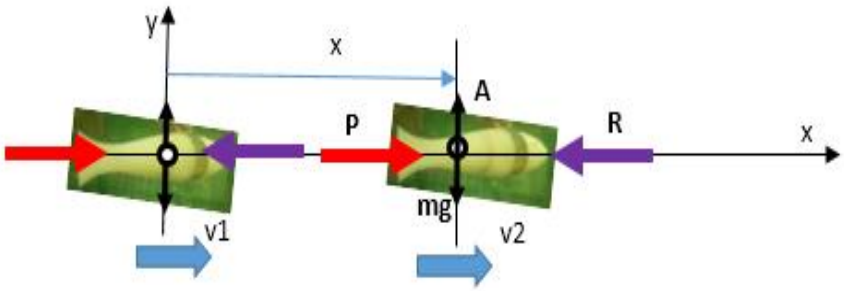

Fig.4.55.Horizontal motion model.

On the vertical axis, the force of gravity *mg* is balanced by the force of *Archimedes* or the force of interaction of the fins with water. In the horizontal direction there is a driving force *P* of the robot and in the opposite direction - resistance force of water *R*.

The differential equation of horizontal motion is as follows (69)

$$m \cdot \ddot{x} = P - b \cdot \dot{x}^2 \cdot sign(\dot{x}) \qquad (69)$$

where m is a mass, $\dot{x}$ is the velocity,$\ddot{x}$ is the acceleration, b is a constant.

In the given optimization problem, the following constraint on the engine force P:

$$0 < P(t) < P_0, \qquad (70)$$

where P_0 is a maximal force; 0– is a minimal force.

In addition, it should be noted that there is a limit to the velocity of motion, that is: V $<V_0$, where V_0 is the maximum velocity, associated with engine power as follows: $P_0<b \cdot V_0$.

Using the Pontryagins maximum principle in one direction motion

Pontryagin's maximum principle is used in optimal control theory to find the best possible control for taking a dynamical system from one state to another, especially in the presence of constraints for the state or input controls [60]. It states that it is necessary for any optimal control along with the optimal state trajectory to solve the so-called Hamiltonian system, which is a two-point boundary value problem, plus a maximum condition of the Hamiltonian. These necessary conditions become sufficient under certain convexity conditions on the objective and constraint functions [61], [62].

$$\ddot{x} = \frac{P}{m} - \frac{b}{m}\dot{x} \qquad (71)$$

Transform :

$$\dot{x_1} = x_2;$$
$$\dot{x_2} = \frac{P}{m} - \frac{b}{m}x_2 \quad (72)$$

Hamiltonian :

$$H = \varphi_1 \cdot x_2 + \varphi_2(\frac{P}{m} - \frac{b}{m}x_2) \quad (73)$$

$$\varphi_1 \text{ and } \varphi_2 \text{ can be calculated}$$

$$\dot{\varphi_1} = -\frac{\partial H}{\partial x_1};\ \ \dot{\varphi_2} = -\frac{\partial H}{\partial x_{21}}; \quad (74)$$

We get :

$\dot{\varphi_1} = 0;\ \varphi_1 = C_1$; C_1 is a constant (75)

$$\dot{\varphi_2} = -C_1 - \varphi_2\left(-\frac{b}{m}\right);\ \varphi_2 \text{ will be exponent} \quad (76)$$

Hamiltonian :

$$H = C_1 \cdot x_2 + (exponent) \cdot (\frac{P}{m} - \frac{b}{m}x_2) \quad (77)$$

The solution for optimal control is:
1) if (exponent) >0, P = P_0;
2) If (exponent) <0, P = 0.

Conclusion:

When moving a robot fish from one position to another, the optimal power consists of two stages:
(a) the maximum engine power must be switched on in the first stage;
(b) the engine power is switched off and braking takes place by the force of water resistance.

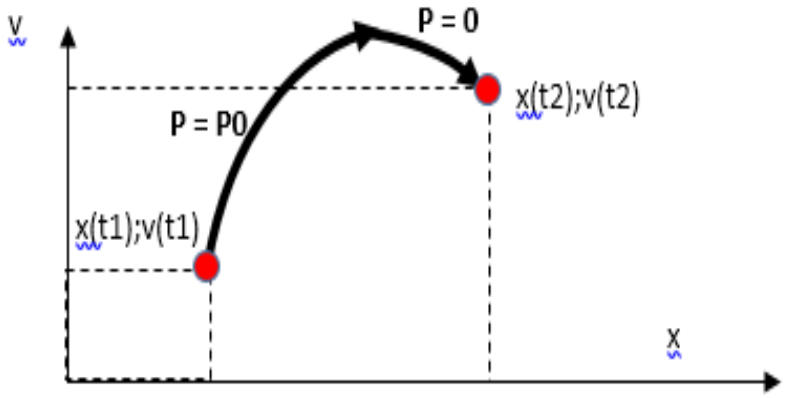

Fig.4.56. Optimal control in phase plane (x, V_0) Velocity V (meters/second) vs displacement X (meters).

If limits exist to velocity $V<V_0$, the optimal control action is given in the same way, motion graphic is shown in Fig. 4.57, $P_0 = b \cdot V_0$ on limit surface.

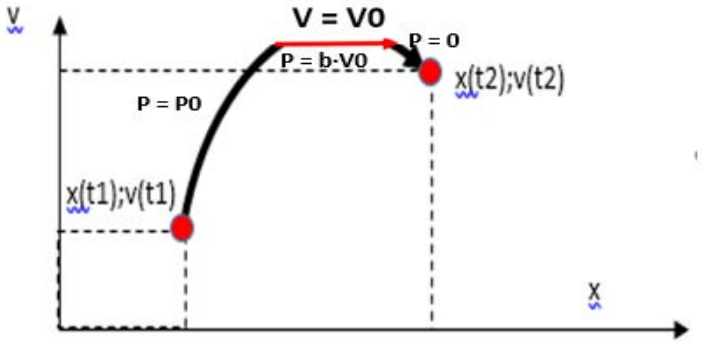

Fig.4.57.Optimal control in phase plane (x, V_0) with limit of velocity ($V <V_0$) Velocity V (meters/second) vs displacement X (meters) .

4.4.3. Vertical motion model optimization with force control.

The model of **vertical** movement of the robot is shown in Fig. 4.58. On the vertical axis, the force of gravity ***mg*** and Archimedes force ***A*** can be put into differential equation (78)

$$m \cdot \ddot{y} = P - m \cdot g + A - b \cdot \dot{y}^2 \cdot sign(\dot{y}); \qquad (78)$$

where m is a mass,

$\dot{y}$, $\ddot{y}$ are the velocity and acceleration in vertical direction, b is a constant.

In given optimization problem there is the same following constraint on the engine force P:

$$0 < P(t) < P_0; \qquad (79)$$

where P_0 is a maximal force;

0– is a minimal force.

In addition, it should be noted that there may be a limit to the velocity of motion, that is: $V < V_0$, where V_0 is the maximum velocity, associated with engine power as:

$P_0 < b \cdot V_0$.

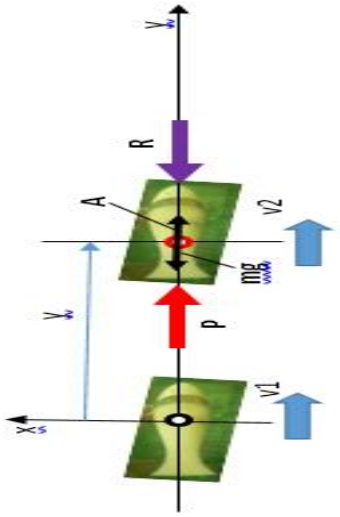

Fig.4.58.Vertical motion model.

In this case, the optimal control is found in a similar way as in the previous case of horizontal movement. The main difference here is that all-time control is complemented by two forces: gravity force and Archimedes force. Since they are constant, the optimal control is similar to the horizontal case. However, the difference is that swimming or sinking rules must be taken into account. If the robot has a neutral buoyancy (A or W = mg), the control corresponds exactly to the horizontal control case.

4.5. Optimization of shape (form) of flow interaction surface

In this section, optimization task for a complex model is taken up to optimize the shape of an object. The task could be solved in the following ways:

(a) numerical;

(b) analytical;

(c) analytical-numerical.

The techniques are explained as below:

In **numerical optimization**, the form is chosen and the parameters are changed at the given criteria and constraints. Then, taking all the results of changing parameter under given criteria and constraints, numerically obtained effects are compared to find the approximate optimal form that is most suitable as a best possible solution.

In **analytical optimization**, analytical correlations must first be obtained for the

expression of the criterion, then they are analyzed analytically. The optimal solution is found from variations of local forms.

Analytical-numerical optimization, as discussed before, yields analytical similarities, the variations of which are found numerically. In this section, we will consider this analytical-numerical method for the two-dimensional shape shown in Fig.4.59.

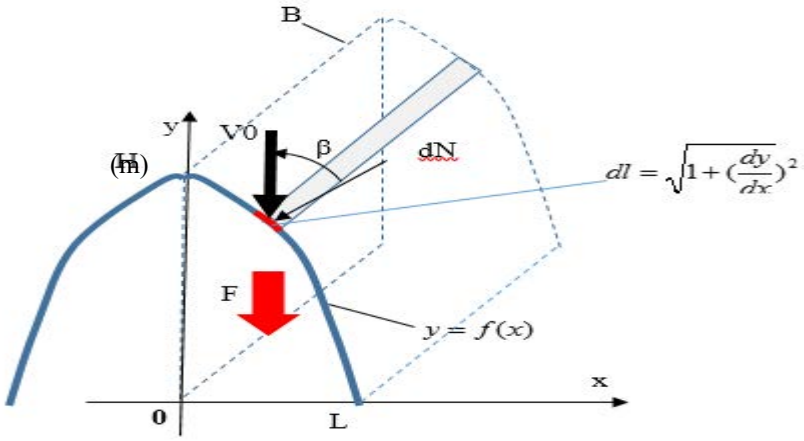

Fig.4.59.Two dimensional shape model.

Optimization problems for a prism with length *B* and form as a given function f (x) can be formulated as follows:

1. At the boundary conditions of the given form y = f (x); y (x = 0) = H; and at y (x = L) = 0. The task is to find the optimal form f (x) that provides the minimum flow force F if the feed rate is V_0. Such a task would be important in the case of energy savings pertaining to a vehicle system or for sports purpose.

2. A similar task is also taken up with the criterion: to find the form f (x) that provides the maximum flow force F. Such a task would be important in energy production systems. Both tasks will be solved in parallel.

As shown in the Fig. 4.59, following analytical relationships (80), (81) are obtained to solve the task of form optimization

$$\begin{gathered} dN = dl \cdot B \cdot [V_0 \cdot \cos(\beta)]^2 \\ dl = \sqrt{1 + \left(\frac{dy}{dx}\right)^2}; \\ \beta = a \cdot \tan\left(\frac{dy}{dx}\right); \\ dF = dN \cdot \cos(\beta); \\ F = \int_x^y dF \end{gathered} \tag{80}$$

$$\partial F = 0; for\ supremum\ or\ infimum \tag{81}$$

Here *dN*, *dF* is the local normal force and local axial force;
dl is a length of local arc;
δF is a variation of force *F* inside limits or on the boundary limits (in case of supremum, infimum).

Task 1.

It should be noted that the form could be searched for as a polynomial or the following function:

$$y = H + C_1 \cdot x + C_2 \cdot x^2 + C_3 \cdot x^3 + \cdots \quad (82)$$

where C_1, C_2, C_3 are the parameters. In the optimization process it is necessary to use relations (82) - (84) and find constants C_1, C_2, C_3, ...*etc*.

Task 2.

Model of two opposite curved planes or convex planes.

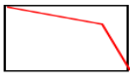

Let us consider a form that differs from the shape of a polynomial in that it is formed by two straight lines (or prism planes) with L = H, Fig. 4.60.

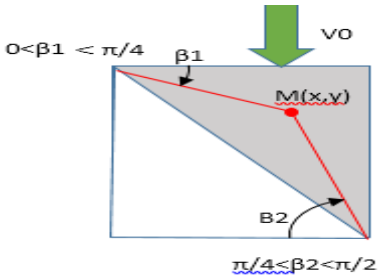

Fig.4.60 Model of two opposite curved planes *L* = *H*.

According to the developed theory, a mathematical relation should be found for each of the length L_1 and L_2. A computer program could be used to find the analytical expression for force (the coefficient D), L_1 and L_2 are given by (83), (84) and (85):

$$\frac{\sin(\beta_2) \cdot \cos(\beta_1)^3 - 1.0 \cdot \cos(\beta_1)^3 \cdot \cos(\beta_2) + \cos(\beta_1) \cdot \cos(\beta_2)^3 - 1.0 \cdot \sin(\beta_1) \cdot \cos(\beta_2)^3}{\cos(\beta_1) \cdot \sin(\beta_2) - 1.0 \cdot \cos(\beta_2) \cdot \sin(\beta_1)} = D \quad (83)$$

$$\frac{-1.0 \cdot (\cos(\beta_2) - 1.0 \cdot \sin(\beta_2))}{5.0 \cdot \cos(\beta_1) \cdot \sin(\beta_2) - 5.0 \cdot \cos(\beta_2) \cdot \sin(\beta_1)} = L_1 \quad (84)$$

$$\frac{\cos(\beta_1) - 1.0 \cdot \sin(\beta_1)}{5.0 \cdot \cos(\beta_1) \cdot \sin(\beta_2) - 5.0 \cdot \cos(\beta_2) \cdot \sin(\beta_1)} = L_2 \tag{85}$$

The length L_1 and L_2 related to L and H by the (86) and (87)

$$L_1 \cdot \cos(\beta_1) + L_2 \cdot \cos(\beta_2) = L \tag{86}$$

$$L_1 \cdot \sin(\beta_1) + L_2 \cdot \sin(\beta_2) = H \tag{87}$$

The next step here is to analyze the analytical expression for D (drag force) numerically with a computer program in 3D space given by (88)

$$\left(\frac{\sin(\beta_2) \cdot \cos(\beta_1)^3 - 1.0 \cdot \cos(\beta_1)^3 \cdot \cos(\beta_2) + \cos(\beta_1) \cdot \cos(\beta_2)^3 - 1.0 \cdot \sin(\beta_1) \cdot \cos}{\cos(\beta_1) \cdot \sin(\beta_2) - 1.0 \cdot \cos(\beta_2) \cdot \sin(\beta_1)}\right.$$
$$\left. + 0.5 \cdot \left(sign(0.785 - \beta_1)\right)\right] \cdot [0.5 - 0.5 \cdot \left(sign(0.785 - \beta_2)\right)] = D \tag{88}$$

The maximum and minimum force F is illustrated in Fig. 4.61

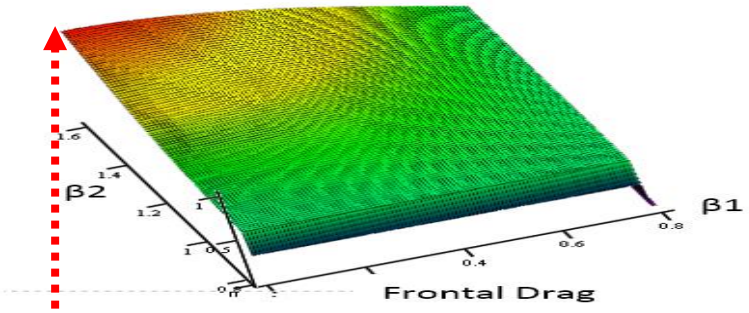

Fig.4.61.Maximum and minimum force F (newtons) solution graph: maximum force F is at $\beta_1 = \boldsymbol{0}$; $\beta_2 = \boldsymbol{\pi/2}$ *(90°)*. The minimum force is at $\beta_1 = \beta_2 = \pi/4$ *(45°)*.

Task 3. Model of two **concave** planes.

The model of two concave planes was analyzed differently when the coordinates x and y of the breaking point were chosen as the variable parameters. A rectangle with sides L and H was considered. As a result, the following expression for the frontal drag force (parameter $D_1(x, y)$) was obtained by a computer program (89):

(89)

$$D_1(x,y)$$
$$= 5.0 \cdot (0.5 \cdot (0.5 \cdot \text{sign}(-\text{x} - \text{y} + 0.2) + 0.5)$$
$$\cdot \left[\frac{x^3}{x^2 + (y-0.2)^2} - \frac{(x-0.2)^3}{y^2 + (x-0.2)^2} \right.$$
$$\left. + \frac{x \cdot (x-0.2) \left[\frac{x \cdot y}{\sqrt{x^2 + (y-0.2)^2} \cdot \sqrt{y^2 + (x-0.2)^2}} - \frac{(x-0.2) \cdot (y-0.2)}{\sqrt{x^2 + (y-0.2)^2} \cdot \sqrt{y^2 + (x-0.2)^2}} \right]}{\sqrt{x^2 + (y-0.2)^2} \cdot \sqrt{y^2 + (x-0.2)^2}} \right]$$
$$+ 5.0 \cdot \left[\frac{(x-0.2)^3}{y^2 + (x-0.2)^2} - \frac{x^3}{x^2 + (y-0.2)^2} \right] \cdot (0.5 \cdot \text{sign}((-\text{x} - \text{y} + 0.2) - 0.5$$

The maximum and minimum force, F is illustrated in Fig. 4.62.

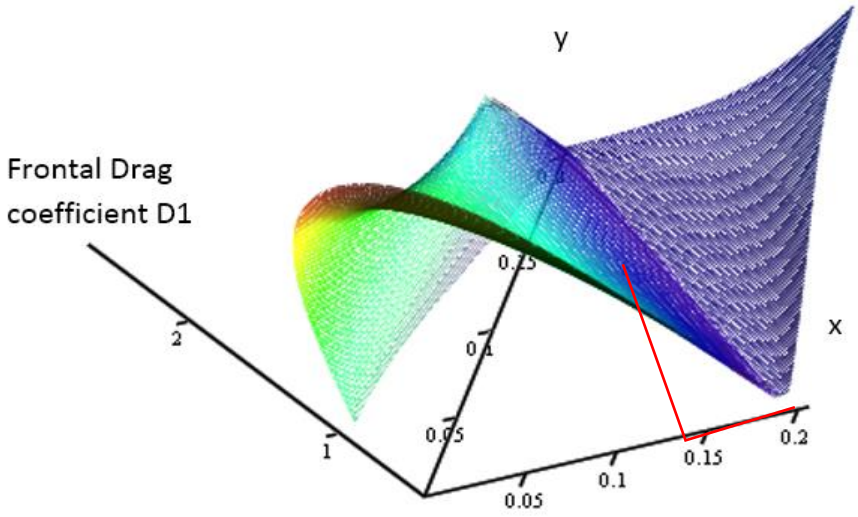

Fig.4.62.Maximum and minimum force F (newtons) solution graph: **maximum** force F is at y = 0 (meters) and 0 < x < L= **0.2.**(meters). The **minimum** force is at $\beta_1 = \beta_2 = \pi/4$ (45°)or x = y.

4.6. Conclusions

1. The developed theory allows obtaining analytical formulas for optimization of fluid-object interaction.
2. By modeling analytical interactions with a computer, it is possible to perform parametric optimization of many parameters in space (even up to 8 parameters and more) for the tasks on damping oscillations or on energy extraction from fluid flow.
3. Control force optimization shows that in real systems it is possible to perform optimal motion control synthesis with such parameters as: object area, object perforation, object position angle to flow and also with object shape selection (for example, in the form of a

broken plane).

4. In the present work a new approximation method was developed for calculating the fluid flow and rigid body interaction according to classical mechanics.

5. As the proposed method is purely mathematical, it allows performing tasks of analysis, optimisation and synthesis for the fluid–rigid body interaction in a simplified way for engineering applications.

6. The developed analytical model can be further extended in performing calculations for flying and diving robot systems.

5. SYNTHESIS OF NEW ENERGY SCAVENGING SYSTEMS

5.1 Single degree of freedom system with varying area prism

A new and novel complex electro-mechanical systems are synthesized by using the phenomenon of fluid-rigid body interaction. The movement of the sharp triangular prism along the x-axis is forming an angle α to the flow. We consider the case where the prism is attached to a base with an elastic spring 3. The energy is obtained by an electro-dynamic braking system 4, Fig.5.1. The differential equation of motion is (90):

$$m \cdot \ddot{x} = -f(x) - D(\dot{x}) - A \cdot \rho \cdot (V_0 \cdot \cos(\beta - \alpha) + \dot{x} \cdot \cos(\beta)^2) \cdot sign(V_0 \cdot \cos(\beta - \alpha) + \dot{x} \cdot \cos(\beta)^2) \quad (90)$$

where $f(x)$ – spring characteristic,
$D(\dot{x})$ – force of electro-dynamic braking system,
A – prism area of pressing zone, as before $A = L \cdot B$.

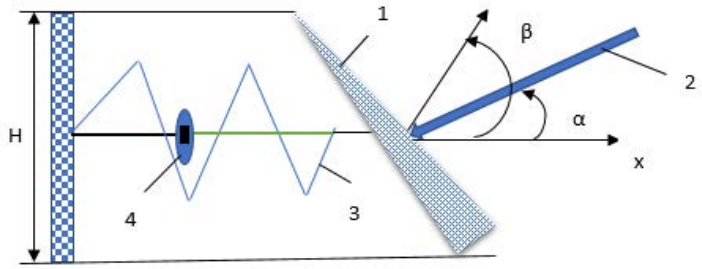

Fig. 5.1.Model for energy extraction by using phenomenon of air – body (prism) interaction, here
1 - sharp triangular prism, 2 - wind flow, 3 - elastic spring,
4 - electro-dynamic braking system.

The resulting (90) allows to solve tasks of analysis, optimization and synthesis encountered in many engineering applications.
For instance, problem of synthesis taks is solved where a change in area A, realized is involved by using perforated plate. Taking into account a linear spring, along with a linear electro dynamic braking system, (91):

$$m \cdot \ddot{x} = -c \cdot x - b(\dot{x}) \cdot \dot{x} - A(\dot{x}, x, t) \cdot \rho(V_0 \cdot \cos(\beta - \alpha) + \dot{x} \cdot \cos(\beta)^2) \cdot sign(V_0 \cdot \cos(\beta - \alpha) + \dot{x} \cdot \cos(\beta)^2); \quad (91)$$

where c – spring constant, $b(\dot{x})$ – control force for electro-dynamic systems,
$A(\dot{x}, x, t)$ – area variation function with time.

The energy optimization task for analysing the power P of the electro - dynamic system is given by (92):

$$P = d(\dot{x}) \cdot \dot{x}^2. \tag{92}$$

Analysing the possibility of obtaining energy from the flow for the change of area for an

$$m \cdot \ddot{x} = -c \cdot x - b(\dot{x}) - (1 + C_1) \cdot A \cdot (a_0 - a_1 \cdot sign(\dot{x} \cdot \Delta v)) \cdot \rho \cdot (V_0 + \dot{x})^2 \cdot sign(-V_0 - \dot{x}), \tag{93}$$

opening or closing the perforation. Assuming a simplest direction of the wind flow parallel to the axis of the prism and with an optimal angle $\beta = 0$ (Fig. 5.1.), the equation of motion in the differential form is given by (93):
where b, C_1, a_0, a_1, Δv are constants.
The results obtained for small variable area prism are shown in Fig. 5.2– 5.5. for parameters: $m = 0.5$ kg; $c = 80$ kg·sec^{-2}; $b = 0.5$ kg· sec^{-1}; $C1 = 0.5$; $A = 0.04$ m^2; $a_0 = 0.75$; $a_1 = 0.25$; $\Delta v = 0.5$ m.sec^{1}; $\rho = 1.25$ kg m^{-3}; $V_0 = 10$ m sec^{-1}.

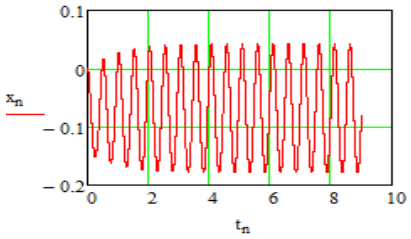

Fig. 5.2. Displacement x_n (meters) in time (seconds) for variable area prism.

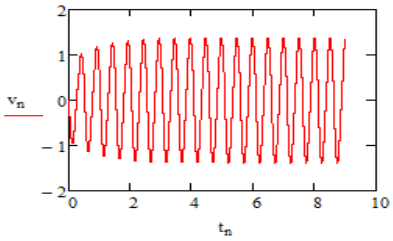

Fig. 5.3. Velocity v_n (meters/second) change in time t_n (seconds) for variable area prism. (sec)

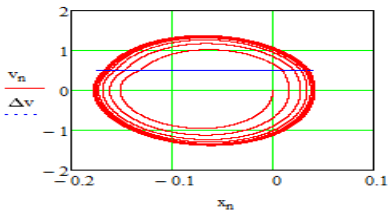

Fig. 5.4. Motion in a phase plane, velocity v_n (meters/second) vs displacement x_n (meters).

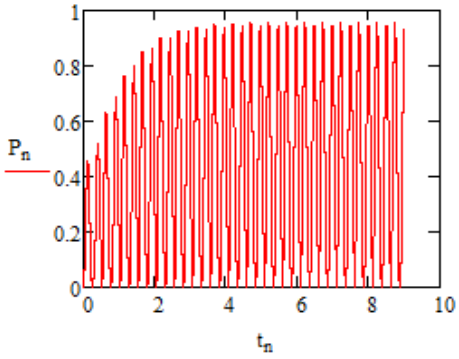

Fig. 5.5. Power P_n (watts) obtained in time t_n (seconds).

5.2 Two degree of freedom system (using rotating perforated plate)

A new electro-mechanical system is synthesized by using flat circular plate with alternate perforated quadrants in fluid flow as shown in Fig. 5.6. Motion analysis in a 2D space is shown in Figs. 5.7–5.9. The system considered consists of the two concentric circular plates fixed at the center, the plate whose front area is subject to fluid flow and is supposed to rotate freely over the other circular plate (non–rotating), both plates have the same area and alternate perforated quadrants, the spring, the linear generator in an incoming flow with a velocity V_0 (10m/s).

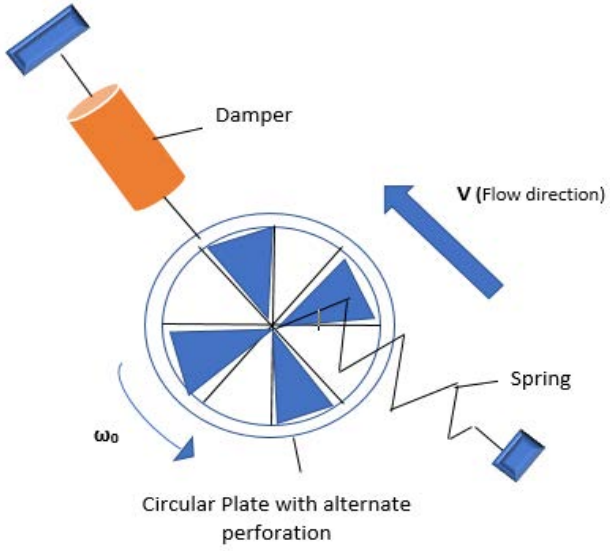

Fig. 5.6. Flat circular plate with alternate perforated quadrants.

V – flow speed, (-b·vx) – force by generators, (-c·x) – spring force, ω0 - angular velocity of rotating part.

$$control = 1 + \frac{\arccos[\cos(\omega_0 \cdot t)}{\pi}$$

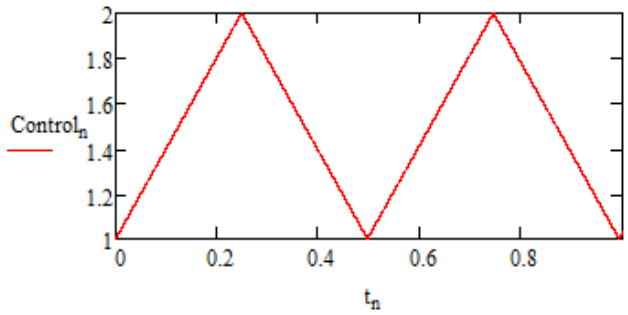

Fig. 5.7. Area control action: t – time (seonds).

Differential equation of circular plate motion in Fig. 5.6 is given by (94):

$$m \cdot \ddot{x} = -c \cdot x - \left[F0 \cdot sign(\dot{x}) - b \cdot \dot{x}\right] + \\ + (1+C) \cdot \frac{A}{\pi} \cdot \left[\text{acos}\left[\cos(\omega 0 \cdot t)\right] + \pi\right] \cdot \rho \cdot (-V0 - \dot{x})^2 \cdot sign(-V0 - \dot{x}), \quad (94)$$

where m – mass, x – displacement, c – stiffness constant for linear spring, F_0, b – constants of linear generator damping, C – coefficient of interaction, V_0 – flow velocity, ω_0 –angular frequency of harmonic control action, A – constant area, ρ – air density.
The task of parametric optimization is as follows:

A combination is to be found with the help of seven parameters - $m, c, F_0, b, \omega_0, A, V_0$ for given constraints on the parameter values that provide the maximum power obtained through the interaction from the fluid flow. The best combination of three parameters - m, c, ω_0 at resonance is taken: $\omega_0 = \sqrt{\frac{c}{m}}$. The graphs for this case are shown in Figs.5.8.-5.9.

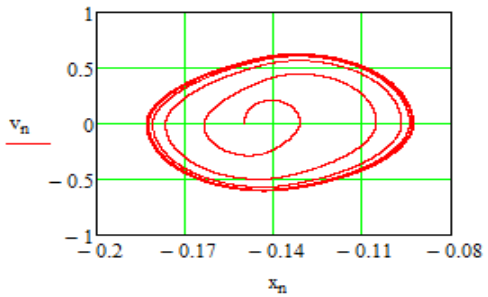

Fig. 5.8. Motion in phase plane velocity v_n (meters/second) vs displacement x_n (meters).

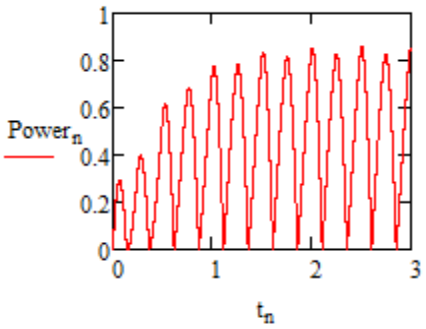

Fig. 5.9. Power (watts) obtained as a time (seconds) function for a small plate.

5.3 Three-degree of freedom system (stretched ribbon)

A new device to produce a flutter of axially stretched flat ribbon model is synthesized. The axially stretched ribbon model is simplified to a system of three degrees of freedom.

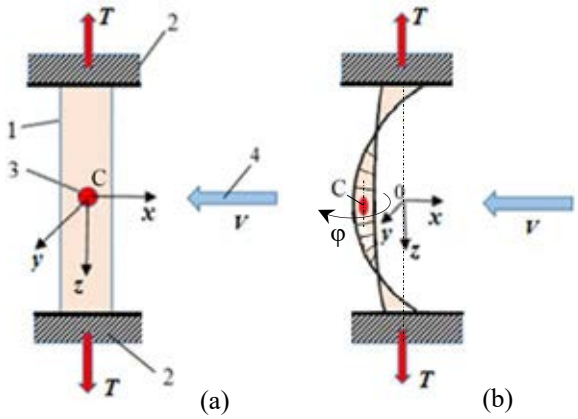

Fig. 5.10 Model of straight flat ribbon: (a) initial condition; (b) deformed state.

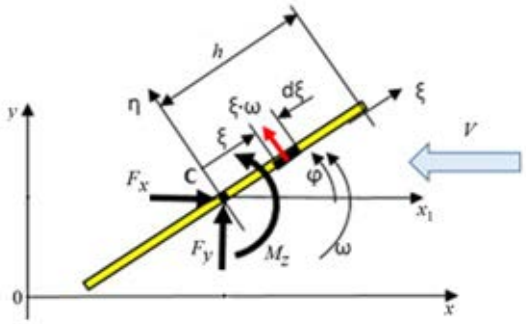

Fig. 5.11. Components of forces and moments in interaction with air flow.

The differential equations of motion of the simplified model as a three-degree of freedom system are as follows (Fig.5.11)

$$m \cdot \ddot{x} = F_x \,;\; m \cdot \ddot{y} = F_y \,;\; J_c \ddot{\varphi} = M_z. \tag{95}$$

Here

$$F_{(x,y)} = P_{e(x,y)} + P_{f(x,y)} + R_{(x,y)}; \tag{96}$$

$$M_z = M_z\left(P_{e(x,y)}\right) + M_z\left(P_{f(x,y)}\right) + M_z\left(R_{(x,y)}\right);$$

In order to determine air flow interaction forces, according to the given 3DOF model of motion, the expression of the relative velocity of a local point in vector form is as follows

$$V_{\xi,n} = \begin{Bmatrix} -(V + \dot{x}\cos(\varphi) - \dot{y}sin(\varphi) \\ (V + \dot{x}\sin(\varphi) - \dot{y}\cos(\varphi) - \xi\omega \end{Bmatrix} \cdot \begin{Bmatrix} i \\ j \end{Bmatrix} \tag{97}$$

From (97) we can find the normal components of the flow interaction N_f and the moment M_f as follows:

$$N_f = (1 + C) \cdot B \cdot \rho \left[\int_{-h}^{h} [(V + \dot{x}\sin(\varphi) - \dot{y}\cos(\varphi) - \xi\omega]^2\right] \xi \cdot d\xi \tag{98}$$

$$M_z\left(P_{f(x,y)}\right) = (1 + C) \cdot B \cdot \rho \left[\int_{-h}^{h} [(V + \dot{x}\sin(\varphi) - \dot{y}\cos(\varphi) - \xi\omega]^2\right] \xi \cdot \varepsilon \cdot d\xi \tag{99}$$

Here

$$\varepsilon = sign[((V + \dot{x}\sin(\varphi) - \dot{y}\cos(\varphi) - \xi\omega], \tag{100}$$

where C is a constant, for example 0.5, B is a width of the plate; ρ is an air density; h is a half of plate height.
Numerical results in MATHCAD are shown in Figs 5.12-5.15:

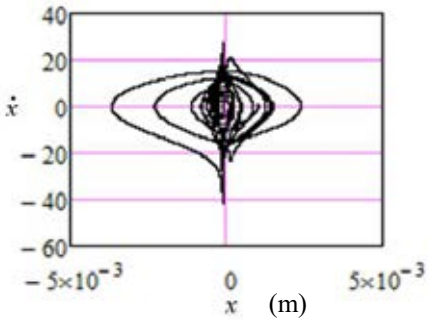

Fig. 5. 12. Centre of mass motion in phase plane x (meters), $\dot{x}$.(meters/second)

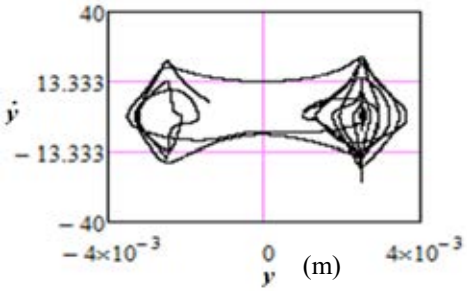

Fig. 5.13. Centre of mass motion in phase plane y (meters) , $\dot{y}$.(meters/second).

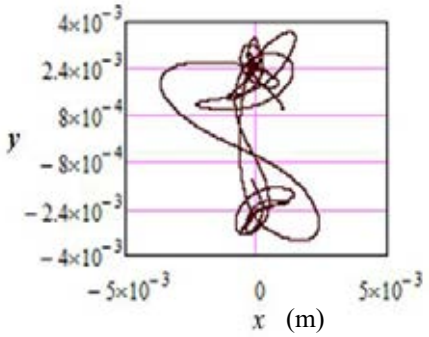

Fig. 5.14. Centre of mass motion in vertical plane y (meters) as against horizontal plane x (meters) .

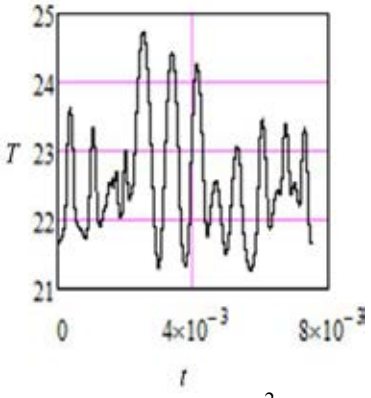

Fig. 5.15. Total tensile strength T (newton/meter^2) of the elastic elements, depending on the time t (milli seconds).

5.4.Conclusions

1. The phenomenon of fluid-rigid body interaction helps in synthesis of approximate mechatronic systems.
2. The task of optimization performed through interaction phenomenon helps to achieve better performance .
3. Since the phenomenon described here has purely mathematical description, in nature it can be extended to any form and to even multi–degree of freedom system.

6. EXPERIMENTAL INVESTIGATIONS

Experiments were carried out in the Armfield wind tunnel available at Riga Technical University. Initially experiments for the square flat plate were performed at a constant uniform speed of 10 m/s in the wind tunnel. The edge length of the flat plate was taken to be 0.16 m and the similar square flat plate with perforations (the area of perforations maintained at half of the total area of the plate) is experimentally investigated. The drag force is measured by using the concepts of balanced weights. Fig. 6.1. shows the flat plate experiment at different angles to the flow for measuring interaction force, drag.

6.1 Experiments in wind tunnel

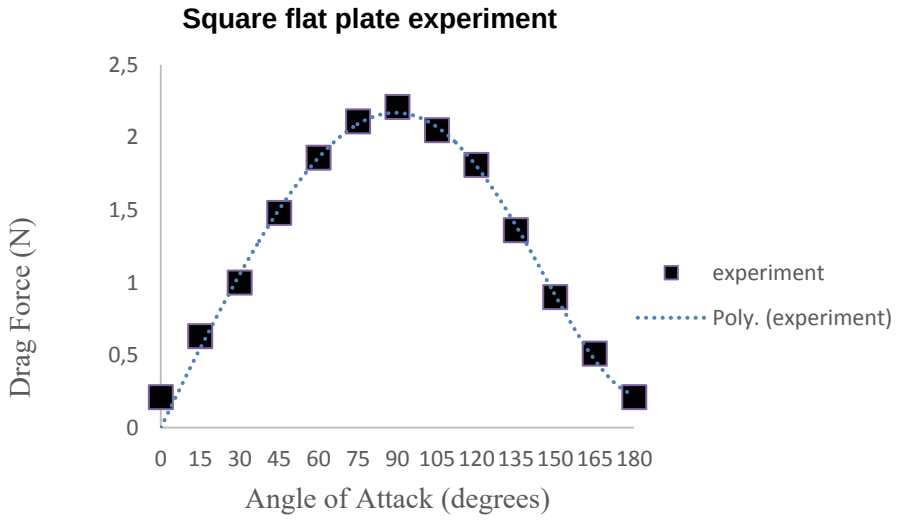

Fig.6.1 Flat plate experiment at constant speed of 10m/s in wind tunnel.

The results of perforated plate experiments as mentioned in Fig. 4.16 were carried out at a constant speed of 10 m/s. Experiments for different alignment of perforations in horizontal and vertical directions were carried out as shown in the Fig.6.3.

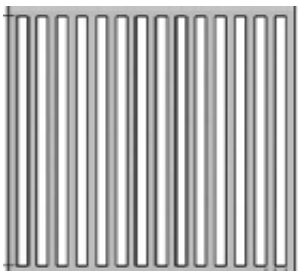

Fig.6.2 Perforated plate with perforations aligned vertically.

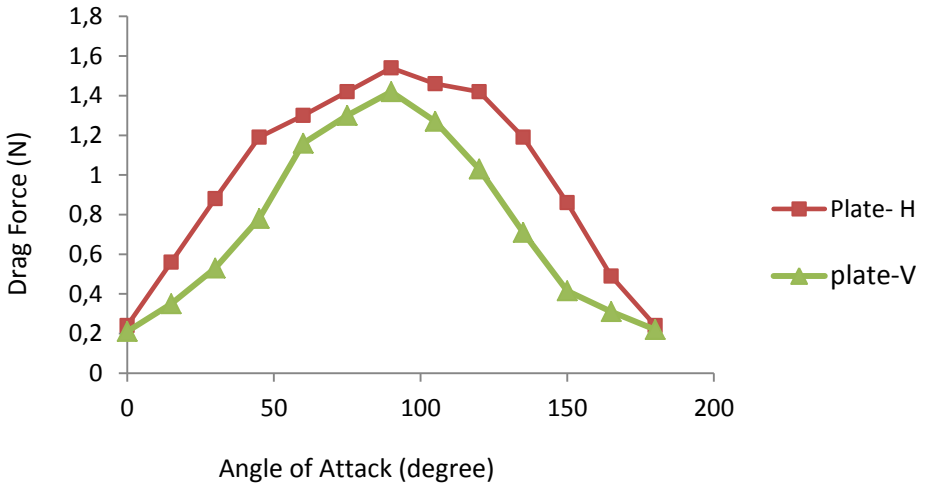

Fig.6. 3.Experiments for perforated plate, perforations aligned in horizontal and vertical direction at a wind speed of 10 m/s.

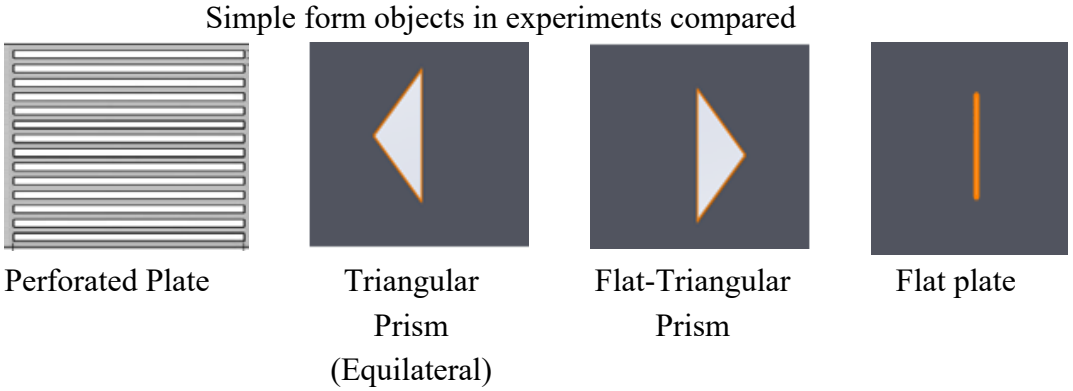

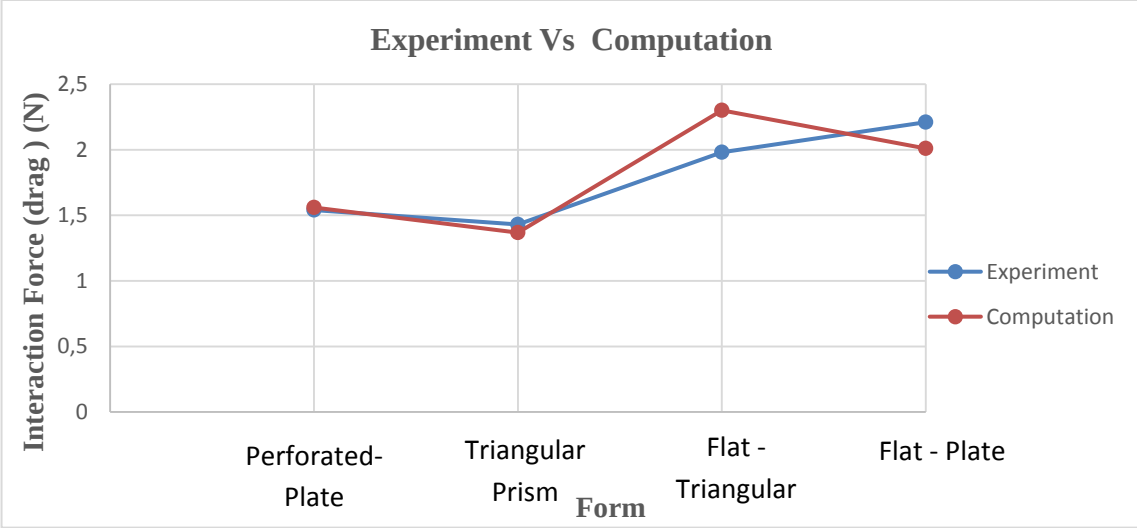

Fig.6. 4.Experiments and computation of interaction force results for different forms at a constant speed of 10 m/s.

6.2 Inspection of new flapping /oscillating device

A new oscillating/flapping device that is fully 3D printed (Fig.6.7) is experimented at different speeds. The model is found to flap/oscillate with much smaller amplitudes at higher speeds. The basic idea is that the concept of flow over the cylinder (due to vortices) would make the plate in the downstream unstable thereby setting the flat plate in flapping motion. From the experiments the fact that with flow induced vibration by inserting plate down of a cylinder would not help to obtain energy, the same is true with the perforated plate. Therefore, in the suction area of a plate, the vortices are inefficient and cannot be used for energy scavenging. ANSYS 3D results for cylinder and flat plate interaction are shown in Fig. 6.5.

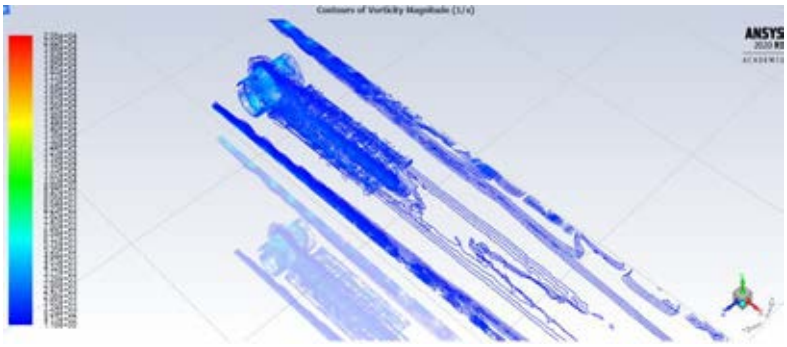

Fig.6.5 Contour of vorticity for cylinder-flat plate model.

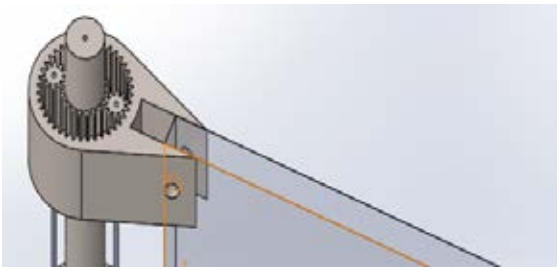

Fig.6.6 3D design of a model from SolidWorks.

Fig.6.7 Prototype of the flapping device.

Fig.6. 8.Flapping device in the wind tunnel.

6.3 Conclusions

1. For any given geometry, the drag force has maximum when aligned normally to the flow.
2. For a given geometry, perforated model has less drag as compared to the non-perforated.
3. The new device model is to be improved to start flapping/oscillations at low speeds.
4. It is not possible to obtain a significant amount of energy with one vibrating flat plate (1DOF).
5. Energy recovery studies shall be performed for a double pendulum (2DOF) system, or for a pendulum with a flexible suspension.

6.4.Validation of theory by experiments

6.4.1. Damping oscillations of thin plates in open air in rotational movement

Experimental setup of a model of one degree of freedom (1DOF) pendulum is shown in Fig. 6.10–6.12. A simple experiment setup in order to validate the theory of interaction coefficient *C* by taking into account the concept of zones (pressure and suction side) was performed. It was noted that in reality the difference between the theory and experimets was only about 1.8% during the starting time period.

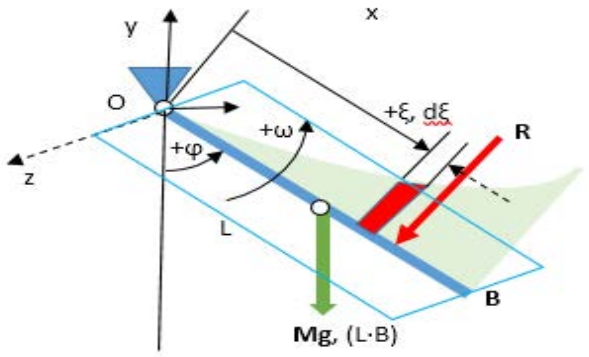

Fig.6.9 Free body diagram of the pendulum.

Fig.6.10 Motion of the pendulum (start from the mean position).

Fig.6.11 Motion of the pendulum oscillating about the mean postion.

Fig.6.12 Motion of the oscillating pendulum-experimental setup.

6.4.2 Comparison of theory and experiment for C =0.5

Differential equation of motion of the physical pendulum is given by (100):

$$\ddot{\varphi} = -3 \cdot g \cdot \left(\frac{1}{2}\right) \cdot \sin(\varphi) - (1 + C) \cdot B \cdot \rho \cdot \left[\frac{3 \cdot L^2}{4 \cdot m} \cdot (\dot{\varphi})^2\right] \cdot sign(\dot{\varphi}), \qquad (100)$$

where φ is the angular displacement, L –length, m-mass, C – coefficient of interaction, B – width of the pendulum.

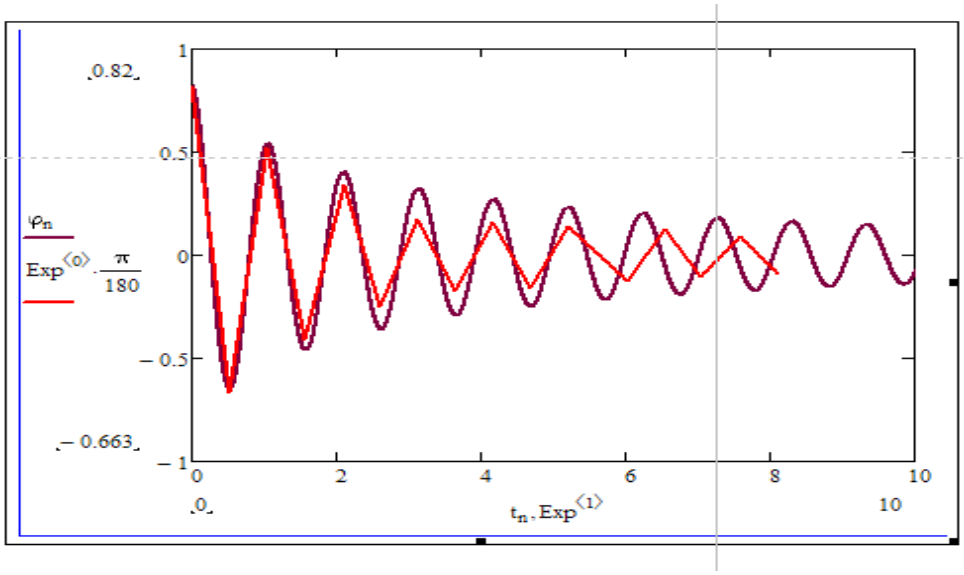

Fig.6. 13.Angular displacement (radians) with time (seconds) (comparison for experiment and numerical calculation).

Starting period for numerical calculation was T_s = 1,0774 s

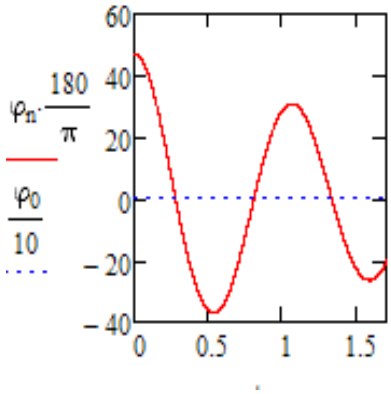

Fig.6. 14.Starting Period (Numerical calculation) angular displacement φ_n (degrees) against time (seconds).

Starting period for experiments was T_{se} = 1,02 s

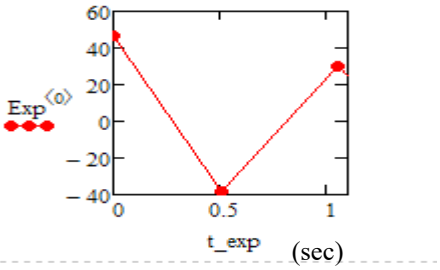

Fig.6. 15.Starting Period (practical experiment) angular displacement φ_n (degrees) against time (seconds) .

6.4.3 Comparison of theory and experiment for C=0,25

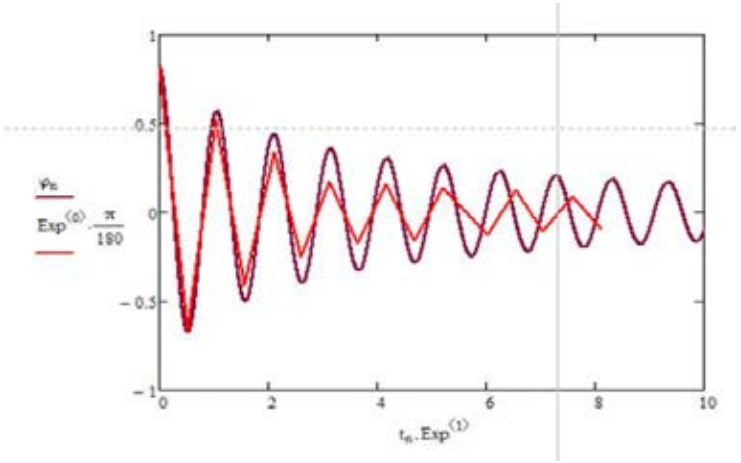

Fig.6.16 Angular displacement (degress)with time (seconds) for C = 0.25 (comparison for experiment and numerical calculation).

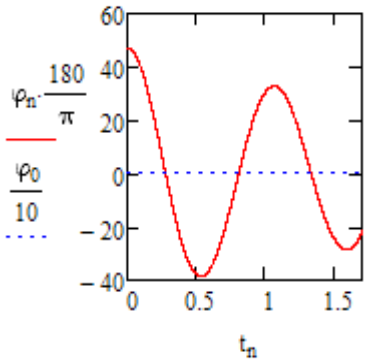

Fig.6.17 Starting Period (Numerical calculation) T_s.=1,0764 s angular displacement φ_n (degrees) against time (seconds) .

6.5. New invention

Within the framework of the mentioned doctoral thesis, in cooperation with other scientists of RTU MTAF, an invention was made regarding the extraction of energy from the vibration motion of a flat plane in the wind flow.

WIND ENERGY CONVERSION EQUIPMENT

Patent authors:

1. Janis Viba, Dr.habil.sc.ing., RTU, MTAF TMMP Department Professor,
2.Vitalijs Beresņevičs, Dr.sc.ing., RTU, MTAF TMMP Department Professor,
3. Martins Irbe, RTU, TMAF, scientific laboratory of Experimental Mechanics of Materials, Researcher,
4.Igors Tipans, Dr.sc.ing., RTU, TMAF TMMP Department, Leading Researcher,
5.Shravan Koundinya Vutukuru, RTU, MTAF TMMP Department, Assistant, Doctoral student,
6. Edgars Kovals, Dr.sc.ing., RTU, TMAF TMMP Department, Senior Laboratory Assistant,
7. Maris Eiduks, RTU, TMAF TMMP Department, Senior Laboratory Assistant.

The invention is related to wind energy, in particular to wind turbines, which convert the kinetic energy of the wind flow into other types of energy (for example, the kinetic energy of the actuator of the machine, or the potential energy of the air compression, or special equipment) (Fig.6.18.).

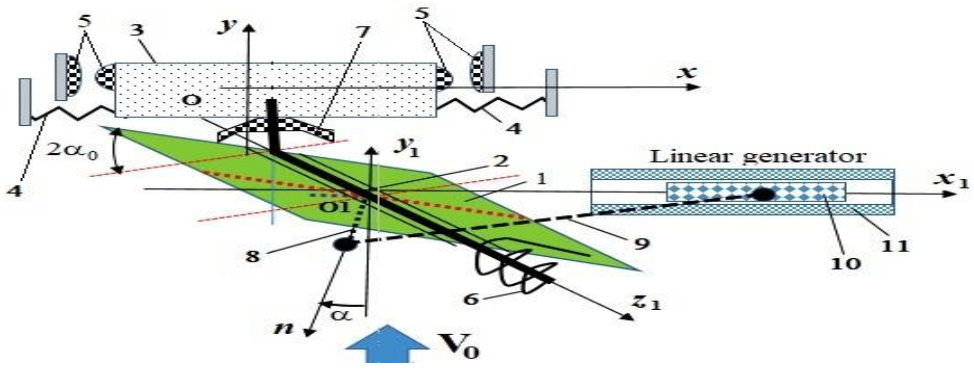

Fig.6.18. Model of the wind energy conversion generator.
1 – Flat blade, 2 – rotating axle, 3 – slider, 4 – spring, 5 – shock absorber, 6 – rotational spring, 7 – rotational shock absorber, 8 – crank, 9 – connecting rod, 10 – slider of linear generator, 11 – electric coil.

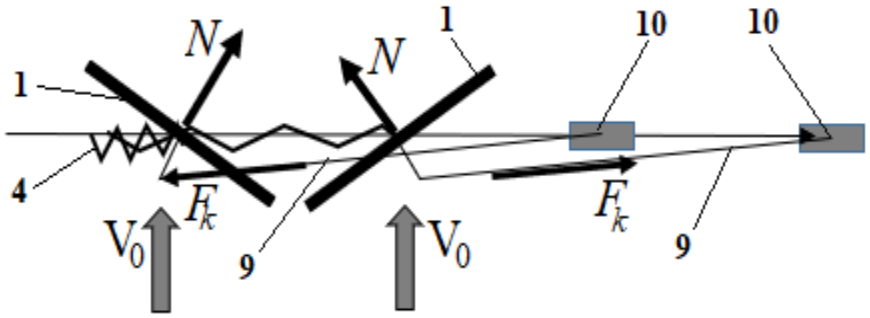

Fig.6.19. Limits positions.

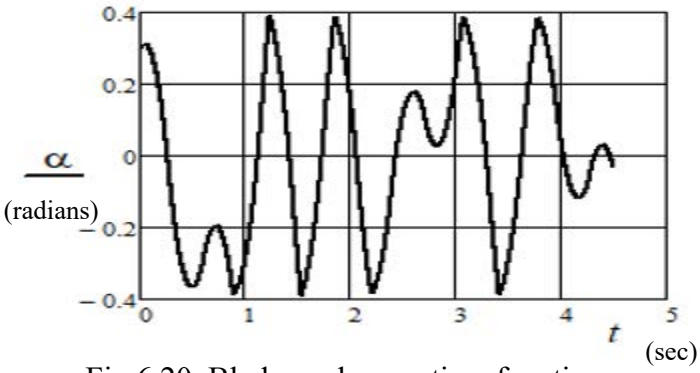

Fig.6.20. Blade angle α as time function.

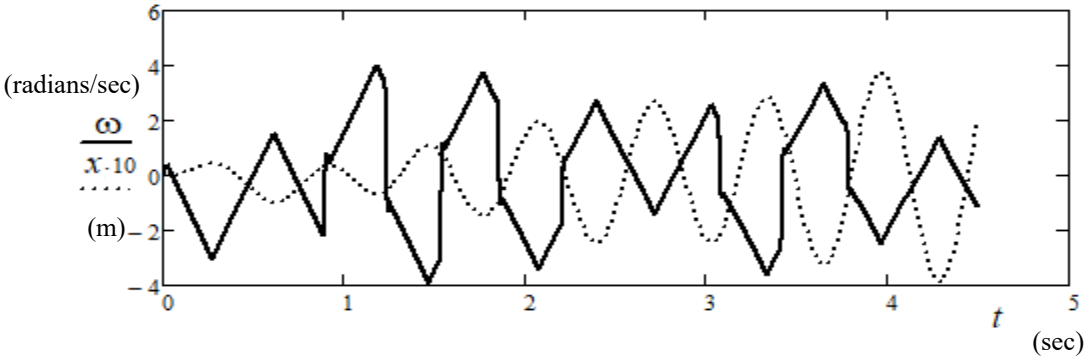

Fig.6.21. Displacement and angular velocity as time t function.

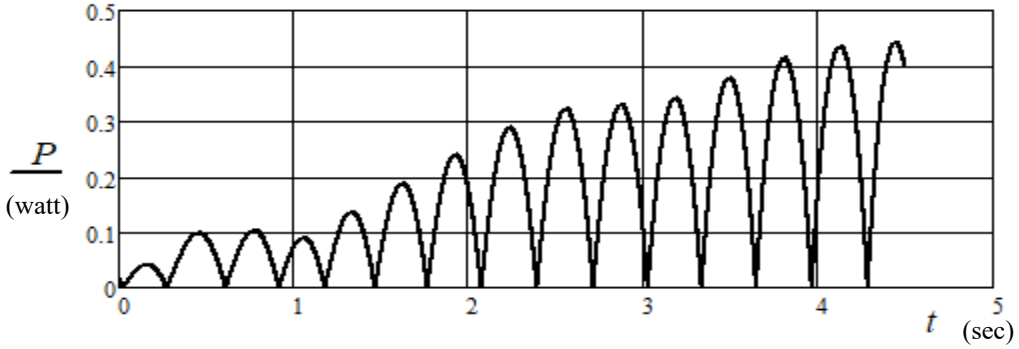

Fig.6.22. Power as time function in starting region.

PRIOR ART

Wind power devices are well-known, the operation of those devices is based on the effect of wind flow on the blades evenly distributed around the circumference of the wind wheel, and the conversion of the kinetic energy of the flow into the mechanical energy of the rotational motion of the wind wheel [65, 66]*. However, these devices do not provide for a change in the orientation of blades during the operation, which does not allow for a rational orientation of the blade against the wind flow at all times. Therefore, the potential for energy conversion in certain wind farms has not been fully exploited and can only be used effectively in relatively strong wind conditions. A wind power plant is known, the rotor of which is equipped with flat blades, and the blades can rotate in relation to the wind flow as a result of its action [67] *. According to the principle of operation of this device, in the rotor rotation stages, where the blade moves in the direction of the wind flow, the relative rotation of the blade is limited by a special support. Thus, in the first stage of movement (in the direction of the wind flow), the working surface area of the blade has a radial orientation towards the rotor axis. Conversely, in the second stage of movement (against the wind flow) the relative rotation of the blade is not limited, so as a result of the effect of wind pressure the blade rotates and its working surface tries to become parallel to the flow. As a result, the air resistance force in the second phase of the movement is significantly reduced. Thanks to the above-described cyclic turns of the blades with two stages, it is possible to significantly reduce the braking forces in the return of the blade in the second stage and thus increase the efficiency of the wind power plant. In the context of this application, the term 'operational efficiency of a wind power installation' means the extraction of maximum net power from existing wind flow at a speed of V_0. However, in a known device [67] * it is not possible to change the orientation of the blade against the wind flow during the rotor rotation, so that the aerodynamic wind interaction force resulting in each first and second stage of movement creates the maximum possible driving torque against the rotor longitudinal axis. This disadvantage prevents the full use of wind energy conversion possibilities, as the position of the blade in the wind flow is close to the optimal (when the resulting aerodynamic force forms the maximum moment in relation to the rotor axis) only in the first stage of movement (in the direction of wind flow). This significantly reduces the efficiency of wind energy conversion. The closest to the invention in terms of technical nature is a wind energy conversion device comprising a rotor and flat blades attached to a rotor with cylindrical axial hinges, the longitudinal axis of the hinges being parallel to the longitudinal axis of the rotor [68] *. The axes of rotation of the rotor and the blades are kinematically connected to each other by a motion conversion mechanism, moreover, the angular velocity or frequency ratio of the rotation of the rotor and the blades is equal to 2 (assumed as a prototype). The conversion mechanism of the prototype device rotates the blades together with the

rotor according to a certain law, as a result of which the orientation of the blades towards the wind flow is optimal at each time, i.e. the resulting aerodynamic force creates a maximum moment in relation to the rotor axis. This provides an opportunity to increase significantly the efficiency of wind energy conversion. However, the prototype device has drawbacks, which are especially evident with the increase in the number of flat blades. The number of blades is increased to improve the efficiency of wind energy conversion and the capacity of the plant. But if the number of blades is more than one, then the front (airflow side) blades cover and obstruct the airflow access to the rear blades. As a result, the airflow to the rear blades can vary in direction and size, and air vortices are formed between the blades in their interior. In general, it slows down the rotation of the central rotor, which has a negative effect on the efficiency of the wind turbine (the net power obtained). Increasing the radial size of the flat blade is used to increase the efficiency of the prototype machine, but it reduces the reliability of the machine by increasing the final speed and noise of the flat blade, which increases the likelihood of injuring living beings with the rotating flat blade.

Purpose and essence of the invention

The object of the invention is to increase the operational safety of a wind energy conversion plant and the operational efficiency of a wind energy plant. To achieve this, the wind energy conversion device is equipped with a flat blade (1) attached to a rotating shaft (2) with a cylindrical axial joint (Fig.6.18). Unlike the prototype, the longitudinal axis of the rotating shaft (2) coincides with the axis of symmetry of the blade, and the rotating shaft (2) is firmly connected to a slider (3), which has the ability to move in special guides. In addition, the forward movement of the slider (3) is limited by springs (4) and shock absorbers (5). In turn, the rotation of the blade around its axis of symmetry is limited by a rotational spring (6) and a shock absorber (7). A crank (8) is firmly attached to the side surface of the flat blade (1) in a direction perpendicular to it, which is hinged to the connecting rod (9). In turn, the connecting rod(9) is hinged to a linear generator in a slider (10), which has the ability to move inside the electric coil (11).

The invention is illustrated by drawing Fig. 6.18 - schematic diagram of the invention device where 1 - flat blade, 2 - rotating shaft, 3 - slider, 4 - springs, 5 - shock absorbers, 6 - rotational spring, 7 - rotary shock absorber, 8- crank, 9 - connecting rod, 10 - linear generator slider, 11 - electric coil. V_0 - wind flow speed is perpendicular to the direction of movement of the slider 3; x_0y - fixed coordinate system; $O_1x_1y_1z_1$ - moving coordinate system related to the axis of rotation 2; n - normal to the flat side surface of the flat blade 1; α is the angle of rotation of the flat blade 1 about z1 axis. Fig. 6.19 shows sequential position of the blade during the operation of the invention: 1 - flat blade, 4 - spring, 9 - connecting rod, 10 - linear generator slider; V_0 - wind flow speed,

which is perpendicular to the direction of movement of the slider 3; N - normal force acting on the flat blade 1; F_k - axial force of the connecting rod 9. Fig. 6.20 shows cyclic change in the angle of rotation α of the flat blade 1 during t. Fig. 6.21. illustrates graphs of the change of the angular velocity ω of the flat blade 1 and the displacement x of the slider 3 at time t. Fig. 6.22 shows cyclic change of power P generated by the invention during time t.

Example of realization of the invention

For carrying out the invention, the wind energy conversion device is equipped with a flat blade 1 attached to a rotating shaft 2 with a cylindrical axial joint (Fig. 6.18). The longitudinal axis of the rotation 2 coincides with the symmetry axis z_1 of the flat blade 1 and is firmly connected to a slider 3 which has the ability to move along special guides in the x-axis direction, the slider 3 being limited by springs 4 and shock absorbers 5. In turn, the rotation of the flat blade 1 around the axis 2 is limited by the rotational spring 6 and the rotational damper 7. A crank 8 is firmly attached to the side surface of the flat blade 1 and is hinged to the connecting rod 9. In turn, the connecting rod 9 is hinged to the linear generator slider 10 which has the ability to move along the inside of the electric coil 11 in the direction of the x_1 axis. The device of the invention operates as follows: at the beginning of the cycle, in the position of the device shown in Fig. 6.18, a wind flow at a speed V_0 perpendicular to the direction of movement of the slider 3 (axis x) acts on the flat blade 1. Force N (Fig. 6.19) is generated in the direction of normal n, which causes the slider (3) to move to the right in the direction of the x-axis. As a result, a compressive force F_k is generated in the connecting rod 9. The compressive force F_k from the connecting rod 9 and the braking linear generator consisting of a slider 10 and electric coil 11 holds the rotating flat blade 1 at the left rotational shock absorber 7. The angle of rotation α in this position of the device reaches its maximum value α_0 clockwise. The spring 4 is applied, then the right damper 5 is deformed until the slider 3 stops in the right extreme position. Then, as a result of the elastic forces from the spring 4 and the right shock absorber 5, the slider 3 moves backwards, to the left. At the beginning of this movement, the connecting rod 9 is stretched, and thus the direction of the force F_k changes to the opposite (Fig. 6.19). The flat blade 1 rotates around the symmetry axis z_1 counterclockwise until it reaches the right rotary damper 7. The angle of rotation α in this position of the device reaches its maximum value α0 counterclockwise. As a result, the normal n position of the flat blade 1 against the wind flow changes at a speed of V_0. The force Fk now presses against the flat blade 1 in the opposite direction to the x axis. As a result, the slider 3 deforms the spring 4 and the left shock absorber 5 by moving to the left until the slider 5 stops in the leftmost position. The cycle will then be repeated as the compressive force F_k reappears in the connecting rod 9. During said cyclic movement, the linear generator slider 10 moves back and forth along the inside of the electric coil 11 along the x_1 axis. As a result, electrical energy is

produced in the linear generator (electric alternating current in the coil 11). The principle of operation of a linear generator is described in the literature [69] and is not the subject of the invention. The inventive device has advantages over the prototype, which can be explained by the specifics of the construction of the invention device. The device of the invention has one flat blade, so in principle it is not possible for the flow of wind to flow between the blades, which reduces the efficiency and safety of the prototype device. In addition, the generation of useful power in the device of the invention is related to the directional movement of the flat blade 1 and the slider 3 (Fig. 6.18), so that the wind flow interaction forces are evenly distributed along the side surface of the flat blade 1. This provides an easy way to increase the efficiency of the invention. This can be achieved by increasing the area A of the side surface of the flat blade 1, because the power to be generated P increases in proportion to the area A according to the formula [70]**:

$$P = C \cdot A \cdot V^3, \qquad [70]^{**}$$

where C - constant, V - relative speed of wind flow against the lateral surface of a flat blade. Such a possibility to increase the operational efficiency does not exist in the prototype device, because the generation of useful power in it is related to the rotational movement of the flat blade. During the rotational movement of the blade, the indicated moment of the wind flow against the axis of rotation can be increased by increasing the radial size of the flat blade. But that reduces the reliability of the equipment, as the speeds of the flat blade end points increase, resulting in increased noise [70]* and increased likelihood of injury to living beings with the rotating flat blade. In the device of the invention, the flat blade does not rotate, as a result of which the noise level is significantly reduced, moreover, the probability of injuring flying creatures is reduced.

In general, it increases the operational safety of the invention device. The performance and efficiency of the invention device is based on mathematical modelling by using Mathcad software [70]*. The modelling was performed by assuming the following equipment and flow parameters of the invention: flat blade dimensions= 0.160 m x 0.160 m x 0.002 m; flat blade mass m = 0.399 kg; the stiffness coefficient of the spring (4) c_1 = 39.177 N / m; the stiffness coefficient of the rotational spring (6) c_2 = 20 Nm / rad; the coefficients of the viscosity of the motion and rotational motion b = 0.01 kg / s and b_2 = 0.1 Nms / rad; wind flow speed V_0 = 10 m / s. The simulation results are shown graphically: the change of the rotational angle α of the flat blade (1) during the cyclic change is shown in Fig. 6.20**,** while the change of the angular speed of the flat blade (1) is shown in Fig. 6.21. In addition, Figure 6.21 shows the slider (3) during the change in displacement x. As a result of the operation of the invention device, the power P was generated, which is confirmed by the graph P = f (t) (Fig. 6.22). In addition, during the modelling, it was demonstrated that as the working surface area A of the flat blade

increases, the generated power P also increases proportionally. Thus, the modeling results confirm the operational safety of the device of the invention and the operational efficiency of the wind power plant.

CLAIM

A wind energy conversion device Fig.6.18, comprising a flat blade 1 attached to a rotating shaft 2 with a cylindrical axial hinge, characterized in that the longitudinal axis of the rotating shaft 2 coincides with the axis of symmetry of the flat blade 1 and is rigidly connected to a slider 3, which has the ability to move along special guides, moreover, the movement of the slider 3 is limited by springs 4 and shock absorbers 5, while the rotation of the flat blade 1 around the rotating axis 2 is limited by rotational movements of a spring 6 and a rotational shock absorber 7, but a crank 8 is firmly attached to the side surface of the flat blade 1, which is hinged to the connecting rod 9, and the connecting rod 9 is hinged to the linear generator slider 10, which has the ability to move along the inside of the electric coil 11.

PATENT SUMMARY

The invention relates to new method for wind to energy conversion based on utilization of flat blade's translation motion. The device is first of its kind to adopt a single flat blade for the only purpose of energy scavenging from air flow. The object of the invention is to increase the operational safety of a wind energy conversion plant and the efficiency of a wind energy plant.

Working principle

Cyclic motion of the device begins with the wind flow as shown in Fig.6.18. The wind flow at a speed of V_0, directed perpendicular to the direction x of motion of the slider 3, acts on the flat blade 1. As a result, compressive force F_k is formed in the connecting rod 9 due to the normal force N that causes movement in the slider 3 as shown in the Fig.6.19. The movement of the slider 3 at the extreme ends is controlled by the spring 4 and shock absorber 5 and also influenced by the blade turning angle. Due to the tension in the connecting rod 9 at the extreme turning angles of the blade a cyclic movement is created. As a result of the cyclic movement, slider 10 of the linear generator inside the electric coil 11 moves forward and backward there by creating an electric energy. The energy could be also termed as "clean energy" or "green energy".

GENERAL CONCLUSIONS

1. In the present work, only air as a surrounding medium is taken into consideration, but the technique with minor variations can be extended for other fluids of interest where rigid body–fluid interactions are to be studied.
2. The task of optimization can also be extended for complex geometries, but only at low speeds.
3. For synthesis of new mechanical systems, object parameters play an important role along with the interaction phenomenon.
4. For analysis of oscillations induced by the flow it is essential role in selection of a damper. A linear damper is deployed, and it is anticipated that use of non-linear damper would increase the overall efficiency of the system under consideration.
5. The coefficient of interaction C can be found by solving tasks of energy scavenging, synthesis and optimization through fluid-rigid body interaction phenomenon. Though viscous nature of the fluid medium is not considered, by using the determination of interaction coefficient C alternative and good results could be achieved.
6. Parametric optimization is needed if a very good efficiency is desired.
7. In case of unsteady flow, the constant pressure at the boundary layer just downstream of the object gets split at the point of symmetry. Thus a variation in pressure on the either side of the symmetry in the downstream side can be observed.
8. The results are only valid for a rigid-body and fluid interaction at low speeds.
9. The concept or technique proposed in the work is first of its kind that helps eliminate complex “space-time” programming techniques and is an advantage to analyse the phenomenon of non-stationary motion in a fluid flow.
10. When considering the interaction phenomenon for a stationary rigid body in air , the viscousity of air is of secondary importance. The object parameters, selection of type of damper, form or shape of the object subjected to the fluid flow and nature of flow - laminar or turbulent - are of primary importance.

REFERENCES

[1] S.P. Bhakade, S.G.Kumbhar, Y.B.Mohite and P.V.Kenga, "A Review on Fluid Structure Interaction Analysis Methodology", International Journal of Trend in Research and Development, Volume 3(3), ISSN: 2394-9333,pp 617-6199.

[2] G. Wei, "A fixed -mesh method for general moving objects in fluid flow",. International journal of modern physics B, vol.19, No. 28 n 29, pp 1719-1722. 2005. doi.org/10.1142/S021798490501030X

[3] T. Wick, "Fluid -structure interactions using different mesh motion techniques'',Journal of Computers and structures. vol. 89(13): 1456-1467. 2011. doi.org/10.1016/j.compstruc.2011.02.019

[4] R. Codina, G. Houzeaux, H.C. Owen & J. Baiges, "The fixed mesh ALE approach for the numerical approximation of flows in moving domain".Vol. 228(5), 1591-1611pp. 2009. doi.org/10.1016/j.jcp.2008.11.004

[5] M. Neumuller, & O. Steinbach, "Refinement of flexible space -time finite element meshes and discontinuous galerkin methods", Computing and visualization in science. Vol.14, 189-205 pp. 2011. doi.org/10.1007/s00791-012-0174-z

[6] A. Gerstenberger, & W.A. Wall , "An extended finite element method based approach for large deformation fluid-structure interaction". European conference on computational Fluid Dynamics. ECCOMAS CFD, Netherlands, TU Delf. 2006

[7] M. Behr, "Simplex space -time meshes in finite element simulations". International journal for numerical methods in fluids.Vol.57 (9), 1421-1434 pp, 2008. **https://doi.org/10.1002/fld.1796**

[8] M.V. Danwitz, V. Karyofylli, N. Hoster & M. Behr . "Simplex space - time meshes in compressible flow simulations". International journal for numerical methods in fluids. vol. 91. 2019. **https://doi.org/10.1002/fld.4743 .**

[9] L.T. Diosady, S.M.Murman, & C. Carton de Wiart, " A higher order space time finite element method for moving body and fluid structure interaction problem", 10th international conference on computational fluid dynamics (ICCFD10) July 9-13 (pp. 1-16) ,2018, Barcelona, Spain..

[10] Santo, G., Peeters, M., Van Paepegem, W., & Degroote, J. (2020). Fluid–Structure Interaction Simulations of a Wind Gust Impacting on the Blades of a Large Horizontal Axis Wind Turbine. Energies, 13(3), 509. https://doi.org/10.3390/en13030509

[11] Boujleben, A., Ibrahimbegovic, A., & Lefrançois, E. (2020). An efficient computational model for fluid-structure interaction in application to large overall motion of wind turbine with flexible blades. Applied Mathematical Modelling, 77, 392-407. https://doi.org/10. 1016/j.apm.2019.07.033

[12] Peralta, G., & Kunisch, K. (2020). Analysis and finite element discretization for optimal control of a linear fluid–structure interaction problem with delay. IMA Journal of Numerical Analysis, 40(1), 140-206. https://doi.org/10.1093/imanum/dry070
[13] Trifunović, S., & Wang, Y. G. (2020). Existence of a weak solution to the fluid-structure interaction problem in 3D. Journal of Differential Equations, 268(4), 1495-1531. https://doi.org/10.1016/j.jde.2019.09.002
[14] Amin, M. M., & Kiani, A. (2020). Multi-Disciplinary Analysis of a Strip Stabilizer using Body-Fluid-Structure Interaction Simulation and Design of Experiments (DOE). Journal of Applied Fluid Mechanics, 13(1), 261-273. [53] https://doi.org/10.29252/jafm.13.01.30253
[15] Shkara, Y., Cardaun, M., Schelenz, R., & Jacobs, G. (2020). Aeroelastic response of a multimegawatt upwind horizontal axis wind turbine (HAWT) based on fluid–structure interaction simulation. Wind Energy Science, 5(1), 141-154. https://doi.org/10.5194/wes-5-141-2020
[16] Yang, Y., Liao, H., Xu, Y., Yang, S., & Niu, J. (2019). Coupled fluid-structure simulation of a vibration-assisted rotary percussion drilling tool. Energy Sources, Part A: Recovery, Utilization, and Environmental Effects, 41(14), 1725-1738. https://doi.org/10.1080/155670 36.2018.1549147
[17] Ullah, H., Hussain, M., Abbas, N., Ahmad, H., Amer, M., & Noman, M. (2019). Numerical investigation of modal and fatigue performance of a horizontal axis tidal current turbine using fluid–structure interaction. Journal of Ocean Engineering and Science, 4(4), 328-337. https://doi.org/10.1016/j.joes.2019.05.008
[18] Shi, F., Wang, Z., Zhang, J., Gong, Z., & Guo, L. (2019). Influences of wind and rotating speed on the fluid-structure interaction vibration for the offshore wind turbine blade. Journal of Vibroengineering, 21(2), 483-497. https://doi.org/10.21595/jve.2018.19356
[19] Nietiedt, S., Goering, M., Willemsen, T., Wester, T. T. B., Kröger, L., Guelker, G., & Luhmann, T. (2019). Measurement of Fluid-Structure Inter-Action of Wind Turbines In Wind Tunnel Experiments: Concept And First Results. International Archives of the iJES – Vol. 8, No. 3, 2020 45 Paper—FSI in Wind Turbines: A Review Photogrammetry, Remote Sensing & Spatial Information Sciences. https://doi.org/10.5194/isprs-archives-xlii-2-w18-143-2019
[20] Badshah, M., Badshah, S., VanZwieten, J., Jan, S., Amir, M., & Malik, S. A. (2019). Coupled Fluid-Structure Interaction Modelling of Loads Variation and Fatigue Life of a FullScale Tidal Turbine under the Effect of Velocity Profile. Energies, 12(11), 2217. https:// doi.org/10.3390/en12112217
[21] Zhu, R., Chen, D. D., & Wu, S. W. (2019). Unsteady Flow and Vibration Analysis of the Horizontal-Axis Wind Turbine Blade under the Fluid-Structure Interaction. Shock and Vibration, 2019. https://doi.org/10.1155/2019/3050694
[22] Laß, A., Schilling, M., Kumar, J., & Wurm, F. H. (2019). Rotor dynamic analysis of a tidal turbine considering fluid–structure interaction under shear flow and waves.

International Journal of Naval Architecture and Ocean Engineering, 11(1), 154-164. https://doi.org/10. 1016/j.ijnaoe.2018.03.002

[23] Li, Z., Wang, Y., Li, T., Liu, F., & Ji, J. (2019). The dynamic characteristics of the ultimate strength of a turbine runner blade under hydraulic excitation. Energy Sources, Part A: Recovery, Utilization, and Environmental Effects, 41(24), 3127-3137.https://doi.org/10.10 80/15567036.2019.1586014

[24] Papoulias, G., Nousias, S., & Moustakas, K. (2019, July). Fluid-structure interaction simulation framework for cerebral aneurysm wall deformation. In 2019 10th International Conference on Information, Intelligence, Systems and Applications (IISA) (pp. 1-7). IEEE. https://doi.org/10.1109/iisa.2019.8900781

[25] Rahmani, S., Jarrahi, A., Saed, B., Navidbakhsh, M., Farjpour, H., & Alizadeh, M. (2019). Three-dimensional modeling of Marfan syndrome with elastic and hyperelastic materials assumptions using fluid-structure interaction. Bio-medical materials and engineering,30(3), 255-266. https://doi.org/10.3233/bme-191049

[26] Fournié, M., Ndiaye, M., & Raymond, J. P. (2019). Feedback stabilization of a two-dimensional fluid-structure interaction system with mixed boundary conditions. SIAM Journal on Control and Optimization, 57(5), 3322-3359. https://doi.org/10.1137/18m1172405

[27] Li, S., Li, R., Wang, Z., Xu, D., Yan, Y., Xu, Y., & Chen, X. (2019). Fluid-Structure Interaction Vibration Response Analysis of the Hydrocyclone Under Periodic Excitation. IEEE Access, 7, 146273-146281. https://doi.org/10.1109/access.2019.2945837

[28] Zhang, Qiwei, Xiangdong Kong, Zhipeng Huang, Bin Yu, and Guo Meng. "Fluid-structureinteraction analysis of an aero hydraulic pipe considering friction coupling." IEEE Access 7 (2019): 26665-26677. https://doi.org/10.1109/access.2018.2890442

[29] Govindarajua, K., Hegdea, P., Badruddinb, I. A., & Alsharifa, I. O. A. M. (2019, March). Fluid Structure Interaction Simulation Study of Travelling Wave Valve-less Micro Pump in Fluid Delivery. In 2019 Advances in Science and Engineering Technology International Conferences (ASET) (pp. 1-5). IEEE. https://doi.org/10.1109/icaset.2019.8714211

[30]Dowell, E. H. & Hall, K.C. (2001, January). "Modelling of Fluid Structure interaction",annual review of fluid mechanics , Vol. 33 pp 445-490. https://doi.org/10.1146/annurev.fluid.33.1.445.

[31] Di Domenico, N., Groth, C., Wade, A., Berg, T. & Biancolini M.E. "Fluid structure interaction analysis : Vortex shedding induced vibrations", AIAS 2017 International conference on stress analysis, Procedia Structural Integrity 8 (2018) , pp 422-423. https://doi.org/10.1016/j.prostr.2017.12.042.

[32]Souček, O. "A brief introduction to fluid structure interactions", http://geo.mff.cuni.cz/jednooci_slepym/os-FSI-intro.pdf.

[33] Christopher, J., Falgout, R.D., Schroder, J.B., Guzik, M.S., & Gao, X. (2020). "A space-time parallel algorithm with adaptive mesh refinement for computational fluid dynamics". *Comput. Visual Sci.* **23,** 13, https://doi.org/10.1007/s00791-020-00334-1.

[34] Christopher, J., Gao, X., Guzik, S.M., and Falgout, R., and Schroder, J.,(2020)" Parallel In Time for a Fully Space-Time Adaptive Mesh Refinement Algorithm", AIAA 2020-0340, Session: CFD Methods II, https://doi.org/10.2514/6.2020-0340.
[35] Falgout, R. D., Friedhoff, S., Kolev, Tz. V., MacLachlan, S. P., and Schroder, J. B., (2014). "Parallel Time Integration with Multigrid", SIAM Journal on Scientific Computing, Vol. 36, No. 6 : pp. C635-C661, https://doi.org/10.1137/130944230.
[36] Bolten, M., Friedhoff, S., Hahne, J. , and Schöps, S., (2020). " Parallel-in-time simulation of an electrical machine using MGRIT". Comput. Visual Sci. **23,** 14. https://doi.org/10.1007/s00791-020-00333-2.
[37]Gander, M.J., and Lunet, T. (2020). "Toward error estimates for general space-time discretizations of the advection equation". *Comput. Visual Sci.* **23,** 16. https://doi.org/10.1007/s00791-020-00328-z.
[38] Rezazadeh, A., Mahmoudi, M., and Darehmiraki, M.(2018)., "Space–time spectral collocation method for one-dimensional PDE constrained optimisation". International Journal of Control Volume 93, Issue 5. https://doi.org/10.1080/00207179.2018.1501161.
[39] Li, S., Shao, X., and Cai, X.C. (2018)." Multilevel space-time additive Schwarz Methods for parabolic Equations", SIAM J. Sci. Comput., 40(5), A3012–A3037. (26 pages). https://doi.org/10.1137/17M113808X
[40] Li, S., Shao, X. & Cai, X.C. (2019). "Highly parallel space-time domain decomposition methods for parabolic problems". *CCF Trans. HPC* **1**, pp.25–34 https://doi.org/10.1007/s42514-019-00003-x
[41] Karri, V.S.K.R. " Flat Plate Vibrations in Wind Analysis for Energy Gain", Mater Thesis, Riga Technical University, Riga, Latvia.
[42] Agamloh, E.B., Wallace, A.K. and Jouanne, A.V.(2008). "Application of fluid–structure interaction simulation of an ocean wave energy extraction device". Renewable Energy,Volume 33, Issue 4,pp. 748-757.
https://doi.org/10.1016/j.renene.2007.04.010.
[43] Liu, Y., Lu, L., Faraci, C. and Zhao, M.(2015). "Mathematical Modeling of Fluid and Structure Interaction in Ocean Engineering". Mathematical Problems in Engineering, Hindawi Publishing Corporation. https://doi.org/10.1155/2015/170301
[44] Rasheed, A., Holdahl, R., Kvamsdal, T. and Åkervik, E.(2014). "A Comprehensive Simulation Methodology for Fluid-structure Interaction of Offshore Wind Turbines". Energy Procedia, Volume 53, pp. 135-145. https://doi.org/10.1016/j.egypro.2014.07.222
[45] Kvamsdal, T., Amundsen, J., Jenssen, C.B. and Oksad, K.M.(1999). "Numerical methods for fluid-structure interactions of slender structures". ECCM'99, European conference on computational mechanics, Munchen ,Germany.
[46] Kvamsdal, T., Jenssen, C.B., Oksad, K.M and Amundsen, J. (1999). "Fluid – structure interaction for structural design".Cmethods for Fluid-structure interactions, Tapir Publications, Trondheim, pp.211-238.
[47] Mumtaz Qadri, M.N., Zhao, F. And Tang, H. (2020). "Fluid-structure interaction of a fully passive flapping foil for flow energy extraction". International Journal of Mechanical Sciences, Volume 177, 105587, https://doi.org/10.1016/j.ijmecsci.2020.105587

[48]Duarte, L., Dellinger, G., Dellinger, N., Ghenaim, A., and Terfous, A. (2021). “Implementation and validation of a strongly coupled numerical model of a fully passive flapping foil turbine”. Journal of fluīds and Structures, Vol. 102, 103248. https://doi.org/10.1016/j.jfluidstructs.2021.103248.

[49] Dumas, G. and kinsey, T.(2006). “Eulerian simulations of oscillating airfoils in power extraction regime”. Advances in fluid mechanics, Vol. VI, pp.245-254. 10.2495/AFM060251.

[50] Richter, T. (2017). “Optimization with Fluid-structure Interactions”. In: Fluid-structure Interactions. Lecture Notes in Computational Science and Engineering, vol 118. Springer, Cham. pp. 357-369. https://doi.org/10.1007/978-3-319-63970-3_9

[51] Triantafyllou, M.S., Triantafyllou, G.S. and Yue, D.K.P. (2000) “hydrodynamics of fishlike swimming”. Annual Review of Fluid Mechanics, vol.32, pp. 33-53.

[52]Tallec, P.L. and Hauret, P.(2003). “Energy conservation in fluid structure interactions.”.Numerical methods for scientific computing,variational probles and applications.

[53] Tallec, P.L and Mouro, J.(2001). “Fluid structure interaction with large structural displacements”. Computer Methods in Applied Mechanics and Engineering,Vol. 190, Issue 24-25, pp.3039-3067.

[54] Gu, J., Cai, F., Müller, N., Zhang, Y. and Chen, H.(2020). “Two-Way Fluid–Solid Interaction Analysis for a Horizontal Axis Marine Current Turbine with LES”. Water , 12, 98. https://doi.org/10.3390/w12010098

[55] Harrison, M.E., Batten, W.M.J., Myers, L.E. and Bahaj, A.S. (2009) “A comaprison between CFD simulations and experiments for predicting the far wake of horizontal axis tidal turbines,”proceedings of the 8th European Wave and Tidal Energy Conference, Uppsala,sweden.pp.566-575.

[56]Hsiang Yu, Y. and Li, Y. (2013) “Reynolds-Averaged Navier Stokes simulation of the heave performance of a two-body floating-point absorber wave energy system”, Computers & Fluids, Vol.73, pp. 104-114. https://doi.org/10.1016/j.compfluid.2012.10.007

[57]De Andres, A.D., Guanche, R., Armesto, J.A., Del jesus, F., Vidal , C. and losada, I.J.(2013). “Time domain model for a two-body heave converter: Model and applications”, Ocean Engineering, Vol. 72, pp.116-123.

[58] Goldstein, H., Poole, C. & Safko, J. 2015. Classical Mechanics. Third Edition, wesley, pp. 625.

[59] Meriam, J. L., Kraige, L.G. & Bolton, J.N. 2015. Engineering Mechanics: Dynamics, 8th Edition, wiley, pp. 736.

[60] Ross, Isaac . “A primer on Pontryagin's principle in optimal control” . San Francisco: Collegiate Publishers(2015). . ISBN 978-0-9843571-0-9. OCLC 625106088.

[61] Mangasarian, O. L. . "Sufficient Conditions for the Optimal Control of Nonlinear Systems". SIAM Journal on Control. (1966), 4 (1): 139–152. doi:10.1137/0304013.

[62] Kamien, Morton I.; Schwartz, Nancy L. "Sufficient Conditions in Optimal Control Theory". Journal of Economic Theory. (1971), **3** (2): 207–214. doi:10.1016/0022-0531(71)90018-4.
[63] Wind energy conversion plant, LVP2020000092, Vība, J., Beresnevich,V., Irbe, M., Tipāns, I., Vutukuru, S.K., Kovals, E. & Eiduks, .M.; OWNER: RTU, application date: 18.12.2020.
[64] Sir Isaac Newton, 1687. Philosophiæ Naturalis Principia Mathematica.
[65*]. Latvian Wind Energy Handbook // EU PHARE Cooperation Program in the Baltic SeaRegion,2001–Internet,resource:
http://www.windenergy.lv/DOC/wind_energy_lv_final.pdf
[66]. Ветроэнергетика / Под ред. Д. де Рензо. - Москва: Энергоатомиздат, 1982, с. 19 - 21.
[67]. Янсон Р.А. Ветроустановки. - Москва: Издательство МГТУ им. Н.Баумана, 2007, с. 16 - 17. Patent of the Republic of Latvia LV 15038. - Prototype.
[68]. Баль В.Б., Геча В.Я., Гончаров В.И. и др. Линейные электрические машины возвратно-поступательного действия - области применения / Вопросы элентимехе 149, с. 3 - 17.
[69]. Dirba J., Levins N., Pugachev V. Electromechanical converters of wind energy. - Riga: RTU Publishing House, 2006.
[70]. Brent Maxfield. Essential Mathcad for Engineering, Science and Math. - London, Elsevier, Academic Press, 2009. 495 p.